SA-CASSCF AND R-MATRIX CALCULATIONS OF LOW-ENERGY ELECTRON COLLISIONS WITH DNA BASES AND PHOSPHORIC ACID

Lilianna Bryjko

A Thesis Submitted for the Degree of PhD
at the
University of St Andrews

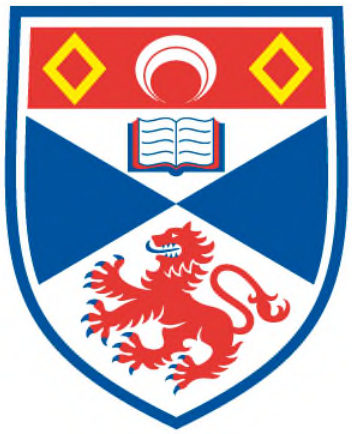

2011

University of St Andrews

School of Chemistry

A thesis submitted for the degree of Doctor of Philosophy

SA-CASSCF and R-matrix calculations of low-energy electron collisions with DNA bases and phosphoric acid

---

Author:

Lilianna Bryjko

Supervisor:

Dr. Tanja van Mourik

January 28, 2011

Contents

Acknowledgements

Firstly many thanks to my family, and to my friends for all their support and encouragement to complete this project all of these years.

I would like to thank my supervisor Dr Tanja van Mourik for her great ideas and her encouragement during this project.

Many thanks due to Professor Tennyson and Doctor Amar Dora for their great support during this project.

Many thanks are also due to Dr Herbert Früchtl for all the help and support all of these years.

Finally thanks due to the EaStCHEM Research Computing Facility and EPSRC for the financial support all of these years.

Abstract

The research presented in this thesis was carried out as part of a collaboration between the groups of Dr Tanja van Mourik at the School of Chemistry, University of St Andrews and Professor Jonathan Tennyson at the Department of Physics and Astronomy at University College London.

This thesis presents State-Averaged Complete Active Space Self Consistent Field (SA-CASSCF) calculations on nucleic acid bases, deoxyribose and phosphoric acid (H_3PO_4). In the case of uracil, for comparison, Multireference Configuration Interaction calculations were also performed. The SA-CASSCF orbitals were subsequently used in R-matrix electron scattering calculations using the close-coupling model.

Of major importance for obtaining accurate SA-CASSCF results is the choice of the active space and the number of calculated states. Properties such as the electronic energy, number of configurations, excitation energy and dipole moment were considered in the choice of active space.

Electron-collision calculations were performed on two of the most stable isomers of H_3PO_4, a weakly dipolar form with all OH groups pointing up and a strongly dipolar form where one OH group points down. A broad shape resonance at about 7 eV was found for both isomers. Ten-state close-coupling calculations suggest the presence of narrow, Feshbach resonances in a similar energy region. Elastic and electronically inelastic cross sections were calculated for both isomers.

The R-matrix calculations on uracil were done by the group from UCL.

R-matrix calculations are currently being done on guanine. Scattering calculations on the other DNA bases will be performed in the near future.

Chapter 1

Introduction

In the past few years, a growing literature has emerged concerning the damage to nucleic acids by low-energy electrons (LEE) with energy between 0 and 20 eV [1–16] produced by ionising radiation. If the electron energy is lower than the ionisation potential of the molecule, damage can be generated through a negative anion-mediated mechanism, which starts with the capture of the electron in a molecular resonance, followed by a transfer of energy and electron density towards a weak bond that subsequently ruptures. There is a wide agreement that the electron capture is mainly due to the DNA and RNA bases, because these molecules have extended aromatic systems. The scattering electron can temporarily be captured by an unoccupied π^* orbital giving rise to a shape resonance. When scattering is connected with electron excitation, Feshbach or core-excited resonances can occur.

It also has been suggested that electron attachment to the phosphate group [17] contributes to DNA strand breaks.

One of the methods used to study low-energy electron-molecule collisions is the R-matrix method [18], which is built around obtaining accurate wave functions for the anion-mediated state, obtained by the temporary capture of the scattering electron by the molecule.

The main aim of the project was to study electron collisions with the DNA and RNA bases and the phosphate group, here modelled by the phosphoric acid molecule.

Different R-matrix models were used, Static Exchange (SE), Static Exchange plus Polarisation (SEP) and Close-Coupling (CC) (see chapter 6). The most accurate of

these, the CC model, requires State-Averaged Complete Active Space Self Consistent Field, SA-CASSCF (shorter CAS) orbitals.

Previously several theoretical calculations on electron collisions with DNA constituents and phosphoric acid were performed [19–23]. Our contribution to these scattering calculations was obtained Feschbach resonances, while calculations of Winstead and McKoy [19–21] and Tonzani and Greene [22, 23] result only in shape resonances (see section 6.3).

Before performing the R-matrix calculations, we first had to: find geometries of the molecules with coordinates transformed to the centre-of-mass coordinates, find Modified Virtual Orbitals (MVOs, see appendix A.4) for uracil, as recommended by Winstead and McKoy [19] and perform the CAS excited state calculations using the Molpro computational package [24].

To transform the coordinates of the molecule from the standard Gaussian [25] format to the coordinates of the centre of mass, and to transform the TZV(2d,p) basis set from GAMESS US [26] to Molpro format [24], scripts were created using the Python Programming Language. The MVOs were calculated using Dalton [27], and here also the basis functions had to be transformed from Molden [28] into Molpro format. For each molecule and basis set programs were written to transform the molecular orbitals from Molpro into R-matrix order.

When performing the scattering calculations on guanine, which is the largest DNA base, using the aug-cc-pVDZ and cc-pVTZ basis sets difficulties with diagonalisation of the Hamiltonian matrix occurred. The polyatomic R-matrix codes have been developed by a number of people in different institutions (Daresbury Laboratory, Royal Holloway, UCL, QUB, etc.) based in part on a diatomic code developed at Daresbury by Cliff Noble and others [29]. All the R-matrix calculations were done using computers at UCL.

This thesis is divided into two parts, theory and results.

The theory section describes in the evolutionary order the methods Hartree-Fock (HF), Configuration Interaction (CI), Complete Active Space Self Consistent Field (CASSCF), and Multireference Configuration Interaction (MRCI). The next chapters discuss the low-energy electron collisions and R-matrix theory. Additional infor-

mation about electron correlation, basis sets, Molpro orbitals, R-matrix calculations and L^2 configurations is provided in the appendix (see appendix A).

The first molecule considered was uracil, and for this molecule the CAS calculations are described in more detail, to illustrate how we chose the active space for the subsequent scattering calculations. The second molecule for which R-matrix calculations were performed was phosphoric acid. For cytosine, adenine, guanine, thymine and 2-deoxyribose only CAS calculations are presented, which may be suitable for subsequent close-coupling calculations. The excitation energies and dipole moments for all molecules were compared with other methods and experimental data. Additional excited state calculations are included in the appendix.

Chapter 2

Deoxyribonucleic and Ribonucleic Acid

Deoxyribonucleic Acid (DNA) is a long polynucleotide polymer of units called nucleotides [17, 30, 31]. It contains the genetic instruction for the development and functioning of living organisms, and the major function of DNA is to encode the sequence of amino acid residues in proteins, using the genetic code. In living organisms DNA exists in the shape of a double helix, where the nucleotide repeats contain both the backbone of the molecule, and a base, which interacts with another base on the other DNA strand in the helix (see figure 2.1).

The four bases in DNA are adenine and guanine (fused five- and six membered heterocyclic compounds called purines) and cytosine and thymine (six membered rings called pyrimidines). Purines on one strand form hydrogen bonds with a pyrimidine on the other strand forming base pairs with adenine binding only to thymine and cytosine only to guanine. Nucleosides are glycosylamines made by attaching a nucleobase to a 2-deoxyribose sugar (for example cytidine, adenosine, guanosine, thymidine). Nucleosides can be phosphorylated by specific kinases in the cell, producing nucleotides, the building blocks of DNA [17]. Each phosphate group is joined to the 3' carbon atom of one deoxyribose and to the 5' carbon atom of another (see chapter 8.7 and figures 8.11 and 8.12). Thus each strand has a 3' end and a 5' end. The two strands are oriented in opposite directions (see figure 2.1).

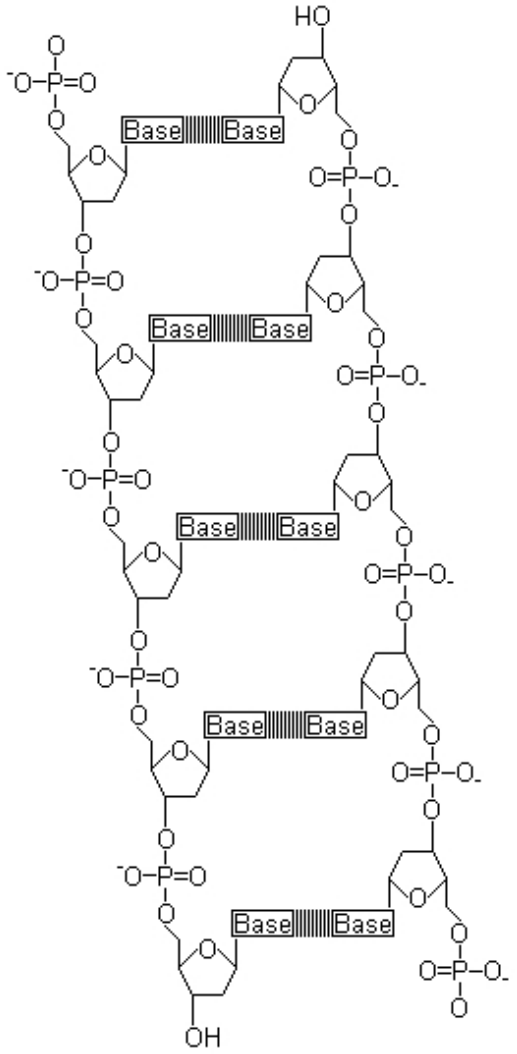

Figure 2.1: Structure of DNA (ChemDraw Ultra 10 [32])

The phosphate linking to the sugar group carries a negative charge because of the chemical interaction between phosphorus and oxygen. In the cell the phosphate groups are neutralised by counter ions (for example Na^+). DNA exists in several possible conformations. The most common in nature are A-DNA, B-DNA and Z-DNA [17]. Ribonucleic Acid (RNA) is also a biologically important molecule that consists of a long chain of nucleotide units. It is very similar to DNA, but RNA is usually single-stranded, and instead of thymine and 2-deoxyribose contains uracil and ribose sugar, respectively. RNA is central to protein synthesis [17].

Chapter 3

The Hartree-Fock Method

The Hartree-Fock (HF) method aims to find the optimal wavefunction, ψ, within the limitation of using a single Slater determinant. Slater determinants are the simplest antisymmetric n-particle functions, from which all other n-particle functions are used in constructing an atomic or molecular wavefunction. Each Slater determinant is normalised in the n-particle space and is constructed from the selection $\phi(r_1)$, $\phi(r_2)$,...$\phi(r_n)$ of spin orbitals [33]:

$$\psi(r_1, r_2, r_3, ...r_n) = \frac{1}{\sqrt{n_{elec}!}} \begin{vmatrix} \phi_1(r_1) & \phi_2(r_1) & \phi_3(r_1) & . & . & . & \phi_n(r_1) \\ . & \phi_2(r_2) & & & & & \\ . & & \phi_3(r_3) & & & & \\ . & & & . & & & \\ . & & & & . & & \\ . & & & & & . & \\ \phi_1(n) & & & & & & \phi_n(r_n) \end{vmatrix} \tag{3.1}$$

Including antisymmetry the energy is a sum of one-electron, Coulomb and exchange terms [34]:

$$E = \sum_i \epsilon_i^n + \sum_{i<j} \int \phi_i^2(r_1) \frac{1}{r_{12}} \phi_j^2(r_2) dr_1 dr_2 - \sum_{i<j} \int \phi_i(r_1)\phi_j(r_2) \frac{1}{r_{12}} \phi_i(r_2)\phi_j(r_1) dr_1 dr_2 \tag{3.2}$$

where $\phi^2(r)$ is the probability of finding an electron at a given point in space. The Hartree-Fock equations are:

$$\left\{H_n + \sum_{j=1} \int \phi_j^2(r_2) \frac{1}{r_{12}} dr_2 \right\} \phi_i(r_1) - \left\{ \sum_{j=1}^{n} \int \phi_j(r_2)\phi_i(r_2) \frac{1}{r_{12}} dr_2 \right\} \phi_i(r_1) = \epsilon_i^{SCF} \phi_i(r_1) \tag{3.3}$$

in the shorter form:

$$\left\{H_n + \sum_j J_j - \sum_j K_j \right\} \phi_i(r_1) = \epsilon_i^{SCF} \phi_i(r_1) \tag{3.4}$$

where the Coulomb and exchange operators are defined as:

$$J_j \phi_i(r_1) = \left(\int \phi_j^2(r_2) \frac{1}{r_{12}} dr_2 \right) \phi_i(r_1) \tag{3.5}$$

$$K_j \phi_i(r_1) = \left(\int \phi_j(r_2)\phi_i(r_2) \frac{1}{r_{12}} dr_2 \right) \phi_j(r_1) \tag{3.6}$$

The Hartree-Fock equations in the Linear Combination of Atomic Orbitals (LCAO) approximation are called the Roothaan equations:

$$\phi_i = \sum_{\mu=1}^{n} c_{\mu i} \chi_\mu \tag{3.7}$$

where each orbital ϕ_i is expressed as a linear combination of atomic orbitals, χ_μ.

The problem for a given basis set is to find values of the expansion coefficients, $c_{\mu i}$, which minimise the energy E. The Schrödinger equation cannot be solved explicitly for the ground state wavefunction. According to the variational principle the energy of an approximate wavefunction, ψ is given by [34]:

$$E = \frac{\int \psi(r) H \psi(r) dr}{\int \psi(r)\psi(r) dr} \tag{3.8}$$

For any normalised wavefunction ψ, the expectation value of the Hamiltonian for ψ

must be greater than or equal to the actual ground state energy:

$$E_{ground} \leq \langle \psi | H | \psi \rangle \tag{3.9}$$

This holds for any trial ψ, by definition, the ground state wavefunction has the lowest energy, and any trial wavefunction will have energy greater than or equal to it.

The Hartree-Fock equations can be solved by an iterative Self Consistent Field (SCF) method, and there are many techniques for helping the iterative procedure to converge [35].
In the first cycle of the SCF procedure all the various atomic integrals for a given basis set and geometry are calculated. Subsequently, a set of expansion coefficients or trial molecular orbitals are guessed, which with the atomic integrals are used to construct the Roothaan-Hartree-Fock operator. Solvation of Fock equations gives another set of 'improved' expansion coefficients used in the second cycle etc. The procedure is repeated until the coefficients are identical within the previous set. With a reasonable set of 'guess' orbitals, 10-20 cycles are usually enough to converge the procedure.

Chapter 4

The Configuration Interaction Method

Configuration Interaction (CI) is a post Hartree-Fock linear variational method for a quantum chemical multi-electron system. Configuration simply describes the linear combination of Slater determinants used for the wavefunction, interaction means the mixing (interaction) of different electronic configurations.

CI uses a variational wavefunction that is a linear combination of configuration state functions (CSFs) (symmetry-adapted linear combinations of Slater determinants) built from spin orbitals. The variationally computed SCF wavefunction and its orbitals are taken as reference to construct several excited states of the appropriate symmetry. The linear variational method is used to find the best possible mixing coefficients C_i [34]:

$$\Psi_{CI} = \sum_i C_i \psi_i = C_0 \psi_{SCF} + \sum_D C_D \psi_D + \sum_T C_T \psi_T + ... \tag{4.1}$$

The subscripts S, D, T etc. show determinants which are singly, doubly, triply etc. excited (one, two or three spin orbitals are swapped with virtual orbitals) relative to the ground state, HF configuration. This leads to a matrix eigenvalue equation:

$$HC = ESC \tag{4.2}$$

where C contains the coefficients, E is energy, H is Hamiltonian matrix with ele-

ments:

$$H_{ij} = \langle \psi_i | H | \psi_j \rangle \tag{4.3}$$

and S is an overlap matrix

$$S_{ij} = \langle \psi_i \psi_j \rangle \tag{4.4}$$

It is usual to take the ψ_i, which are called CSFs, to be orthonormal so that S is an identity or unit matrix which simplifies the above matrix equation.
The processes involved in a SCF-CI calculation:

1. Choose basis set and compute integrals
2. Carry out an SCF procedure and obtain orbitals
3. Transform the integrals over the basis functions to integrals over molecular orbitals
4. Construct CSFs and compute H (and S)
5. Find eigenvalues (E) and eigenfunctions (C)

A special case of the Configuration Interaction method is Full Configuration Interaction (FCI) in which all Slater determinants (CSFs) of the proper symmetry are included in the variational procedure (all Slater determinants obtained by exciting all possible electrons to all possible virtual orbitals) [36].

Chapter 5

Multi-reference Configurational Methods

5.1 Multi-configurational Self Consistent Field

Multi-configurational Self Consistent Field (MCSCF) is an extension of configuration interaction (CI) and uses a linear combination of CSFs or configuration determinants (not a single reference as CI based on HF orbitals) to approximate the exact electronic wavefunction of an atom or molecule. In the MCSCF method not only the coefficients in front of the determinants (see equation 4.1) are optimised by the variational principle, but also the molecular orbitals used for constructing the determinants (see equation 3.7) are made optimum. The MCSCF optimisation is iterative just like the SCF procedure (if the 'multi-configuration' is only one, it is simply HF) [37] and has been developed for treating static correlation effects (see appendix A.2).

When static correlation is weak, Hartree-Fock theory provides a correct description of the wavefunction, but for most excited states, for molecules that are close to dissociation, and for electronic degeneracy, Hartree-Fock is a poor approximation. Large static correlation effects often indicate that there is no single Slater determinant that dominates the wavefunction. A viable way is to include the static correlation using a CI-expansion that covers all the important effects and subsequently using this many-determinant reference as a starting point for recovery of the dynamic

correlation. Such approaches are multi-reference methods [38].

Several MCSCF methods have been described and historically they are divided into: Optimised Valence Configurations [39–41], Generalised Brillouin Theorem [42–47], Second Order Methods [48–59] and First Order Procedure [60, 61].

5.2 Complete Active Space Self Consistent Field

The Complete Active Space Self Consistent Field (CASSCF, shorter CAS) method [62], also called Full Optimised Reaction Space (FORS), is one of the most popular approaches of the MCSCF method [37]. CASSCF is full CI in the active space[1]. The method is developed also for calculating the ground state.
The selection of configurations is done by partitioning the MOs into an active, closed and virtual space.

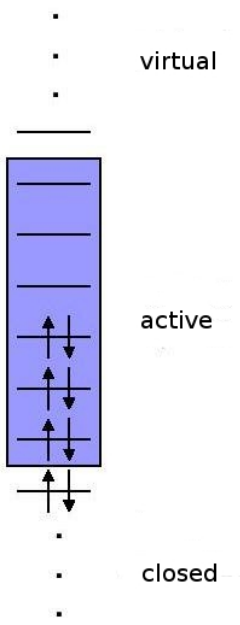

Figure 5.1: An example of an active space as required in CASSCF theory. The example corresponds to a six-electrons-in-six-orbital selection [63]

The closed orbitals are doubly occupied, while the active orbitals have occupation numbers varying between 0 and 2. The virtual orbitals are unoccupied.
In the CASSCF method the total electronic wavefunction is formed as a linear combination of CSFs. The number of configurations is given by the Weyl-Robinson formula [64, 65]:

[1]In CASSCF type wavefunctions the CI coefficients do not have the same significance as for a single reference CI based on HF orbitals. In a full CI the orbitals may be rotated among themselves (which has influence on the magnitude of the coefficients in front of each CSF) without affecting the total wavefunction. In the single reference CI the CSFs can only be characterised by the number of spin orbitals that are swapped with virtual orbitals from the HF determinant.

$$n_{(CSF)} = \frac{2S+1}{M+1}\binom{M+1}{M-(N/2)-S}\binom{M+1}{N/2-S} \tag{5.1}$$

where S is the total spin, N is the total number of active electrons, and M is the number of active orbitals.

Because CASSCF calculations are dependent on the number of active electrons and particularly on the number of active orbitals generating many electron configurations, the orbital optimisation is practically independent of the number of closed orbitals.

Another general problem with CASSCF calculations is the choice of which state for which the orbitals are to be optimised. This choice has an influence on the relative energies of the calculated excited states and can change their energetic ordering. One way to partially avoid this problem is to perform a state-averaged calculation, in which the orbitals are optimised with respect to the weighted mean of all states of interest [66, 67]. A state averaged calculation is performed when the same set of MOs is used for a number of electronic states of the same spin and symmetry. The CI problem is solved for a number of roots (R) and the orbitals are optimised for the average energy, E_{aver}, of the states [68]:

$$E_{aver} = \sum_{i=1}^{R} \omega_I E_I \tag{5.2}$$

where ω_I are weights which can be chosen.

There is no clear-cut way to choose the active space. Usually, for small molecules, CASSCF calculations are done with a full valence active space. For conjugated systems all π orbitals should be included in the active space [37]. Another way is to choose a one-to-one active space that has one anti bonding orbital for each bonding orbital. An unbalanced choice of active orbitals leads to an unbalanced treatment of the excited states. For example, if the chosen active space consists of only π orbitals, the calculated spectrum contains only π excited states. Other states, for instance $n \rightarrow \pi^*$ states are not found, although in general they cannot a priori be excluded, since they might become important in the course of the studied photo-initiated process. A too small active space and the concomitant neglect of large

parts of dynamical electron correlation can be the reason of significant errors and an unbalanced treatment of different classes of electronic states.

Some convergence problems can occur, if an active orbital has an occupation number very close to 2 (the energy is dependent upon only weak rotations between this orbital and the closed orbitals) or when an orbital has a very small occupation number (rotations between this orbital and the virtual orbitals become near-redundant). In this situation the optimisation method by Werner and Knowles [24, 69–71] may be used, which enables calculations with active orbital occupation numbers as high as 1.995 and as low as 0.001 without convergence problems. This is the method that is implemented in Molpro [24].

5.3 Multireference Configuration Interaction

Multireference Configuration Interaction (MRCI) is one of the methods that can recover the dynamical correlation (see appendix A.2) energy in multiconfigurational systems. MRCI is equivalent to the CI method, but taking as starting point an MCSCF wavefunction and building the different excitations from the different configurations belonging to Ψ_{MCSCF}. In MRCI(SD) all single and double excitations out of all determinants that are included in the MCSCF wavefunction are considered.

Several MRCI methods have been described for example: by Siegbahn [72, 73] Buenker and Peyerimhoff [74, 75], Brook and Schaefer [76, 77], Duch and Karwowski [78, 79], Tavan and Schulten [80], Taylor [81], Liu and Yoshimine [82] and Lischka et al. [83]. The most commonly used MRCI program is probably that of Werner and Knowles [24, 70, 71, 84], whose determinant-based internally contracted scheme facilitates extending the correlation treatment to the valence inactive electrons.

In general, an MRCI(SD) wave function can be written [84]:

$$\Psi = \sum_I c^I \Psi_I + \sum_S \sum_a c_a^S \Psi_S^a + \sum_D \sum_{ab} C_{ab}^D \Psi_D^{ab} \tag{5.3}$$

where a,b denote external orbitals (not occupied in the reference configurations), S and D denote internal N-1 and N-2 electron-hole states. Ψ_I, Ψ_S^a, Ψ_P^{ab} are respectively internal, singly external and doubly external configurations. The reference space is a subset of the internal configurations Ψ_I.

Two different contraction schemes which reduce the number of variational parameters are used in MRCI:

- **"Externally" contracted CI** (of Siegbahn [85, 86]).

  The singly and doubly external configurations are contracted as:

$$\Psi_S = \sum_a \alpha_a^S \Psi_S^a \tag{5.4}$$

$$\Psi_D = \sum_{ab} \alpha_{ab}^D \Psi_D^{ab} \tag{5.5}$$

The contraction coefficients α are obtained by first order perturbation theory.

- **"Internally" contracted CI** (first discussed by Mayer [87] and Siegbahn [88] and implemented by Werner and Reinsch [89]). In this method the configurations are generated by applying pair excitation operators to the reference wave function as a whole. This generates linear combinations of the configurations Ψ_D^{ab} with different internal states D.

Three different orbital subspaces are distinguished [84]:

- **Core orbitals** - doubly occupied in all configurations and not correlated.
- **Valence orbitals** (i,j,k,l,...) - occupied in the reference configurations and correlated in the CI wave function.
- **External orbitals** (a,b,c,d,...) - unoccupied in the reference wave function.

The set of N-2 electron states D is obtained from all possible two-electron annihilation acting on each reference configuration. The N-1 electron states S are generated from the N-2 electron states D by adding one electron to the valence space, and the internal configurations are obtained from the N-1 electron states S by adding another electron. Defining the internally contracted configuration space, it is useful to employ one-electron creation and annihilation operators, which remove an electron from i and j orbitals which are occupied in the reference wave function and add this electron to unoccupied orbitals in the reference wave function, a and b. The internally contracted doubly external configurations are defined as:

$$\Psi_{ijp}^{ab} = \frac{1}{2}(\widehat{E}_{ai,bj} + p\widehat{E}_{bi,aj})\Psi_0 \tag{5.6}$$

where $p = 1$ for external singlet pairs and $p = -1$ for triplet pairs. Ψ_0 is the reference wave function, which may be composed of many configurations Ψ_R:

$$\Psi_0 = \sum_R a^{(R)} \Psi_R \tag{5.7}$$

One of the advantages of this scheme is that the number of contracted internal states is independent on the number of reference configurations. It depends only on the number of correlated orbitals. For m correlated orbitals can be obtained at most m^3 contracted internal N-1 electron states by two annihilation and one creation, and m^2 contracted N-2 electron states by two annihilation.

Chapter 6

R-matrix

6.1 Low-energy electrons

In the past few years, a growing literature has emerged concerning the damage to nucleic acids by low-energy electrons (LEE) with energies between 0 and 20 eV [1, 2, 4–16] produced by ionising radiation. The process follows the creation of thousands of low-energy electrons, stripped off from molecules in the cell either directly by radiation or else by its first products, highly energetic primary electrons, that can cause electron-impact ionisation.

The nucleic acid can be ionised and damage produced through the dissociation of the cation [90] when the electron energy is higher than the ionisation threshold for DNA (between 7.85 and 9.4 eV, as measured for the DNA bases [91]). If the electron energy is lower, damage can still be generated, but through a negative anion-mediated mechanism, which starts with the capture of the electron in a molecular resonance, followed by the transfer of energy and electron density towards a weak bond that subsequently ruptures.

There are many controversial issues that concern the location of the initial capture site [1, 68], the dynamics of the metastable anion generated by electron capture (called transient molecular anion), and the identification of the final bond that ruptures [5, 13–15, 92–95].

There is a wide agreement that the electron capture is mainly due to the DNA and RNA bases, because these molecules have extended aromatic systems. The scatter-

ing electron can temporarily be captured by an unoccupied π^* orbital giving rise to a shape resonance. When scattering is connected with electron excitation, Feshbach or core-excited resonances can occur.

The mechanism of DNA-LEE interaction is important because the low-energy secondary electrons are the most abundant radiolysis species generated upon impact of high-energy radiation [96] and therefore highly pertinent to issues such as the development of radiotherapy. Low-energy collisions with molecules can result in a variety of different processes such as [97]:

- Elastic scatterring:

$$AB + e^- \rightarrow AB + e^- \tag{6.1}$$

- Electronic excitation:

$$AB + e^- \rightarrow AB^* + e^- \tag{6.2}$$

- Vibrational excitation:

$$AB(v'') + e^- \rightarrow AB(v') + e^- \tag{6.3}$$

- Rotational excitation:

$$AB(N'') + e^- \rightarrow AB(N') + e^- \tag{6.4}$$

- Dissociative attachment:

$$AB + e^- \rightarrow A^- + B \tag{6.5}$$

$$AB + e^- \rightarrow A + B^- \tag{6.6}$$

- Impact dissociation:

$$AB + e^- \rightarrow A + B + e^- \tag{6.7}$$

- Impact ionisation:

$$AB + e^- \rightarrow AB^+ + e^- + e^- \tag{6.8}$$

Because of loss of symmetry and increase of degrees of freedom, electron-molecule collisions are significantly more difficult to treat theoretically than electron-atom collisions. A common feature of all these processes is that they can be considered to go via an intermediary, AB^-. One of the methods used to consider low-energy electron-molecule collisions is the R-matrix method [18], which is built around obtaining accurate wave functions for this intermediary and hence gives a theoretical framework capable of modelling all the above processes.

6.2 R-matrix theory

The R-matrix method was introduced into atomic physics by Burke and his associates [98–102] in the early 1970's. Burke and his co-workers applied the R-matrix method to many problems in the electron scattering and photoionisation of simple and complex atoms [103]. The method was generalised and applied by Schneider [104, 105], Hay and Schneider [106] and Schneider and Morrison [107] and then by Burke, Mackey and Shimamura [108], Buckley, Burke and Lan [109] and Noble, Burke and Salvini [110] to treat electron-molecule collisions.

Besides the R-matrix method, there are two other close-coupling expansion-based methods which are used for electron-molecule collision studies. These methods are based on the Kohn variational principle [111] and the Schwinger variational principle [112–114].

The R-matrix method is based on the splitting of coordinate space into two regions, an inner and an outer region, separated by a spherical boundary of radius r = a centred on the centre of mass of the molecule [115, 116]. The inner region contains all the electronic charge cloud of the target molecule. In the inner and outer regions the interaction between the electron and the target molecule has different features. Inside the R-matrix sphere, the scattering electron lies within the molecular-charge cloud, and exchange interactions and electron-electron correlation must be taken into consideration. In the outer region, exchange and correlation are negligible and only long-range multipolar interactions between the scattering electron and the target are included, which makes it possible to reduce the scattering problem in the external region to the solution of a set of coupled, ordinary differential equations.

When the system (N-electron molecule plus one scattering electron) has energy E then it has a wavefunction, $\psi^{N+1}(E)$, given by [18]:

$$(H_{N+1} - E)\psi^{N+1}(E) = 0 \tag{6.9}$$

where H_{N+1} is the Hamiltonian of the N-electron molecule plus one scattering electron.

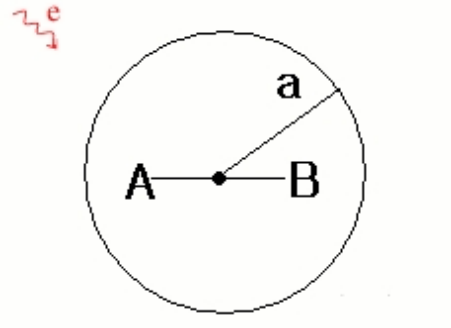

Figure 6.1: The R-matrix method divides space into an inner and outer region. The inner region contains the wave function of the target molecule, AB. In the outer region only the scattering electron can be presented. The boundary is given by a sphere of radius a, centred on the target centner of mass [18].

In fixed-nuclei [1] R-matrix theory the wavefunction of the inner region has the form [117, 118]:

$$\Psi^{N+1}(E) = \sum_k A_k(E)\psi_k^{N+1} \tag{6.10}$$

where ψ_k^{N+1} is an energy-independent solution of the inner region problem and the $A_k(E)$ are coefficients whose values change as the total energy E is changed. These ψ_k^{N+1} need to be constructed only once for all scattering energies and in the inner region they are expansions over CSFs, which are composed of linear combinations of Slater determinants (see equation 3.1). These determinants involve spin orbitals, ϕ_i (see equation 3.7), which are combinations of functions centred on the nuclei and on the centre of gravity of the molecule.

In the inner region the wave function is usually written [29]:

$$\psi_k^{N+1} = A\sum_{ij} a_{ijk}\phi_i^N(x_1...x_N)u_{ij}(x_{N+!}) + \sum_i b_{ik}\chi_i^{N+1}(x_1...x_{N+1}) \tag{6.11}$$

where the target contains N electrons and functions are labelled as N or N+1 according to whether they refer to the target or the compound scattering system, respectively. ϕ_i^N is the wave function of the i^{th} target state and u_{ij} are extra orbitals introduced to represent the scattering electron, called continuum orbitals.

[1] The nuclei are fixed at a particular geometry and then solve for the electronic part of the total wave function.

The continuum basis set needs to be centred on the target centre-of-mass. The polyatomic R-matrix procedure was developed, initially by Nestman et al. [119] and used Gaussian Type Orbitals (GTOs) [35] to represent both the target and continuum functions in the inner region. An alternative GTO-based procedure was implemented by Morgan [120] and other more specialised, electron-molecule R-matrix procedures [121–125] have been developed more recently. The choice of the continuum orbitals depends on the particular target state, ϕ_i^N, since the two must couple together to give the correct overall spatial and spin symmetry of the total wave function ψ^{N+1}.

The electrons which space-spin coordinates are represented by x_i, must obey the Pauli principle and therefore are anti-symmetrised by the operator A. The second summation in equation 6.11 involves configuration where all electrons are placed in the target, referred to as L^2 configurations (see appendix A.5.1 and A.5.2). Such configurations are essential in even the simplest scattering model as they allow for relaxation of the orthogonalisation between the continuum orbitals and those belonging to the target. In more sophisticated models the L^2 configurations are also used to model the effects of target polarisation (see appendix A.5.1).

The radial distance where the energy-independent solutions from the inner region are used to construct an energy-dependent R-matrix is called the boundary.

In the outer region the wavefunction can be written [29]:

$$\psi^{N+1}(E) = \sum_{i=1}^{n} \phi_i^N(x_1...x_N) F_i(r_{N+1}) Y_{l_i,m_i}(\theta,\phi) \Xi_{\frac{1}{2}} \tag{6.12}$$

where the sum runs over the n channels of the problem. For molecular problems, there are usually several channels associated with each target state. F_i corresponds to the energy-dependent wave function of the projectile in the i^{th} channel, Y_{l_i,m_i} are spherical harmonics, where the (l_i, m_i) match with the asymptotic channel associated with the i^{th} target state and its angular momentum quantum numbers. The function $\Xi_{\frac{1}{2}}$ is a spin one-half electron spin function.

The quality of the scattering calculation is strongly dependent on obtaining a good representation of the target wavefunctions and the associated target properties. A

particular problem that faces scattering studies is the need to represent all target states using a single set of orbitals. The SCF solution to the Hartree-Fock approximation yields orbitals which often give a satisfactory representation of the ground state but are less appropriate for excited states. The ways of improving the orbital representation for a multistate problem is employment of the CASSCF orbitals. The CASSCF method obtains orbitals optimised simultaneously for a number of electronic states.

The UK polyatomic R-matrix code is built on the Sweden-Molecule quantum chemistry package of Almöf and Taylor [126, 127] and now is used by a large number of different groups around the world [128–140]. The program Quantemol-N [141] is also available to facilitate the use of the polyatomic version of the codes by non-experts. The general application of the R-matrix method to polyatomic molecules employing the UK polyatomic R-matrix code has been described in the literature [18, 116, 142, 143]. There are also many examples [144–151] describing the employment of the R-matrix method to study electron-collisions with different molecules.

6.3 Resonances

The temporary trapping of an electron to form a quasibound or short-lived state is known as a resonance. Resonances are generally characterised by type, configuration, symmetry, position, and width. The formation and behaviour of resonances is the key to many processes in electron-molecule scattering.
Resonance states are often characterised as:

- **Shape resonance**, where the scattering electron temporarily occupies a low-lying unoccupied orbital in the ground state of the target molecule. They are generally rather short-lived meaning that they appear as broad features as a function of energy in the scattering observables. They provide the most common route for dissociative attachment [152]. For example, if the ground state of an electronic system can be labeled as s^2p^0 with a doubly occupied s orbital and with a virtual orbital p (see figures 6.2 and 6.3), and if f_E corresponds to an incident electron of kinetic energy E, then in case of a shape resonance the $p \rightarrow f_E$ transition is the only one required for the emission of an electron.

$$s^2p^0 + e^-(E) \rightarrow s^2p^1 \tag{6.13}$$

- **Feshbach resonance**, where the scattering electron temporarily occupies an unoccupied orbital of an electronically excited state of the target molecule. They are generally narrower than shape resonances and provide the main route to dissociative recombination [153]. In case of a Feshbach resonance both transitions $p \rightarrow f_E$ and $p \rightarrow s$ are required to emit one electron (see figure 6.2).

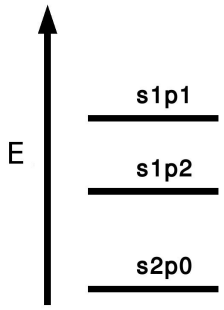

Figure 6.2: Orbitals in the case of a Feshbach resonance

$$s^2p^0 + e^-(E) \rightarrow s^1p^2 \tag{6.14}$$

with not allowed

$$s^1p^2 \rightarrow s^1p^1 + e^-(E' > 0) \tag{6.15}$$

- **Core-excited shape resonance**. This resonance, like a Feshbach resonance, is associated with electronic excitation of the target but, like a shape resonance, the electron is trapped by a barrier in the potential at an energy above that of the excited state. In case of a core-excited shape resonance one of the fragments is left in the excited state s^1p^1 and only the $p \rightarrow f_E$ transition is required to emit one electron (see figure 6.3).

$$s^2p^0 + e^-(E) \rightarrow s^1p^2 \tag{6.16}$$

with allowed

$$s^1p^2 \rightarrow s^1p^1 + e^-(E' > 0) \tag{6.17}$$

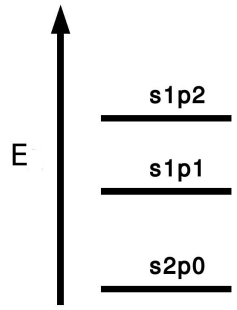

Figure 6.3: Orbitals in the case of a core-excited shape resonance

Resonances can be characterised by position (E^{res}) and width Γ^{res}. One of the R-matrix programs to obtain the resonances is RESON [154], which reads the file of energy points and corresponding eigenphases. The eigenphase sum, δ, is obtained from the sum of the eigenvalues of the K-matrix (this is a symmetric matrix whose dimension is the number of open channels, see section 8.6.3), K^D_{ii}, as [29]:

$$\delta(E) = \sum_i arctan(K^D_{ii}) \tag{6.18}$$

Eigenphase sums provide a very useful diagnostic of scattering calculations.

The standard method for characterising an isolated resonance is to represent the eigenphase sum in the region of the resonance using the Breit-Wigner form [155]:

$$\delta(E) = \delta_0(E) + \sum_{i=1}^{m} tan^{-1} \frac{\Gamma_i^{res}}{2(E_i^{res} - E)} \tag{6.19}$$

where $\delta_0(E)$ is the background eigenphase. Hazi [156] showed that it is correct to fit the eigenphase sum, δ, as a function of collision energy, E.

In RESON Tennyson and Noble [154] implemented a recursive procedure for detecting and performing Breit-Wigner fits to resonances. This procedure scans $\delta(E)$ and marks those points where the numerically computed second derivative, $\frac{d^2E}{d\delta^2}$ changes signs from positive to negative [2]. A finer grid is constructed about each of

[2]The second derivative of a function f measures the concavity of the graph of f. If the second derivative of a function changes sign, the graph of the function will switch from concave down to

these points which is then used as the input to a Breit-Wigner fit. These points are marked as the location of possible resonances. RESON can handle eigenphase sums which are smoothed (i.e. increase by π). Narrow resonances can be missed if the energy grid is too coarse. In our calculations resonances were obtained using the program RESON and by analysis of the eigenphase sums and their derivatives.

concave up, or vice versa. A point on a curve at which the second derivative changes sign is called an inflection point.

6.4 Scattering models

The basic scattering models are [157]:

- **The Static Exchange (SE)** model. This is the most basic model, in which the target wavefunction is represented at the HF level. The SE model cannot treat many physical processes such as electron impact electronic excitation. It also cannot model Feshbach resonances since these also involve electronic excitation of the target. The SE model can only give shape resonances which are usually significantly too high in energy. Within the SE approximation the only possible L^2 configurations (see appendix A.5.1) are ones in which the scattering electron occupies otherwise unoccupied, or virtual spin-orbitals of the target.

- **The Static Exchange Plus Polarisation (SEP)** model, in which single excitations out of the target (HF) wavefunction are used to represent target polarisation effects. Polarisation effects can be included by promoting one electron from the target into a virtual orbital and also putting the scattering electron into a virtual orbital giving a two particle-one hole (2p,1h) configuration. The SEP model can give good resonance parameters for shape resonances and is also capable of representing Feshbach resonances, which arise from two particle-one hole (2p,1h) L^2 configurations (see appendix A.5.1), which correspond to target excitations.

- **The Close-Coupling (CC)** approximation uses a CAS representation of the target wavefunction. A CC expansion can give a complete treatment of the scattering process, and the calculations are particularly good at representing Feshbach resonances associated with the target excited states (see appendix A.5.2). The CC model includes several target states, but these can in principle be represented by any CI model. The simplest L^2 configurations (see appendix A.5.2) for the CAS CC model can be written as [157]:

$$(core)^m(CAS)^n$$

$$(core)^m(CAS)^{n-1}(virtual)^1$$

where the first set of configurations can represent Feshbach resonances, and the second shape resonances. It has been common to contract the second set of CSFs with the target CI wave function [145,158]. In this contracted model the occupation of each virtual orbital of the appropriate symmetry only contribute one CSF no matter how large the target CI expansion is. The CC calculations without this contraction are called uncontracted calculations. In calculations using the uncontracted model molecular partitioned R-matrix calculations are used [159] in which less than 10% of the eigenvalues are computed.

.

Chapter 7

Methodology

The main aim of the project was to generate State-Averaged Complete Active Space Self Consistent Field, SA-CASSCF (shorter CAS) molecular orbitals and to perform R-matrix calculations in a collaboration with Prof. Jonathan Tennyson's group at UCL [160].

Because the UK R-matrix codes (http://ccpforge.cse.r1.ac.uk/gf/project/ukrmol-in/) use spherical harmonic functions, all calculations were done with spherical harmonic basis functions. The R-matrix calculations were performed with the centre of mass coordinates of the molecule.

The types of electronic orbitals that may be present in organic molecules are σ, π, n, π^* and σ^*. Photochemists designate electronic excitations by an arrow from the lower energy orbital to the upper energy state and $n \rightarrow \pi^*$, $\pi^* \rightarrow \pi^*$, $n \rightarrow \sigma^*$, $\sigma \rightarrow \sigma^*$. $n \rightarrow \pi^*$ and $\pi \rightarrow \pi^*$ excitations, which are the most characteristic transitions, are normally observed in the near-UV and visible regions [161].

To establish a model methodology to obtain the target orbitals, a series of calculations was performed with the CAS method with several basis sets and different active spaces using the MOLPRO 2006.1 computational package [24] on a computer cluster with 2.4 GHz AMD Opteron processors.

A key problem with CAS calculations is scaling with system size: there is a factorial dependence on both the number of active electrons and particularly on the number of active orbitals generating many-electron configurations (full CI within the active space) [37]. For atomic or conjugated systems the CAS space, typically, includes

the valence π-orbitals. In heteroatomic systems one may want to include also the lone pair orbitals and electrons to allow for $n \rightarrow \pi^*$ excitations [63].

Some R-matrix calculations were performed with Modified Virtual Orbitals (MVOs) [157, 162] (see appendix A.4) obtained from the DALTON 2.0 molecular electronic structure program [27].

The optimisation of the molecular geometries was performed using the Gaussian03 computational package [25]. The basis sets used in the calculations are 6-31G, 6-31G*, 6-31+G* [163], cc-pVDZ, aug-cc-pVDZ and cc-pVTZ [164, 165] with segmented contraction (see www.bse.pnl.gov/bse/portal). Some calculations were performed with the TZV(2d,p) and 6-311++G** [163] basis sets. The TZV(2d,p) basis set was converted from GAMESS US [26] to Molpro [24] format.

For scattering calculations, the excitation energies should lie below the ionisation potential of the molecule and the functions should not be too diffuse (see appendix A.1).

Scattering calculations were performed using the UK R-matrix codes (see chapter 6). For the SE and SEP calculations, Restricted Hartree-Fock (RHF) wavefunctions were used. The CC calculations used a CAS model (see chapter 6). In the case of phosphoric acid, C_1 symmetry was used and the active space consisting of 14 electrons distributed over 10 orbitals (see chapter 8.6). In the case of guanine, a planar, C_s symmetric, molecule was considered employing an active space consisting of 12 electrons distributed over 9 orbitals (see chapter 8.4). The scattering calculations with phosphoric acid were performed with an R-matrix radius $a = 15a_0$, the SE and SEP scattering models employed the 6-31G, cc-pVDZ, aug-cc-pVDZ, and cc-pVTZ basis sets, and the CC model with the aug-cc-pVDZ and cc-pVTZ basis sets (see chapter 8.6). The scattering calculations with guanine are currently being performed using $a = 13a_0$ and the cc-pVDZ basis set. Resonances were obtained using the program RESON and by analysis of the eigenphase sums and their derivatives.

Chapter 8

Results and Discussions

8.1 Uracil

Different theoretical [166–173] and experimental [174–180] investigations of uracil were aimed at obtaining insight into the physical, chemical and biological properties of the molecule. The most stable uracil tautomer is 2,4-dioxouracil [181–183] (see figure 8.1).

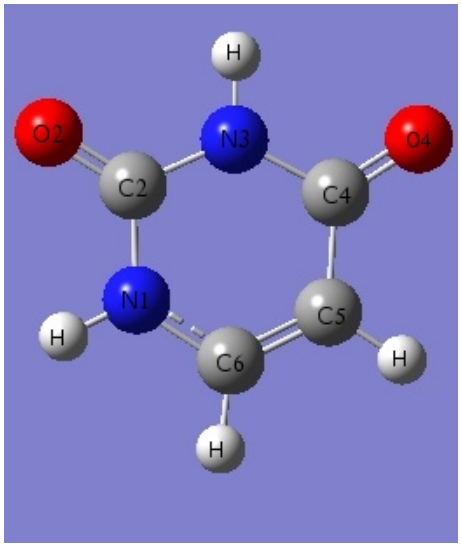

Figure 8.1: The structure of 2,4-dioxouracil (Gaussview 4.1.2 [25])

8.1.1 Methodology

The geometry of uracil, optimised with the MP2 method and the 6-31G* basis set, was taken from Ref. [19]. Uracil in its equilibrium geometry has C_s symmetry [65, 184].

The 58 electrons of uracil occupy 24 σ orbitals of symmetry A' and 5 π orbitals of symmetry A". The full π active space of uracil consists of 10 electrons distributed over 8 active MOs. Including a lone pair MO located on each oxygen yields 14 electrons distributed over 10 MOs in the active space. The biggest active space consisted of 14 electrons distributed over 16 active MOs.

The next step was performing MRCI calculations (see chapter 5.3), taking as starting point the CAS wavefunction. MRCI calculations using the MOLPRO 2006.1 computational package [24] are possible with the Pople and Davidson correction [185] and with two different options. The first one is with closed orbitals, which are doubly occupied in all CSFs and are correlated through single and double excitations, and the second one is with core orbitals, which are doubly occupied in all configurations and not correlated (see appendix A.3). The Pople and Davidson correction approximately correct the lack of size-extensively in MRCI. In this thesis we use the Davidson correction. The Davidson correction estimates the energy of configuration interaction up to quadruple excitations from the energy of configuration interaction up to double excitations.

The data about scattering calculations on uracil, performed by Dr Amar Dora are in appendix F.

8.1.2 CAS calculations

Several different active spaces were tested. The ground state energy, ground state dipole moment and the vertical excitation energies were taken into consideration. The choice of the active space, the number of calculated states and the basis sets have the main influence upon the results. An unbalanced choice of active orbitals leads to an unbalanced treatment of the excited states. For example, if the chosen active space consists of only π orbitals, the calculated spectrum contains only

$\pi \rightarrow \pi^*$ excited states. The addition of σ orbitals to the active space yields also $n \rightarrow \pi^*$ or $\pi \rightarrow \sigma^*$ excitations. Because the calculations were performed with the state-averaged CAS, a different choice of calculated states yields different values of the ground and excited state energies and dipole moments.

According to the Weyl-Robinson formula (see equation 5.1), increasing the number of active orbitals and electrons gives more configurations (CSFs). The triplet states have a larger number of configurations than the corresponding singlet states. For example, looking at table B.7 (see appendix B), for 14 electrons distributed over 10, 14 and 16 active orbitals the number of configurations is 2352, 1378080, and 13899270 for the singlet A' state, and 3458, 2504645, and 26544650 for the triplet A' state, respectively. The largest calculations were performed with five states and the active space consisting of 14 active electrons distributed over 16 orbitals using the 6-31G basis set (see appendix B.1, table B.7). These calculations took 40 days (CPU times 3189955.37 seconds).

The excited state energies

For scattering calculations, the excitation energies should lie below the ionisation potential of the molecule, which for the case of uracil is 9.3 eV [186–188].

In table 8.1 are compared the results obtained with 16 states and the 6-31G and cc-pVDZ basis sets. Here (a,b) means: a-number of electrons, b-number of orbitals in the active space. Columns **(12,9)** include the data from table B.2 (see appendix B.1.1), columns **(14,10)** from table 8.3 and columns **(14,11)** from table B.6 (see appendix B.1.3). A comparison of the calculations with the (12,9), (14,10) and (14,11) active spaces shows that larger active spaces lead to lower values of the ground state energy, and all 15 excited states calculated with the (14,10) and (14,11) active spaces have vertical excitation energies below the ionisation potential of uracil, 9.3 eV [187]. Because the results calculated with the (14,10) active space differ only slightly from the results calculated with the (14,11) active space, the (14,10) active space was chosen to generate the target orbitals for the scattering calculations.

Table 8.1: The CAS X^1A' ground state energy (in Hartree) and the vertical excitation energies (in eV) as a function of active space and basis set. The calculations were performed with 16 states.

	(12,9)		**(14,10)**		**(14,11)**	
	6-31G	*cc-pVDZ*	*6-31G*	*cc-pVDZ*	*6-31G*	*cc-pVDZ*
X^1A'	-412.34728	-412.55905	-412.350985	-412.563490	-412.361860	-412.574134
$2^1A'$	6.68	6.61	6.61	6.59	6.61	6.55
$3^1A'$	7.05	7.13	6.96	7.00	6.95	6.99
$4^1A'$	8.44	8.56	8.63	8.77	8.62	8.76
$1^1A''$	4.42	4.59	4.69	4.92	4.69	4.91
$2^1A''$	7.27	7.34	6.17	6.49	6.18	6.52
$3^1A''$	9.40	9.61	7.73	7.89	7.73	7.89
$4^1A''$	10.42	10.98	7.88	7.96	7.89	7.96
$1^3A'$	3.72	3.79	3.79	3.87	3.79	3.86
$2^3A'$	5.26	5.40	5.31	5.49	5.29	5.48
$3^3A'$	6.16	6.53	6.04	6.36	6.05	6.37
$4^3A'$	7.46	7.55	7.58	7.70	7.56	7.67
$1^3A''$	4.25	4.41	4.52	4.75	4.52	4.74
$2^3A''$	7.18	7.25	5.97	6.29	5.97	6.32
$3^3A''$	9.34	9.54	7.62	7.78	7.63	7.78
$4^3A''$	9.61	9.88	7.86	7.93	7.87	7.93

To investigate how the results depend on the number of states several comparisons were performed.

In the CAS calculations the energy average for all states under consideration was optimised. This yields a single set of compromise orbitals for all states. In table 8.2 are shown the ground state energy and the vertical excitation energies calculated with 32, 16 and five states, with the 6-31G and cc-pVDZ basis sets and with the active space consisting of 14 active electrons distributed over 10 orbitals (see also tables 8.3, B.4, and B.3). Because the excitation energies should lie below the ionisation energy of the molecule, 16-states calculations appear to be a good choice to obtain orbital sets for subsequent scattering calculations.

Table 8.2: The X^1A' ground state energy (in Hartree) and the vertical excitation energies (in eV) obtained with the (14,10) active space for singlet and triplet uracil depending on the number of calculated states. The orbital space consists of: closed 22,0; occupied 24,8.

	6-31G			**cc-pVDZ**		
	32 states	**16 states**	**5 states**	**32 states**	**16 states**	**5 states**
X^1A'	-412.34784	-412.35099	-412.35569	-412.56001	-412.56349	-412.56920
$2^1A'$	6.60	6.61		6.56	6.59	
$3^1A'$	6.92	6.96		6.96	7.00	
$4^1A'$	8.53	8.63		8.66	8.77	
$5^1A'$	8.97			9.13		
$6^1A'$	9.34			9.43		
$7^1A'$	10.08			10.23		
$8^1A'$	10.45			10.61		
$1^1A''$	4.61	4.69	4.39	4.84	4.92	4.65
$2^1A''$	6.03	6.17		6.35	6.49	

Continued on Next Page...

Table 8.2 – Continued

	6-31G			cc-pVDZ		
	32 states	**16 states**	**5 states**	**32 states**	**16 states**	**5 states**
$3^1A''$	7.62	7.73		7.78	7.89	
$4^1A''$	7.88	7.88		7.93	7.96	
$5^1A''$	9.74			9.99		
$6^1A''$	9.96			10.41		
$7^1A''$	10.38			10.96		
$8^1A''$	11.63			11.98		
$1^3A'$	3.75	3.79	3.76	3.82	3.87	3.83
$2^3A'$	5.25	5.31	5.42	5.42	5.49	5.56
$3^3A'$	5.93	6.04		6.24	6.36	
$4^3A'$	7.51	7.58		7.61	7.70	
$5^3A'$	8.57			8.53		
$6^3A'$	8.98			9.18		
$7^3A'$	9.15			9.23		
$8^3A'$	9.93			10.28		
$1^3A''$	4.44	4.52	4.20	4.67	4.75	4.47
$2^3A''$	5.84	5.97		6.17	6.29	
$3^3A''$	7.52	7.62		7.68	7.78	
$4^3A''$	7.86	7.86		7.91	7.93	
$5^3A''$	9.63			9.93		
$6^3A''$	9.70			10.01		
$7^3A''$	9.87			10.31		
$8^3A''$	10.01			10.46		

Table 8.3 shows the data obtained from the active space consisting of 14 electrons distributed over 10 orbitals. Winstead and McKoy [19], in their scattering calculations on uracil, employed the 6-311++G** and TZV(2d,p) basis sets. Therefore we also performed some CAS calculations with uracil using the same basis sets. The TZV(2d,p) basis set was employed in the subsequent R-matrix calculations, but only with the SE and SEP models [157]. The aug-cc-pVDZ, 6-31++G**, TZV(2d,p), and cc-pVTZ basis sets were too diffuse for scattering calculations on uracil with the CC model, therefore in the cc-pVDZ basis set was employed.

Looking at the values of the excitation energies, in the case of planar uracil, no big differences are observed between the excitation energies calculated using the basis sets with diffuse functions, and the excitation energies obtained with the 6-31G, 6-31G*, cc-pVDZ, and cc-pVTZ basis sets (see appendix B.1.2, table B.4).

Table 8.3: The X^1A' ground state energy (in Hartree) and the vertical excitation energies (in eV) for singlet and triplet uracil calculated with 16 states and the (14,10) active space. The orbital space consists of: closed 22,0; occupied 24,8.

State	**6-31G**	**cc-pVDZ**	**aug-cc-pVDZ**	**6-31++G****	**TZV(2d,p)**
X^1A'	-412.3510	-412.5635	-412.5851	-412.6354	-412.6656
$2^1A'$	6.61	6.59	6.46	6.53	6.50
$3^1A'$	6.96	7.00	6.94	6.96	6.95
$4^1A'$	8.63	8.77	8.62	8.65	8.65
$1^1A''$	4.69	4.92	4.92	4.89	4.92
$2^1A''$	6.17	6.49	6.47	6.44	6.48
$3^1A''$	7.73	7.89	7.87	7.86	7.87
$4^1A''$	7.88	7.96	7.90	7.93	7.93
$1^3A'$	3.79	3.87	3.84	3.83	3.84
$2^3A'$	5.31	5.49	5.48	5.46	5.48
$3^3A'$	6.04	6.36	6.34	6.31	6.35
$4^3A'$	7.58	7.70	7.62	7.66	7.65
$1^3A''$	4.52	4.75	4.76	4.73	4.75
$2^3A''$	5.97	6.29	6.28	6.25	6.29
$3^3A''$	7.62	7.78	7.76	7.75	7.76
$4^3A''$	7.86	7.93	7.87	7.90	7.90

The ground state energies

Inspection of table 8.4, which compares the values of the RHF and CAS ground state energy, shows that the larger basis sets yield lower ground state energies. Only the 16-states calculation with the active space consisting of 12 electrons distributed over 9 orbitals (see appendix B.1.1, table B.2) using the cc-pVDZ basis set gives a lower value of the ground state energy than the calculations which the aug-cc-pVDZ basis set. CAS should give a lower energy than RHF calculations because of the variation principle, and because RHF is the reference for CAS. Our results agree with this. We performed state-averaged (CAS) calculations and here also the number of considered states plays a role. Performing calculations with a smaller number of states yield a lower value of the ground state energy (see appendix B.1). Considering CAS calculations with the same number of states, it is observed that an increase of the active space gives lower values of the ground state energy.

Table 8.4: Comparison of the RHF, CAS and MRCI ground state energy (in Hartree) for different basis sets (see appendix B.1).

	States	**6-31G**	**6-31G***	**cc-pVDZ**	**aug-cc-pVDZ**	**cc-pVTZ**
				E^{RHF}		
		-412.2777	-412.4625	-412.5024	-412.5279	-412.6159
				E^{CAS}		
(12,9)	16	-412.3473	-412.5199	-412.5590	-412.5568	-412.6686
(12,9)	5	-412.3553	-412.5293	-412.5686	-412.5910	-412.6797
(14,10)	16	-412.3510	-412.5244	-412.5635	-412.5851	-412.6739
(14,10)	5	-412.3557	-412.5299	-412.5692	-412.5917	-412.6803
(14,11)	16	-412.3619	-412.5351	-412.5741	-412.5881	-412.6850
(14,11)	5	-412.3665	-412.5408	-412.5801	-412.6009	-412.6919
				E^{MRCI}		
(14,10)	16	-412.4785	-412.7227	-412.7666	-412.8061	-412.9154
$(14,10)^{D1}$	16	-412.4874	-412.7388	-412.7830	-412.82701	-412.9368

[1]Calculations with Davidson correction

The ground state dipole moments

The observed dipole moment for uracil using the microwave spectroscopic method is 3.87 D [189], while in a dioxane solution it is 4.16 D [179]. Because of the fact that our calculations were performed for gas phase molecule, 3.87 D is the best value for use as a reference. In table 8.5 are compared the RHF, CAS and MRCI ground state dipole moments. Considering the number of states, better results were obtained with five than with 16 states. The choice of the cc-pVDZ basis set gives the most accurate values of the ground state dipole moment. The gas-phase ground state dipole moment calculated with the 5-state calculations using the (12, 9) and (14,11) active space and the cc-pVDZ basis set (3.95 D) is nearest to the experimental value (3.87 D).

Table 8.5: Comparison of the RHF, CAS and MRCI ground state dipole moment, μ (in D), as a function of the active space (see tables in appendix B.1).

	States	**6-31G**	**6-31G***	**cc-pVDZ**	**aug-cc-pVDZ**	**cc-pVTZ**
				μ^{RHF}		
		5.35	5.02	4.93	5.09	5.02
				μ^{CAS}		
(12,9)	16	4.19	4.04	3.96	4.45	4.02
(12,9)	5	4.19	4.03	3.95	4.06	4.02
(14,10)	16	4.27	4.14	4.06	4.20	4.15
(14,10)	5	4.19	4.04	3.96	4.07	4.02
(14,11)	16	4.27	4.13	4.07	4.19	4.16
(14,11)	5	4.19	4.03	3.95	4.34	4.05
				μ^{MRCI}		
(14,10)	16	4.39	4.34	4.25	4.47	4.39
(14,10)^{D2}	16	4.43	4.29	4.19	4.37	4.28
				μ^{expt} [189]		
				3.87		

[2]Calculations with Davidson correction

8.1.3 MRCI calculations

MRCI calculations were performed and were compared with the CAS results. As the main direction of the project was performing CAS calculations to obtain orbitals for subsequent scattering calculations, MRCI calculations were performed only for uracil.

Table **8.6** shows the MRCI and its reference CAS ground state energy, the vertical excitation energies, the ground state dipole moment and real time of the calculations with the 6-31G and cc-pVDZ basis sets. Two options were considered, one with 24σ closed orbitals and the second one with 24σ core orbitals (see appendix A.3). Calculations with closed orbitals, which are more accurate, take longer time and yield a lower value of the ground state energy. In this case the active space included only π orbitals, which is why only $\pi \rightarrow \pi^*$ excitations resulted. As expected MRCI calculations with closed orbitals give lower singlet excited states than calculations with the core option, and both are lower in energy than their reference CAS energies. The first singlet excited state obtained with the 6-31G basis set has a higher energy (6.51, 6,18, 6.07 eV for CAS, $MRCI^{core}$, and $MRCI^{closed}$, respectively) than the state calculated with the cc-pVDZ basis set (6.49, 6,15, 6.07 eV for CAS, $MRCI^{core}$, and $MRCI^{closed}$, respectively). The next singlet excited states show lower values for the 6-31G basis set. However, for the triplet excited states, the lowest energies were obtained with core orbitals using the 6-31G basis set. The first three triplet excited energies obtained with the closed option using the 6-31G basis set are noticeably higher in energy than their reference CAS results.

In this case also, the CAS calculations yield lower values of the ground state dipole moment than the MRCI calculations.

Table 8.6: The MRCI X^1A' ground state energy (in Hartree), the vertical excitation energies (in eV), the ground state dipole moment μ (in D) and time of the calculations for singlet and triplet uracil. The orbital space consists of **closed or core** 24,0; occ 24,8.

	6-31G			**cc-pVDZ**		
	CAS^{Ref}	$MRCI^{core}$	$MRCI^{closed}$	CAS^{Ref}	$MRCI^{core}$	$MRCI^{closed}$
X^1A'	-412.35140	-412.40571	-412.97341	-412.56486	-412.66142	-413.49097
$2^1A'$	6.51	6.18	6.07	6.49	6.15	6.07
$3^1A'$	7.02	6.80	6.85	7.11	6.90	6.87
$4^1A'$	8.37	7.85	7.72	8.50	7.99	7.91
$1^3A'$	3.83	3.80	3.96	3.91	3.91	3.96
$2^3A'$	5.37	5.20	5.45	5.58	5.44	5.57
$3^3A'$	6.14	5.93	6.23	6.49	6.28	6.44
$4^3A'$	7.44	7.01	7.04	7.58	7.14	7.17
μ	4.28	4.39	4.41	4.06	4.22	4.13
time	21 [sec]	18[min]	33[day]	59 [sec]	59[min]	38[day]

Table 8.7 compares the CAS, MRCI and MRCI calculations with the Davidson correction using the 6-31G and cc-pVDZ basis sets. The Davidson correction of the MRCI method yields a noticeably lower value of the ground state energy (see table 8.4) and dipole moment (see table 8.5). The MRCI and CAS excitation energies calculated with the cc-pVDZ basis set are higher in value than the energies obtained with the 6-31G basis set. Using both basis sets, the first three singlet $\pi \rightarrow \pi^*$ excitations with the Davidson correction yield the most favourable values in comparison with experiment (see table 8.8), but they are still too high. Among these three methods, the CAS calculations yield the lowest and the MRCI calculations with the Davidson correction the highest value of the first singlet $n \rightarrow \pi^*$ and the first triplet $\pi \rightarrow \pi^*$ and $n \rightarrow \pi^*$ excitations. Comparing the MRCI excitation energies with other basis sets (see appendix B.2, tables B.8 and B.9), the lowest excitation energies of the first three singlet $\pi \rightarrow \pi^*$ excitations were obtained with the aug-cc-pVDZ basis set. For both MRCI and CAS calculations the first singlet excited state is $n \rightarrow \pi^*$, but the second singlet excited state for MRCI is $\pi \rightarrow \pi^*$, and for CAS is $n \rightarrow \pi^*$.

Table 8.7: Comparison of the ground (in Hartree) and the excitation energies (in eV) calculated with CAS and MRCI and MRCI with Davidson correction using the cc-pVDZ and 6-31G basis sets. The MRCI orbital space consists of core 22,0; occ 24,8. (The reference CAS calculations were done with 16 states and the (14,10) active space, see table B.4).

	CAS		**MRCI**		**MRCI^D**	
	cc-pVDZ	*6-31G*	*cc-pVDZ*	*6-31G*	*cc-pVDZ*	*6-31G*
X^1A'	-412.5635	-412.3510	-412.7666	-412.4785	-412.7830	-412.4874
$2^1A'$	6.59	6.61	6.18	6.17	6.05	6.06
$3^1A'$	7.00	6.96	6.84	6.72	6.75	6.63
$4^1A'$	8.77	8.63	8.01	7.76	7.76	7.52
$1^1A''$	4.92	4.69	5.24	4.97	5.28	5.01
$2^1A''$	6.49	6.17	6.76	6.44	6.79	6.48
$3^1A''$	7.89	7.73	7.92	7.69	7.97	7.66
$4^1A''$	7.96	7.88	7.83	7.74	7.86	7.70
$1^3A'$	3.87	3.79	3.96	3.86	3.97	3.87
$2^3A'$	5.49	5.31	5.56	5.33	5.55	5.32
$3^3A'$	6.36	6.04	6.44	6.10	6.43	6.09
$4^3A'$	7.70	7.58	7.24	7.06	7.10	6.93
$1^3A''$	4.75	4.52	5.04	4.77	5.09	4.81
$2^3A''$	6.29	5.97	6.54	6.21	6.57	6.24
$3^3A''$	7.78	7.62	7.83	7.62	7.81	7.59
$4^3A''$	7.93	7.86	7.80	7.72	7.73	7.67

8.1.4 Comparison with experiment and different calculations

The excited states of uracil have been studied theoretically previously with ab initio methods ranging from configuration interaction with single excitation (CIS) [190–192] to highly correlated Multireference Perturbation (CASPT2) methods [73, 193, 194], MRCI methods and density functional approaches for excited states [195–198]. The first circular dichroism (CD) spectrum was recorded by Miles et al. [199], who interpreted the first four transitions in uridine and thymidine as $\pi \rightarrow \pi^*$ and related them to the benzene spectrum. It is generally agreed that the first band corresponds to a $\pi \rightarrow \pi^*$ transition. Most authors agree with Miles et al. that the second state has the same character. Sprecher and Johnson [200] suggest, however, that an $n \rightarrow \pi^*$ transition might be responsible for this feature in the spectrum. Novros and Clark [201] observed a small out-of-plane component in the polarised absorption spectrum of 1-methyl-uracil crystals at 4.7 eV, which might point in the same direction. Such an assignment would locate the $n \rightarrow \pi^*$ transition at ca. 5 eV.
Our CAS calculations showed that the first singlet excitation is $n \rightarrow \pi^*$, which for the active space consisting of 14 electrons distributed over 10 orbitals, depending on the basis set, ranges from 4.69 to 4.93 eV (see tables 8.3 and B.4), which gives quite good agreement with the values obtained by Novros and Clark. Also gas-phase spectra were reported [202, 203]. Unfortunately, these appear to be broad as well with an overall shape similar to those in solution, albeit further blue-shifted: the long-wavelength absorption band is found at 244 nm (ca. 41 000 cm^{-1} or 5.08 eV) with a weak shoulder at 205 nm (ca. 48 800 cm^{-1} or 6.05 eV), and the short-wavelength band appears at 187 nm (ca. 53 500 cm^{-1} or 6.63 eV). These values have been interpreted as vertical $\pi \rightarrow \pi^*$ excitation energies. Our first singlet $\pi \rightarrow \pi^*$ vertical excitation energy for each of the active spaces and basis sets under consideration lies above 6 eV (see tables B.2, 8.3, B.4, and B.6), which constitutes a noticeable difference with experiment. The main aim of our CAS calculations was to use the CAS orbitals for UK R-matrix calculations. We considered only state-averaged calculations and selected an active space that gives singlet and triplet $n \rightarrow \pi^*$ and $\pi \rightarrow \pi^*$

excitations below the ionisation energy of uracil. Also because of limitations of the R-matrix programs we could not use the aug-cc-pVDZ and cc-pVTZ basis sets and active spaces larger than (14,10). The discrepancies between our results and experiment are probably due to these restrictions. The closest to the experimental ground state dipole moment was obtained with the cc-pVDZ basis set. The SE and SEP calculations were performed with several basis sets, while for the more advanced CC model, the cc-pVDZ basis set with the (14,10) active space was employed [157].
Table 8.8 compares the MRCI and CAS excitation energies of uracil to experimental data and to the calculations with different methods like CASPT2 and Time Dependent Density Functional Theory (TDDFT) [198].
Noticeable differences between the MRCI and CAS $\pi \rightarrow \pi^*$ excitation energies and the experimental data are observed. Methods like TDDFT give lower values of the excitation energy, which are closer to those obtained by experiment.
The CASPT2 and TDDFT calculations show that the first singlet excitation state is $n \rightarrow \pi^*$ and the second $\pi \rightarrow \pi^*$, the first triplet excitation state is $\pi \rightarrow \pi^*$, and the second $n \rightarrow \pi^*$, which is in close accordance with the MRCI and CAS calculations (using the aug-cc-pVDZ basis set, see table 8.3). The results differ depending on the basis set and the active space.
We could not use basis sets as large as aug-cc-pVDZ or cc-pVTZ, or active spaces bigger than the (14,10) active space. Thus we selected the (14,10) active space and the cc-pVDZ basis set for use in the R-matrix calculations. Because we aimed to obtain only energies below the ionisation potential of the molecule, the 16-states calculations were chosen.

Table 8.8: Comparison of the CAS and MRCI excitation energies (eV) with experimental data and with calculations using the CASPT2 and TDDFT methods.

	CAS	**MRCI**	**CASPT2**	**TDDFT**	**Expt Range**
	t. 8.3	t. B.8	[73]	[198]	[200, 202, 204–214]
	cc-pVDZ	cc-pVDZ	ANO	cc-pVDZ	
$2^1A'$	6.59	6.18	5.00	5.27	4.6-5.1
$3^1A'$	7.00	6.84	5.81	5.92	5.8-6.1
$4^1A'$	8.77	8.01	6.46	7.28	6.3-6.6
$1^1A''$	4.92	5.24	4.54	4.63	at ca. 5
$2^1A''$	6.49	6.76	6.00	6.60	
$3^1A''$	7.89	7.92	6.37	5.76	
$4^1A''$	7.96	7.83	6.95	6.19	
$1^3A'$	3.87	3.96		3.42	
$2^3A'$	5.49	5.56		4.71	
$3^3A'$	6.36	6.44		5.44	
$4^3A'$	7.70	7.24		5.92	
$1^3A''$	4.75	5.04		4.23	
$2^3A''$	6.29	6.54		5.49	
$3^3A''$	7.78	7.83		6.43	
$4^3A''$	7.93	7.80		6.00	

8.1.5 Conclusions

Considering only $n \rightarrow \pi^*$ and $\pi \rightarrow \pi^*$ transitions, calculations with three active spaces were considered, the active space consisting of 12 electrons distributed over 9 orbitals (see appendix B.1.1, table B.2), the active space consisting of 14 electrons distributed over 10 orbitals (see appendix B.1.2 and table 8.3) and the active space consisting of 14 electrons distributed over 11 orbitals (see appendix B.1.3, table B.6). Comparing the calculations with the (12,9), (14,10) and (14,11) active spaces shows that the larger active space leads to a lower value of the ground state energy, and all 15 excited states calculated with the (14,10) and (14,11) active space have vertical excitation energies below the ionisation potential of uracil, 9.35 ± 0.01 eV [187]. As the results calculated with the (14,10) active space differ only slightly from the results calculated with the (14,11) active space, the (14,10) active space was chosen to generate the target orbitals for the scattering calculations. CAS calculations with the (12,9) active space using the cc-pVDZ basis set yield a dipole moment that is closest to the experimental value of 3.87 D [19]. An only slightly higher value of the ground state dipole moment (4.06 D) was obtained with the (14,10) active space using the same basis set, therefore the cc-pVDZ basis set was chosen for subsequent R-matrix calculations. MRCI calculations were also performed. The reference CAS calculations were done with 16 states and the (14,10) active space (see appendix B.1.2 and table 8.3). The first three singlet $\pi \rightarrow \pi^*$ excitations obtained with our MRCI calculations yield more favourable values in comparison with experiment than the CAS calculations, but they are still too high (see table 8.8).

8.2 Cytosine

Cytosine and uracil are RNA pyrimidine bases (in DNA thymine replaces uracil, see chapter 2). The 1H-2-keto 4-amino form of cytosine was considered [215–219].
Tonzani and Greene [23] found three shape resonances for cytosine: a very sharp one at 1.7 eV (0.5 eV wide), a second one at 4.3 eV (0.7 eV wide), and the third at 8.1 eV (0.8 eV wide). The electron-molecule collision calculations performed by Winstead and McKoy [21] for cytosine resulted in resonances at 0.5, 2.4, and 6.3 eV. Experimental temporary anion states of cytosine obtained by Aflatooni et al. [2] are at 0.32, 1.53 and 4.50 eV.

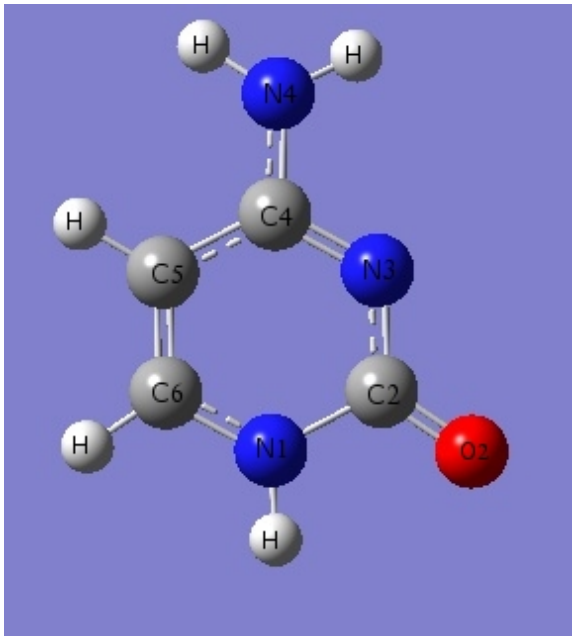

Figure 8.2: The structure of 1H-2-keto 4-amino cytosine (Gaussview 4.1.2)

8.2.1 Methodology

The geometry of 1H-2-keto 4-amino cytosine was obtained from optimisation employing the B3LYP method [220–223] and the 6-31+G* basis set.
Two types of symmetry were considered, planar, C_s and nonplanar, C_1 symmetry. Planar cytosine is a transition state and the optimised nonplanar molecule possesses

slightly lower energy (-394.949754 Hartree) than its planar counterpart (-394.949726 Hartree).

The 58 electrons of cytosine occupy 24 σ orbitals of symmetry A' and 5 π orbitals of symmetry A". Like for uracil, the full π active space of cytosine consists of 10 electrons distributed over 8 active MOs, and we therefore used the same active space as was used for the scattering calculations on uracil (see section 8.1.1). In the nonplanar molecule 58 electrons occupy 29 orbitals, and the full active space includes 37 orbitals.

The ionisation potential of cytosine is 8.68 eV [187].

8.2.2 CAS calculations

Tables 8.10 and 8.9 compare the CAS ground state energy, the ground state dipole moment and the vertical excitation energies for planar and nonplanar 1H-2-keto 4-amino cytosine respectively, calculated with 16 states and with the active space consisting of 14 electrons distributed over 10 orbitals, (14,10). For the nonplanar molecule the CI calculations with the cc-pVDZ basis set were not converged and were therefore not included in table 8.9. In table 8.10 are also presented the excitation energies obtained by experiment and from calculations with different methods. The first singlet excitation has $\pi \rightarrow \pi^*$ character. The exception is the result obtained using the 6-31G basis set, where the first singlet excitation is $n \rightarrow \pi^*$ (see table 8.10). These results are different to those of uracil where the first singlet excited state is $n \rightarrow \pi^*$ (see table 8.3). The first two triplet excited states are of type $\pi \rightarrow \pi^*$. Here also, the character of the excitations is noticeably different from the case of uracil, where the first triplet excited state is $\pi \rightarrow \pi^*$, but the second triplet excited state is $n \rightarrow \pi^*$ (see table 8.3).

Considering the calculations with the nonplanar molecule (see table 8.9), using the 6-31G basis set the first three singlet excitations are noticeably lower in value than the excitation energies calculated with the other basis sets. However, considering higher excited singlet states, the lowest values were obtained using the aug-cc-pVDZ basis set (see section 8.7). For example the 7th state calculated with the aug-cc-pVDZ basis set has the value 6.33 eV; using any of the other basis sets the same

state remains constantly above 7 eV.

The absorption spectra of an aqueous solution of cytosine show broad peaks near 4.66 and 6.29 eV and weak peaks or shoulders near 5.39 and 5.85 eV [224–232]. In general, the absorption spectrum of cytosine is solvent dependent [224, 227]. Compared to the first absorption peak of cytosine near 4.66 eV, the corresponding peak of cytidine and 3-methylcytosine is found to be near 4.57 eV and 4.29 eV, respectively, in aqueous solution [226, 230, 231]. However, our CAS calculations showed that the first excitation has $\pi \rightarrow \pi^*$ character and is higher in value (excluding the calculations with the 6-31G basis set) which, depending on the basis set, ranges from 4.97 to 5.05 eV. There is significant experimental and theoretical evidence for the existence of an $n \rightarrow \pi^*$ transition near 5.3 eV in cytosine [233]. Obtained from our calculations, the first $n \rightarrow \pi^*$ transition ranges from 4.88 to 5.23 eV. The one nearest to the experimental value is the $n \rightarrow \pi^*$ excitation calculated using the cc-pVDZ basis set (5.23 eV). Zaloudek et al. [229] have suggested the existence of another $n \rightarrow \pi^*$ transition near 5.6 eV. Our second $n \rightarrow \pi^*$ transition ranges from 5.14 to 5.51 eV. Here also the $n \rightarrow \pi^*$ excitation calculated using the cc-pVDZ basis set (5.51 eV) is the nearest to the experimental value.

Recent, high-level CR-EOM-CCSD(T) (Completely Renormalised Equation of Motion Coupled Cluster method with singles, doubles and noniterative triples [234,235]) calculations predict the $\pi \rightarrow \pi^*$ and $n \rightarrow \pi^*$ states to have vertical excitation energies of 4.76 and 5.24 eV [236] respectively. A hybrid MM approach using ab initio MRCI with double excitations (MRCI2/MM) calculations give 5.14, 5.29 and 5.93 eV for the $\pi \rightarrow \pi^*$ and two $n \rightarrow \pi^*$ excitations, respectively [237]. Considering our calculations, the nearest to the first CR-EOM-CCSD(T) $\pi \rightarrow \pi^*$ excitation was obtained with the 6-31G basis set, 4.90 eV. The $\pi \rightarrow \pi^*$ MRCI2/MM excitation is higher in value (5.14 eV) than ours, which ranges from 4.90 to 5.05 eV. The first $n \rightarrow \pi^*$ CR-EOM-CCSD(T) energy (5.24 eV) is in good agreement with our excitation energy calculated using the cc-pVDZ basis set (5.23 eV). MRCI2/MM gives the nearest to the experimental value (5.3 eV [233]) of the first $n \rightarrow \pi^*$ excitation energy, 5.29 eV. The second $n \rightarrow \pi^*$ MRCI/MM transition (5.93 eV) is higher in value than the experimental one (5.6 eV [229]) and our results, which range, depending on the

basis set, from 5.14 to 5.51 eV (see table 8.10).

Thus the character of the first excitations of cytosine is different than that of uracil, and our CAS calculations are in quite good agreement with the experimental data. We compared the results to some of the most recent results obtained with the CR-EOM-CCSD(T) [236] and MRCI2/MM [237] methods, but the excited states of cytosine have also been studied theoretically previously with a variety of ab initio methods [238–249].

As for uracil and the other DNA bases, the excited-state calculations were performed to provide orbitals for subsequent R-matrix calculations. The next section provides recommendations for the choice of active space and basis set for scattering calculations on cytosine.

Table 8.9: The X^1A' ground state energy (in Hartree), the vertical excitation energies (in eV) and the ground state dipole moment, μ (in D) for nonplanar cytosine calculated with 16 states and the (14,10) active space.

State	**6-31G**	**6-31G***	**aug-cc-pVDZ**	**cc-pVTZ**
E^{RHF}	-392.433675	-392.609032	-392.676288	-392.757498
X^1A	-392.499958	-392.665608	-392.696576	-392.781885
2^1A	4.85	5.02	5.01	5.04
3^1A	4.90	5.22	5.10	5.42
4^1A	5.12	5.51	5.32	6.04
5^1A	5.94	6.16	5.81	6.21
6^1A	6.28	6.39	5.89	6.56
7^1A	7.59	7.95	6.33	7.15
8^1A	8.01	8.15	6.83	7.33
1^3A	3.47	3.63	3.94	3.84
2^3A	4.60	4.76	4.98	5.36
3^3A	4.69	5.07	5.24	5.61
4^3A	4.93	5.31	5.52	5.86
5^3A	5.33	5.54	5.67	5.87
6^3A	5.85	6.06	5.78	6.02
7^3A	6.94	7.06	5.84	6.44
8^3A	7.59	7.86	6.16	7.14
μ^{RHF}	7.89	7.30	7.27	7.21
μ^{CAS}	6.54	6.25	6.90	6.97

Table 8.10: The X^1A' ground state energy (in Hartree), the vertical excitation energies (in eV) and ground state dipole moment, μ (in D) for planar cytosine calculated with 16 states and the (14,10) active space. The orbital space consists of: closed 22,0; occupied 24,8.

State	**6-31G**	**6-31G***	**cc-pVDZ**	**aug-cc-pVDZ**	**cc-pVTZ**
E^{RHF}	-392.434955	-392.608958	-392.649332	-392.676271	-392.757484
X^1A'	-392.500747	-392.664478	-392.703927	-392.726912	-392.808984
$2^1A'$	4.90	5.05	5.04	4.97	5.02
$3^1A'$	6.27	6.36	6.34	6.26	6.32
$4^1A'$	7.98	8.12	8.15	7.97	8.09
$1^1A''$	4.88	5.22	5.23	5.18	5.21
$2^1A''$	5.14	5.49	5.51	5.46	5.49
$3^1A''$	5.94	6.17	6.13	6.11	6.13
$4^1A''$	7.59	7.88	7.84	7.75	7.80
$1^3A'$	3.49	3.63	3.63	3.59	3.62
$2^3A'$	4.60	4.74	4.75	4.70	4.74
$3^3A'$	5.33	5.55	5.56	5.53	5.57
$4^3A'$	6.94	7.07	7.06	7.00	7.05
$1^3A''$	4.72	5.06	5.06	5.02	5.04
$2^3A''$	4.95	5.30	5.33	5.28	5.32
$3^3A''$	5.85	6.07	6.02	6.02	6.03
$4^3A''$	7.60	7.87	7.84	7.74	7.79
μ^{RHF}	7.94	7.36	7.17	7.33	7.28
μ^{CAS}	6.59	6.34	6.18	6.27	6.26
μ^{expt}	**6.02** [250]				

Continued on Next Page...

Table 8.10 – Continued

	Expt [224–232]	**Ref. [234, 235]**	**Ref. [237]**
$2^1A'$	4.66	4.76	5.14
$3^1A'$	6.29		
$2^1A''$	5.39	5.24	5.29
$3^1A''$	5.85		5.93

8.2.3 Recommendations for R-matrix calculations

Electronically, cytosine is like uracil and the same (14,10) active space is recommended for the subsequent R-matrix calculations with the close-coupling model. At first the calculations will be performed with planar cytosine, but the symmetry of the molecule (how nonplanarity influences the results) could also be a point of interest for the scattering calculations.

The lowest ground state dipole moment, which is nearest to the experimental value (6.02 D) [250], was obtained with the cc-pVDZ basis set, 6.18 D (see table 8.10 and see table 8.1.2 in chapter 8.1). However, for nonplanar cytosine the ground state dipole moment is higher in value and, depending on the basis set, ranges from 6.25 to 6.97 D. As for the other DNA bases, the aug-cc-pVDZ and cc-pVTZ basis sets are too large for calculations with the close-coupling R-matrix model on cytosine and also here the cc-pVDZ basis is recommended for the scattering calculations.

8.3 Thymine

Thymine is also known as 5-methyl uracil and is a pyrimidine nucleobase in DNA [251] (see figure 8.3). In double stranded DNA, thymine pairs with adenine.

The excited states of thymine have been studied theoretically previously with a variety of ab initio methods [68, 73, 191, 196, 252]. For example Lorentzon et al. [73] computed, using the CASPT2 method, $\pi \rightarrow \pi^*$ transition energies for thymine of 4.9, 5.9, 6.1 and 7.1 (7.0) eV. $n \rightarrow \pi^*$ energies were calculated to be 4.4, 5.9, 6.1 and 6.7 eV, respectively.

Some shape resonances for thymine were found by Tonzani and Greene [23] and Winstead and McKoy [21]. Tonzani and Greene [23] found resonances at 2.4 eV (0.2 eV wide), at 5.5 eV (0.6 eV wide), and at 5.5 eV (1 eV wide). Winstead and McKoy [21] found the resonances for thymine at 0.3, 1.9, and 5.7 eV. Those are closer to the experimental resonances obtained by Aflatooni et al. [253] at values 0.29, 1.71 and 4.05 eV. Here also, as in the case of the other DNA bases, further calculations could be performed to obtain core-excited and Feshbach resonances.

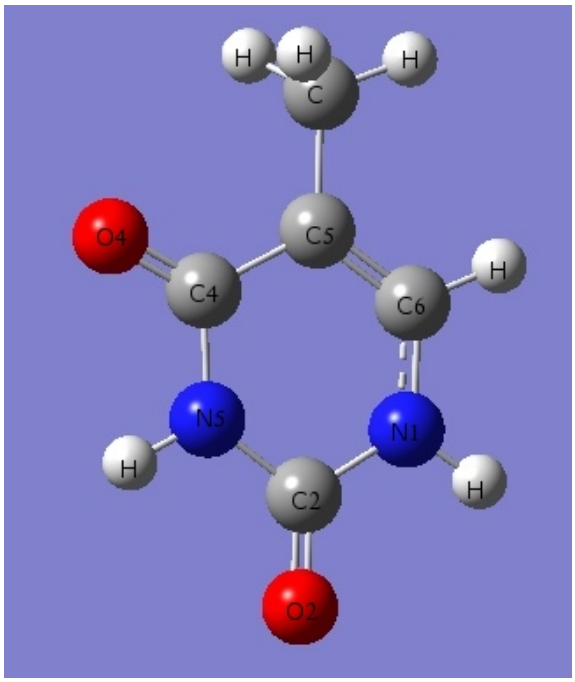

Figure 8.3: The structure of thymine (Gaussview 4.1.2)

8.3.1 Methodology

The geometry of thymine was obtained from optimisation employing the B3LYP method and the 6-31+G* basis set.

Because of the presence of the methyl group thymine is a nonplanar, C_1 symmetric molecule. The energy of the optimised structure is -454.158107 Hartree and the dipole moment is 4.62 D. The 66 electrons of thymine occupy 33 orbitals and the full valence active space includes 42 orbitals. The CAS calculations were performed with the active space consisting of 10 electrons distributed over 10 orbitals, (10,10), and 14 electrons distributed over 10 orbitals, (14,10).

The ionisation potential of thymine is 8.87 eV [187].

8.3.2 CAS calculations

Table 8.11 compares the results obtained with the active space consisting of 10 electrons distributed over 10 orbitals, (10,10), and table 8.12 contains the results from the calculations with the active space consisting of 14 electrons distributed over 10 orbitals, (14,10). In all calculations seven states, with the excitation energies below the ionisation energy of thymine, were calculated. In table 8.12 are also presented experimental excitation energies and results obtained using three different methods (Coupled Cluster Singles and Doubles (CCSD), CAS, and CASPT2).

Lorentzon et al. [73] mentioned that the excitation energies are similar for uracil and thymine. Table 8.12 also lists our excitation energies of uracil obtained using the (14,10) active space and the cc-pVDZ basis set (see table 8.3) and the CAS excitation energies of thymine calculated by Lorentzon et al. [73] with an atomic natural orbital (ANO) type basis set. Lorentzon et al. [73] performed calculations with 10 π active electrons and with an increasing number of active π orbitals, and the four lowest $n \rightarrow \pi^*$ transitions ($^1A''$) were computed with an active space including eight π and two σ orbitals. It is observed that the CAS excitation energies do not differ too much for both molecules.

The calculations using the CCSD [252], CAS and CASPT2 [73] methods for uracil and thymine show that the first singlet excitation is of type $n \rightarrow \pi^*$, and the next two excitations obtained with the CAS method have $n \rightarrow \pi^*$ and $\pi \rightarrow \pi^*$ character, respectively. The second and third singlet excitation energy obtained with the CASPT2 method are of type $\pi \rightarrow \pi^*$. The CCSD method shows the second singlet excitation of $\pi \rightarrow \pi^*$ and the third of $n \rightarrow \pi^*$ type. The experimental data give smaller values and a different character of the singlet excitation energies than the calculations. According to the Circular Dichroism spectra of thymidine [225, 254–257], the first singlet excitation has $\pi \rightarrow \pi^*$ character. Similarly, Polarised Reflection Spectra of single crystals of thymine show $\pi \rightarrow \pi^*$ excitations at values of 4.5 and 5.8 eV [208, 258].

Considering these methods the nearest to the experimental data are the excitation energies obtained with CASPT2. Multiconfigurational second-order perturbation approach is one of the most advanced methods using as the starting point a CAS wavefunction [35].

Differences between the excitation energies calculated with the smaller, (14,10) and bigger (10,10) active space are observed. Both active spaces give excitation energies below the ionisation potential of thymine, but the first singlet excitations obtained with the (14,10) active space are lower in value than those obtained with the (10,10) active space. An exception are the results calculated using the aug-cc-pVDZ basis set, where the first singlet excitation energy computed with the (14,10) active space is higher (5.40 eV) than the energy calculated with the (10,10) active space (5.12 eV). The first singlet excitation energies calculated using the 6-31G* (4.68 eV) and cc-pVDZ (4.69 eV) basis set and the (14,10) active space are near the first singlet $\pi \rightarrow \pi^*$ excitations obtained by Circular Dichroism spectroscopy of thymidine (4.5-4.7 eV) [225, 254–257].

Considering the results calculated with the bigger, (10,10), active space, it is observed that the lowest values of the singlet excitation energies were obtained using the aug-cc-pVDZ basis set (see table 8.11). Here the first excitation energies range from 5.13-5.50 eV, in good agreement with the $n \rightarrow \pi^*$ experimental excitation, 4.9-5.2 eV [225, 254–257].

Table 8.11: The X^1A' ground state energy (in Hartree) and the vertical excitation energies (in eV) and the ground state dipole moment, μ (in D) for singlet and triplet thymine calculated with seven states and the (10,10) active space.

State	**6-31G**	**6-31G***	**cc-pVDZ**	**aug-cc-pVDZ**	**cc-pVTZ**
E^{RHF}	-451.301740	-451.502141	-451.545221	-451.571174	-451.668257
X^1A	-451.422186	-451.613279	-451.635643	-451.637590	-451.757320
CSFs	19404				
2^1A	5.13	5.36	5.50	5.12	5.50
3^1A	7.34	7.78	7.01	6.12	6.94
4^1A	7.76	7.79	7.47	6.92	7.03
CSFs	29700				
1^3A	3.85	3.90	3.88	3.73	3.84
2^3A	4.90	5.13	5.27	5.06	5.28
3^3A	5.81	6.03	6.16	6.03	6.18
μ^{RHF}	5.19	4.82	4.74	4.91	4.83
μ^{CAS}	4.23	4.00	4.08	4.77	4.20

Table 8.12: The X^1A' ground state energy (in Hartree) and the vertical excitation energies (in eV) and the ground state dipole moment, μ (in D) for singlet and triplet thymine calculated with seven states and the (14,10) active space. Data for uracil obtained using the (14,10) active space and the cc-pVDZ basis set (see table 8.3) are also included.

State	**6-31G**	**6-31G***	**cc-pVDZ**	**aug-cc-pVDZ**	**cc-pVTZ**
E^{RHF}	-451.301740	-451.502141	-451.545221	-451.571174	-451.668257
CSFs	4950				
X^1A	-451.372959	-451.569928	-451.612257	-451.577622	-451.732563
2^1A	5.02	4.68	4.69	5.40	4.80
3^1A	6.28	7.23	7.19	6.35	6.90
4^1A	7.33	7.48	7.45	7.23	7.26
CSFs	6930				
1^3A	4.83	3.76	3.75	3.74	3.81
2^3A	5.04	4.56	4.56	5.33	4.60
3^3A	5.99	5.76	5.77	6.24	5.58
μ^{RHF}	5.19	4.82	4.74	4.91	4.83
μ^{CAS}	3.97	4.33	4.26	4.69	4.08
μ^{expt}	**4.51** [250]				

	CCSD [252]	**t. B.4**	**CAS [73]**	**CASPT2 [73]**	**Expt. [225, 254–257]**
$2^1A'$	5.60	6.59	6.75	4.88	4.5-4.7
$3^1A'$	6.78	7.00	7.15	5.88	5.8-6.0
$4^1A'$	7.05	8.77	8.33	6.10	6-3-6.6

Continued on Next Page...

Table 8.12 – Continued

	CCSD [252]	**t. B.4**	**CAS [73]**	**CASPT2 [73]**	**Expt. [225, 254–257]**
$1^1A''$	5.14	4.92	5.22	4.39	4.9-5.2
$2^1A''$	6.57	6.49	6.77	5.91	
$3^1A''$	7.67	7.89	8.14	6.15	

8.3.3 Recommendations for R-matrix calculations

Calculations with two different active spaces were performed for nonplanar thymine. The CAS excited state calculations were designed to yield orbitals that can be used for the R-matrix close-coupling model. This limited the active spaces and basis sets that can be used. This is also the reason that the results differ somewhat from the experimental data. Based on previous calculations on phosphoric acid, which is electronically smaller than thymine (see chapter 8.6), the (10,10) active space is probably too large for scattering calculations on thymine. Therefore at first the (14,10) active space is recommended. Excluding the aug-cc-pVDZ and cc-pVTZ basis sets which are probably too diffuse for R-matrix calculations on thymine, the nearest to the experimental dipole moment (4.51 D) [250] was obtained with the (14,10) active space using the 6-31G* basis set. Calculations with the cc-pVDZ basis set give a slightly smaller value of the ground state dipole moment and very similar excitation energies to those obtained with the 6-31G* basis set. In the case of thymine, as for the other DNA and RNA bases, the cc-pVDZ basis set is recommended as a starting point for scattering calculations.

8.4 Guanine

Guanine can exist in different tautomeric forms, depending on its environment [68, 259–261, 261–266]. The most stable one is the keto-N7H tautomer [259] (see figure 8.4).

The excited states of guanine have been studied theoretically previously with a variety of ab initio methods [260, 261, 266–271, 271–276].

Tonzani and Greene [23] performed scattering calculations on keto-N9H guanine and they found four resonances: at 2.4 eV (0.2 eV wide), at 3.8 eV (0.25 eV wide), a third at 4.8 eV (0.35 eV wide), one at 8.9 eV (0.6 eV wide), and a broad resonance around 12 eV. Winstead and McKoy [21, 277] found three low-energy resonances for guanine, associated with temporary trapping of the projectile electron in a vacant π^* molecular orbital, at energies 1.55, 3.8, and 4.8 eV. Aflatooni et al. [2] employed low-energy electron transmission spectroscopy (EPS) [278] to observe the formation of temporary π^* anion states. They found resonances for guanine (enol tautomer) at 0.46, 1.37 and 2.36 eV.

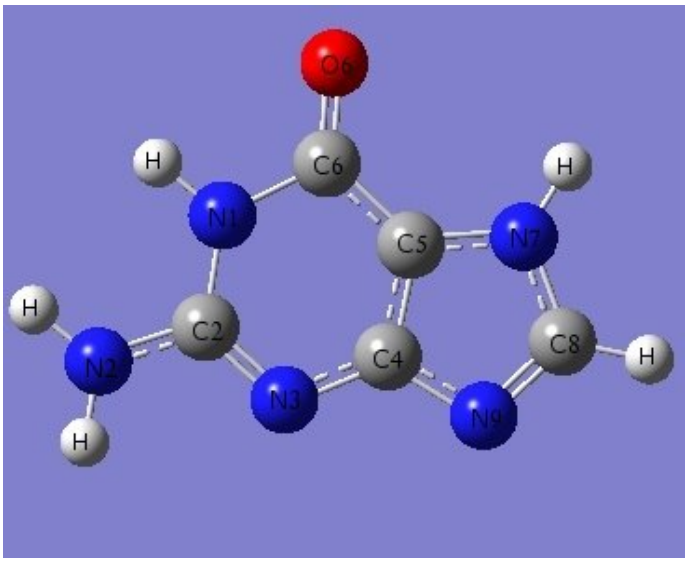

Figure 8.4: The structure of keto-N7H guanine (Gaussview 4.1.2)

8.4.1 Methodology

The geometry of keto-N7H and keto-N9H guanine was obtained from optimisation employing the B3LYP method and the 6-31+G* basis set.

Two types of symmetry of keto-N7H guanine were considered, planar with C_s and nonplanar with C_1 symmetry. The planar structure is a transition state. The optimised nonplanar molecule possesses a lower energy and dipole moment (-542.577446 Hartree, 1.80 D) than its planar counterpart (-542.576074 Hartree, 2.22 D).

In the planar structure the 78 electrons of guanine occupy 32 σ orbitals of symmetry A' and 7 π orbitals of symmetry A". The full π active space of guanine consists of 14 electrons distributed over 11 active MOs. In the nonplanar molecule 78 electrons occupy 39 orbitals, and the full valence space includes 49 orbitals. The experimental value of the ionisation potential of guanine is 7.77 eV [279].

R-matrix calculations are currently performed with planar keto-N7H guanine and the cc-pVDZ basis set, using an R-matrix box of radius $a = 13a_0$ and 15 virtual orbitals.

8.4.2 CAS calculations

Several active spaces were considered, but guanine is a relatively big molecule (78 electrons), and some difficulties with the R-matrix calculations occurred. In tables C.1, C.2 (see appendix C) are presented the calculations for planar and nonplanar guanine using the active space consisting of 16 electrons distributed over 12 orbitals, (16,12), with 16 states. This active space is too big for the R-matrix calculations, but includes all π orbitals. Table C.1 shows calculations performed with 16 states which result in the first three singlet $\pi \rightarrow \pi^*$ excitations below 7.5 eV, but the third and fourth singlet $n \rightarrow \pi^*$ excitations are above 9 eV. An exception is the third excitation energy obtained using the aug-cc-pVDZ basis set, which is 8.44 eV. The 16-states calculations with the nonplanar molecule (see table C.2) show all seven singlet states below 8 eV.

Table 8.13 shows the results that are currently being used in scattering calculations, obtained with the active space consisting of 12 (4σ, 6π) electrons distributed

over 9 orbitals, (12,9), and compares them to the experimental data obtained by Clark in crystalline 9-ethylguanine [280], and to one of the most recent calculations preformed by Kowalski et al. [275] CR-EOMCCSD(T), in conjunction with the combined quantum mechanical (QM/MM) molecular mechanics approach. In table 8.14 are presented the results calculated with the nonplanar molecule, using the same active space. All seven excitation energies lie below 7 eV for both planar and nonplanar guanine.

Experimentally the existence of $n \rightarrow \pi^*$ transitions near 5.21, 6.32, and 7.08 eV, and $\pi \rightarrow \pi^*$ transitions near 4.46, 5.08, 6.20 and 6.57 eV in crystalline 9-ethylguanine has been suggested by Clark [280] (see table 8.13). According to the reassigned Resonant Two Photon Ionisation (R2PI) spectra [281–283], the first excitation of the enol-N9H-trans, keto-N7H-imino-cis, keto-N7H-imino, and enol-N7H tautomeric forms [260] has $\pi \rightarrow \pi^*$ character and its value is at 4.31, 4.20, 4.12, and 4.07 eV, respectively. It could be suggested that the first $\pi \rightarrow \pi^*$ excitation of keto-N7H guanine should also lie below 5 eV, but our calculations, both for planar and nonplanar guanine, show the first singlet $\pi \rightarrow \pi^*$ excitations above 5 eV.

The CR-EOM-CCSD(T) calculations of guanine in the DNA environment (12-mer fragment of B-DNA) [275] show the first $\pi \rightarrow \pi^*$ excitation of guanine at 5.05 eV, and the first $n \rightarrow \pi^*$ excitation at 5.70 eV (see table 8.13).

The first singlet excitation in 9-ethylguanine suggested by Clark [280] and the first excitations from Kowalski et al. [275] have $\pi \rightarrow \pi^*$ character. Our calculations with the (16,12) active space agree with this (see table C.1). The calculations with the (12,9) active space predict the first singlet excitation to be of $n \rightarrow \pi^*$ character (see table 8.13). The first $n \rightarrow \pi^*$ excitation calculated with the (12,9) active space and eight states ranges from 4.96 to 5.27 eV. The value calculated with the aug-cc-pVDZ basis set, 5.23 eV, is nearest to the experimental data, 5.21 eV, obtained by Clark [280] (see table 8.13). However, the first $n \rightarrow \pi^*$ excitation obtained with the (16,12) active space is higher in energy and ranges from 6.24 to 6.55 eV (see table C.1).

The experimental ground state dipole moment for keto-N9H guanine is 6.02 D [250]. The dipole moment obtained from our B3LYP/6-31+G* optimisation is 7.10 D for

planar keto-N9H guanine, and nearer to the experimental value, 6.80 D, for the nonplanar molecule. Keto-N7H guanine has a lower value of the ground state dipole moment, and as in the case of keto-N9H guanine, the dipole moment of the optimised B3LYP/6-31+G* structure is higher for the planar (2.22 D) than for the nonplanar (1.80 D) molecule. Our value of the ground state dipole moment, calculated with the planar keto-N7H guanine, ranges from 2.60 to 3.00 D with eight-states calculations and the (12,9) active space (see table 8.13), and from 1.91 to 2.75 D with 16-states calculations and the (16,12) active space (see table C.1). CAS calculations also show that the ground state dipole moment of the nonplanar molecule has a lower value than that of planar guanine and ranges from 1.32 to 2.46 D with eight-states calculations and the (12,9) active space (see table 8.14) and from 1.64 to 2.34 with 16-states calculations and the (16,12) active space (see table C.2).

Table 8.13: The ground X^1A' state total energy (in Hartree), the vertical excitation energies (in eV) and the ground state dipole moment, μ (in D) for planar keto-N7H guanine calculated with eight states and the (12,9) active space. The orbital space consists of: closed 30,3; occupied 32,10.

State	**6-31G**	**6-31G***	**cc-pVDZ**	**aug-cc-pVDZ**	**cc-pVTZ**
E^{RHF}	-539.132044	-539.383391	-539.437628	-539.473107	-539.580966
CSFs	1316				
X^1A'	-539.197916	-539.440893	-539.494558	-539.527593	-539.636097
$2^1A'$	6.09	6.12	6.09	5.97	6.02
$3^1A'$	6.96	6.98	6.99	6.85	6.93
CSFs	1204				
$1^1A''$	4.96	5.25	5.27	5.23	5.27
CSFs	1680				
$1^3A'$	3.62	3.68	3.68	3.60	3.63
$2^3A'$	5.41	5.55	5.56	5.51	5.53
$3^3A'$	6.08	6.26	6.29	6.27	6.30
CSFs	1722				
$1^3A''$	4.81	5.09	5.11	5.09	5.12
μ^{RHF}	2.14	2.09	2.10	1.95	2.03
μ^{CAS}	3.00	2.75	2.74	2.60	2.68

Continued on Next Page...

Table 8.13 – Continued

	Expt. [280]	**Ref. [275]**
$2^1A'$	4.46	5.05
$3^1A'$	5.08	
$4^1A'$	6.20	
$1^1A''$	5.21	5.70
$2^1A''$	6.32	
$3^1A''$	7.08	

Table 8.14: The ground X^1A state total energy (in Hartree), the vertical excitation energies (in eV) and the ground state dipole moment, μ (in D) for nonplanar keto-N7H guanine calculated with eight states and the (12,9) active space.

State	**6-31G**	**6-31G***	**cc-pVDZ**	**aug-cc-pVDZ**	**cc-pVTZ**
E^{RHF}	-539.127964	-539.384838	-539.439430	-539.474278	-539.582042
CSFs	2520				
X^1A	-539.190771	-539.440590	-539.494479	-539.511243	-539.644369
2^1A	5.04	5.35	5.37	5.46	6.08
3^1A	5.90	5.99	5.99	6.06	6.62
4^1A	6.63	7.12	7.16	6.95	7.81
CSFs	3402				
1^3A	3.90	3.97	3.99	3.78	3.89
2^3A	4.83	4.94	4.97	5.40	5.18
3^3A	4.87	5.18	5.20	5.57	5.71
4^3A	6.22	6.34	6.36	6.66	7.09
μ^{RHF}	1.93	1.74	1.70	1.58	1.62
μ^{CAS}	2.46	1.94	1.85	1.78	1.32

8.4.3 Recommendations for R-matrix calculations

The character of particular excitations obtained with the (16,12) active space agree with the experimental results, but the excitation energies are noticeably higher (see table C.1). This active space was too big for R-matrix calculations and a smaller active space, consisting of 12 electrons distributed over 9 orbitals, was used in the scattering calculations.

R-matrix calculations are generally performed for molecules with some symmetry, and problems occurred with nonplanar guanine (which has C_1 symmetry). Therefore we considered only the planar molecule. This is adequate as guanine is planar in base pairs.

We could not use the aug-cc-pVDZ and cc-pVTZ basis sets in the scattering calculations on guanine, because in the case of guanine these basis sets are too large.

In the R-matrix calculations with uracil [157], the choice of the virtual orbitals had noticeable influence upon the results. A larger number of virtual orbitals gave more favourable results. Therefore our scattering calculations on guanine are being performed with at least 15 virtual orbitals. However, considering our excitation energies obtained with eight states and the (12,9) active space (see table 8.13), it is observed that the results calculated using the 6-31G* and cc-pVDZ basis sets only slightly differ, and they are nearest to the experimental data [280]. As cc-pVDZ basis set was chosen for the final calculations with uracil [157], therefore we also chose this basis set for the scattering calculations on guanine.

We are performing R-matrix calculations with only the most stable tautomer of guanine, but it could be also an interesting point to see how the resonances change using different isomers and active spaces.

.

8.5 Adenine

N9H-adenine is predicted to be the most stable tautomer [181,218,251,284–286] and we therefore performed calculations for this tautomer.

The excited states of adenine have been studied theoretically previously with a variety of ab initio methods [196, 252, 264, 276, 287].

The shape π resonances of adenine were found theoretically by Tonzani and Greene [23] and Winstead and McKoy [21], and experimentally by Aflatooni et al. [253]. According to Tonzani and Greene [23], the first resonance for adenine occurs at 2.4 eV (0.2 eV wide), the second at 3.2 eV (sharp and 0.2 eV wide), then another centred at 4.4 eV (0.3 eV wide), while at 9 eV they obtained a broader resonance at 0.5 eV in width. Winstead and McKoy [21] found the resonances for adenine at 1.1, 1.8 and 4.1 eV, which are closer to the experimental data obtained by Aflatooni et al. [253] (0.54, 1.36 and 2.17 eV) than the resonances calculated by Tonzani and Greene [23].

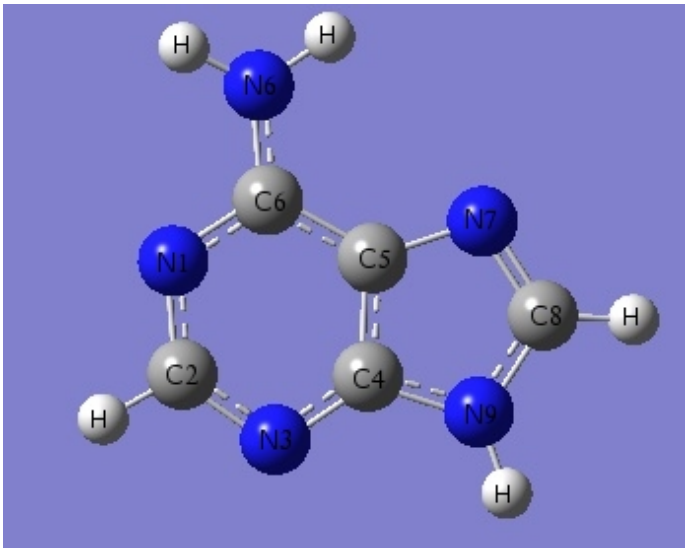

Figure 8.5: The structure of adenine-N9H (Gaussview 4.1.2)

8.5.1 Methodology

The geometry of adenine-N9H was obtained from optimisation employing the B3LYP method and the 6-31+G* basis set.

Two types of symmetry were considered, planar, C_s and nonplanar, C_1 symmetry. As in the case of guanine and cytosine, planar adenine is a transition state. The optimised nonplanar molecule possesses slightly lower energy, but a larger dipole moment (-467.339875 Hartree, 2.50 D) than its planar counterpart (-467.339857 Hartree, 2.46 D).

The 70 electrons of adenine occupy 29 σ orbitals of symmetry A' and 6 π orbitals of symmetry A". The full π active space of adenine consists of 12 electrons distributed over 10 active MOs (see section 8.1.1). In the nonplanar molecule 70 electrons occupy 35 orbitals, and the full active space includes 45 orbitals.

The experimental ionisation potential of adenine is 8.55 ± 0.10 eV [187, 288].

8.5.2 CAS calculations

Adenine is a smaller molecule than guanine and contains eight electrons fewer. In table 8.15 are compared the results for planar adenine obtained with the active space consisting of 12 electrons distributed over 9 orbitals, (12,9), to the experimental data and to the values calculated with different methods.

Table 8.16 shows the CAS ground state total energy, the vertical excitation energies and the ground state dipole moment obtained with eight states for the nonplanar molecule. However as in the case of the previous DNA bases, the scattering calculations will first be performed on the planar molecule, which is more adequate to model adenine in a DNA base pair [31].

In the case of adenine calculations with the bigger (16,12) active space were performed with 16 states. Looking at the tables D.1 and D.2 it is observed that all calculated 15 excited states lie below the ionisation potential of adenine. Thus, the CAS calculations that will yield the orbitals for use in R-matrix calculations can probably include more than eight states.

Recently several high-level spectroscopic investigations were performed to study the

$\pi \rightarrow \pi^*$ and $n \rightarrow \pi^*$ transitions of adenine. Based on the Resonance Enhanced Multiphoton Ionisation (REMPI) and fluorescence spectroscopy investigations of supersonic jet-cooled adenine, Kim et al. [289] have suggested that the first transition of adenine has $n \rightarrow \pi^*$ and the second has $\pi \rightarrow \pi^*$ character; they are located at 4.40 eV and 4.48 eV, respectively. However, Luhrs et al. [290] do not support the assignment of the $n \rightarrow \pi^*$ transition suggested by Kim et al. [289], based on a similar study of adenine and 9-methyladenine (9MA). According to their investigation the spectral origin of the first $\pi \rightarrow \pi^*$ transition of adenine and 9MA is located at 4.48 eV and these results agree with the observation made by Kim et al. [289]. Nir et al. [291] have found similar results based on R2PI investigation of laser desorbed adenine.

However, all our first singlet $\pi \rightarrow \pi^*$ excitations, both for the planar and nonplanar molecule, lie above 5 eV. Calculations with both active spaces also show the first singlet excitation of type $\pi \rightarrow \pi^*$ (see tables 8.15 and D.1). An exception are the calculations with the (12,9) active space using the 6-31G basis set, where the first excitation is $n \rightarrow \pi^*$.

Clark has tentatively assigned the existence of $n \rightarrow \pi^*$ transitions near 5.08 and 6.08 eV in the crystal of 2'-deoxyadenosine [292] and the existence of $\pi \rightarrow \pi^*$ transitions near 4.51, 4.68, and 5.82 eV in crystal 9-methyladenine [293]. The existence of an $n \rightarrow \pi^*$ transition near 5.38 eV was also revealed in a stretched polymer film of 9-methyladenine [294].

The first singlet $n \rightarrow \pi^*$ transition from our calculations lies above 5.5 eV. The second singlet $n \rightarrow \pi^*$ transition ranges, depending on the basis set, from 6.09 to 6.40 eV (see table D.1). The second $n \rightarrow \pi^*$ excitation calculated using the 6-31G basis set is the nearest to the experimental data obtained by Clark (6.08 eV) [292]. Our $\pi \rightarrow \pi^*$ excitations obtained with the (16,12) and (12,9) active spaces are higher in value than the excitation energies calculated with TDDFT [196] and CASPT2 [276] (using ANO-type basis sets, the (10,10) active space for $\pi \rightarrow \pi^*$, and the (12,11) active space for $n \rightarrow \pi^*$ excitations, see table 8.15).

These two methods result in quite similar values of the $\pi \rightarrow \pi^*$ excitation energies, but still higher than the experimental data [289, 293]. The TDDFT $n \rightarrow \pi^*$ [196]

and CASPT2 $\pi \rightarrow \pi^*$ [276] values of the excitation energies are nearest to the experimental data [292, 293].
As in the cytosine chapter: 'The next section' provides recommendation for R-matrix calculations on adenine.

Table 8.15: The ground X^1A' state total energy (in Hartree), the vertical excitation energies (in eV) and the ground state dipole moment, μ (in D) for planar adenine-N9H calculated with eight states and the (12,9) active space. The orbital space consists of: closed 27,2; occupied 29,9.

State	**6-31G**	**6-31G***	**cc-pVDZ**	**aug-cc-pVDZ**	**cc-pVTZ**
E^{RHF}	-464.292106	-464.513393	-464.558845	-464.586147	-464.676974
CSFs	1316				
X^1A'	-464.359613	-464.575105	-464.619731	-464.645350	-464.736700
$2^1A'$	6.22	6.33	6.31	6.26	6.29
$3^1A'$	7.77	7.14	7.10	6.99	7.03
CSFs	1204				
$1^1A''$	5.79	6.41	6.37	6.36	6.36
CSFs	1680				
$1^3A'$	4.20	4.42	4.41	4.34	4.37
$2^3A'$	5.46	5.45	5.45	5.42	5.42
$3^3A'$	6.02	5.81	5.80	5.75	5.78
CSFs	1722				
$1^3A''$	5.56	6.07	6.04	6.03	6.03

Continued on Next Page...

Table 8.15 – Continued

State	**6-31G**	**6-31G***	**cc-pVDZ**	**aug-cc-pVDZ**	**cc-pVTZ**
μ^{RHF}	2.62	2.47	2.41	2.46	2.44
μ^{CAS}	2.77	2.44	2.40	2.43	2.42
$\mu^{expt.}$	**2.27** [250, 295]				

	Expt. [289]	**Expt. [293]**	**Expt. [292]**	**CASPT2 [276]**	**TDDFT [196]**
$2^1A'$	4.48	4.51		5.13	5.27
$3^1A'$		4.68		5.20	5.00
$4^1A'$		5.82		6.24	6.32
$1^1A''$			5.08	6.15	4.97
$2^1A''$			6.08	6.86	5.61
$3^1A''$					

Table 8.16: The ground X^1A' state total energy (in Hartree), the vertical excitation energies (in eV) and the ground state dipole moment, μ (in D) for nonplanar adenine-N9H calculated with eight states and the (12,9) active space.

State	**6-31G**	**6-31G***	**cc-pVDZ**	**aug-cc-pVDZ**	**cc-pVTZ**
E^{RHF}	-464.291272	-464.513490	-464.559023	-464.586227	-464.677060
CSFs	2520				
X^1A	-464.357089	-464.573759	-464.618761	-464.621287	-464.734502
2^1A	6.09	6.04	6.11	5.34	5.36
3^1A	6.35	6.75	6.19	6.47	5.89
4^1A	6.60	7.15	7.11	7.12	6.34
CSFs	3402				
1^3A	4.17	4.24	4.22	5.10	4.14
2^3A	5.52	5.62	5.64	5.32	5.26
3^3A	5.97	5.88	5.90	5.39	5.58
4^3A	5.98	6.15	6.04	6.41	5.60
μ^{RHF}	2.70	2.53	2.46	2.51	2.49
μ^{CAS}	2.56	2.45	2.52	2.66	2.75

8.5.3 Recommendations for R-matrix calculations

As a start point scattering calculations will be performed on planar adenine. The same (12,9) active space as used for guanine is recommended. Looking at the 16-states calculations using the (16,12) active space (see table D.1), it is observed that all calculated states lie below the ionisation energy of the molecule. The calculations that will yield the orbitals for use in R-matrix calculations can probably include more than eight states. Here also an interesting point could be the investigation how the number of calculated states affects the scattering results, a result that was observed in the case of phosphoric acid (see chapter 8.6).

Based on the previous scattering calculations on the other DNA bases, the (16,12) active space and basis sets such as aug-cc-pVDZ and cc-pVTZ could be too large for R-matrix calculations on adenine.

CAS calculations performed on uracil using the cc-pVDZ basis set give a dipole moment nearest to the experimental value (see chapter 8.1 and table 8.5). Also in the case of planar adenine the dipole moment that was the closest to the experimental value (2.27 D) was obtained using the (12,9) active space with the cc-pVDZ basis set (2.40 D). Therefore, for scattering calculations on adenine this basis set is recommended.

8.6 Phosphoric Acid

It has been suggested that electron attachment to the phosphate group also contributes to DNA strands breaks.

Simons' group [13–15] showed that electrons of ca. 1.0 eV can attach to a base to form a π^* anion, which then can break a 3' or 5' O-C σ bond connecting the phosphate to either of two sugar groups. Li et al. [296] performed calculations on a sugar-phosphate-sugar model system using the Own n-layered integrated MO and MM method (ONIOM) (using B3LYP/6-31+G* as the high level and Austin Model 1, AM1, as the low level) and found that the activation barrier for bond rupture of the anion's phosphate-sugar C-O bond is only 0.5 eV, indicating that very-low-energy electrons can induce DNA strand breaks. Berdys at al. [14, 15] found that near 0 eV electrons may not easily attach directly (i. e. vertically) to the phosphate units, but can produce a metastable $P = O$ π^* anion above 2 eV.

Pan et al. [94, 95] in linear and supercoiled DNA observed desorption of H^- as the result of temporary capture of electrons by the bases, with a small contribution from a core-excited resonance on the sugar group, OH^- desorption by the localisation of electrons on the protonated form of the phosphate group, and production of O^- via the temporary localisation of electrons on the π^* double bond of the phosphate group. Pan and Sanche [93] measured dissociative-electron attachment (DEA) to the monosodium salt of phosphoric acid, NaH_2PO_4, in the condensed phase, confirming DNA damage can be induced by low-energy electrons. A single broad peak whose maximum fell at 8.8, 8.0, 7.3 eV, depending on whether the anion detected was H^-, O^-, or OH^-, was observed. König et al. [297] measured DEA spectra for the dibuthyl and triethyl phosphate ester, and observed a variety of anionic fragments. Using dibuthyl phosphate [298] they found that the compound undergoes effective dissociative electron attachment within a low-energy resonant feature at 1 eV and a further resonance peaking at 8 eV. The DEA reactions are associated with the direct cleavage of the C-O and the P-O bond but also the excision of the PO^-, PO_3^- and $H_2PO_3^-$ units. They propose that the most direct mechanism of single strand breaks occurring in DNA is due to DEA directly to the phosphate group.

To investigate the role of the phosphate group in breaking of DNA, scattering calculations were performed for phosphoric acid. In the case of phosphoric acid there are only few experimental and theoretical data to compare with.
Limited experimental information on the resonances in the molecules related to the phosphate group in DNA are available from dissociative electron-attachment and electron-transmission measurements. Aflatooni et al. [299], in their DEA study of trimethyl phosphate (TMP), observed a peak at 7.4 eV which was assigned to a core-excited resonance. Recent electron-transmission measurements by Burrow et al. [300] indicated resonances at 2.1 and 4.6 eV in the TMP total scattering cross section, which were assigned as shape resonances associated with low-lying valence orbitals. Recently scattering calculations for phosphoric acid were performed by Tonzani and Greene [22] and Winstead and McKoy [20]. Tonzani and Greene [22] found two resonances, one at 7.7 eV and the other at 12.5 eV, with respective widths of 2.0 and 1.5 eV, whereas four resonances at 5.00, 7.00, 8.5, and 10 eV were observed by Winstead and McKoy.

8.6.1 Methodology

The three hydroxyl groups can be in up or down position with respect to the P=O group. Starting structures were created by taking into account all possible combinations of the positions of the hydroxyl groups. These were optimised with tight convergence and the B3LYP method and the 6-31+G* basis set. Three stationary points were found: the first one with C_1 symmetry and two hydrogen up and one hydrogen down (uud) (see figure 8.6), the second one with C_3 symmetry and three hydrogens up (uuu) (see figure 8.6) and one transition state with one imaginary frequency and C_{3v} symmetry and three hydrogen down (ddd) (see figure 8.7). Our structures are similar to those obtained by Yekutiel et al. [301].

R-matrix scattering calculations were performed with the SE, SEP and CC models. The CC model used CAS orbitals, obtained with an active space consisting of 14 electrons distributed over 10 orbitals. At first calculations with five states were considered, but better scattering results were obtained using as the input ten-states

CAS orbitals.

The scattering calculations were performed with a box of radius a=15a_o. Calculations with a=10a_o gave unphysical eigenphase sums, while calculations with a=13a_o appeared physically correct but gave resonance structures that disappeared when a was increased. The R-matrix codes are more familiar with symmetry molecules, what is the reason that for bigger, but planar molecue as guanine the calculations with a box of radius a=13a_o are enough to give correct results (see section 8.4.1).

At first the SE and SEP models employed the 6-31G, cc-pVDZ and aug-cc-pVDZ basis sets, whereas the CC calculations used the aug-cc-pVDZ basis set. However, the aug-cc-pVDZ basis set was fount to be too diffuse for R-matrix calculations and was replaced with the cc-pVTZ basis set (see tables and figures in appendix E.2). GTO continuum basis sets were used which followed the prescription of Faure et al. [302]. Because the representation of low-lying resonances depends on the virtual orbitals [19, 157], to get converged results it was necessary to retain at least 15 virtual orbitals. The cross sections of molecules with large dipole moments become very large at low scattering energies and low scattering angles. These cross sections are difficult to determine experimentally and require special treatment theoretically [303], therefore the Born correction was applied. Those were done by Dr Amar Dora using the program POLYDCS [205]. The automatic resonance detection program RESON [304] and visual inspection of the eigenphase sums were used for identification of any possible resonances.

Because phosphoric acid belongs to the nonabelian symmetry point group C_3, the electronic excited state calculations were carried out using C_1 symmetry.

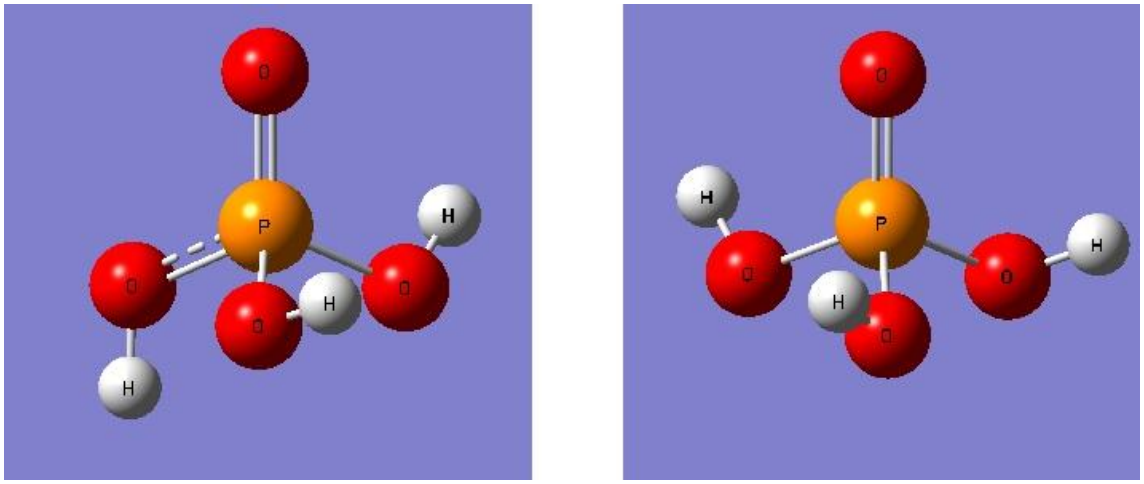

Figure 8.6: The structure of uud and uuu conformers of phosphoric acid (B3LYP/6-31+G*, Gaussview 4.1.2)

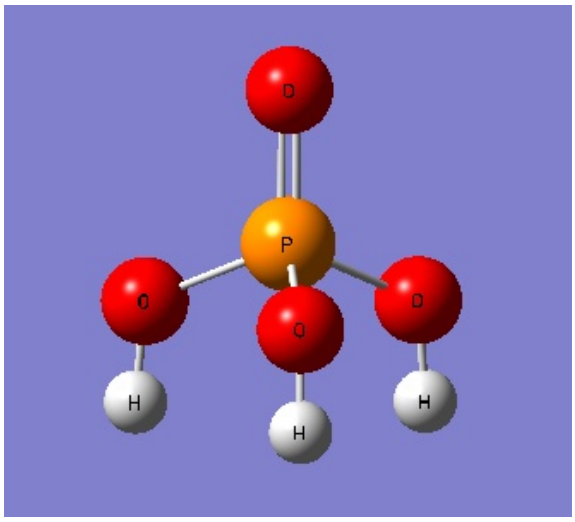

Figure 8.7: The structure of (ddd) transition state of phosphoric acid (B3LYP/6-31+G*, Gaussview 4.1.2)

8.6.2 CAS Calculations

At first the R-matrix calculations with the close-coupling model were performed with the aug-cc-pVDZ basis set (see appendix E). Tables E.1 and E.2 compare the ground state energy, the vertical excitation energies, and the ground state dipole moment of the two conformers of phosphoric acid calculated using the 6-31G, cc-pVDZ and aug-cc-pVDZ basis sets, and the active space consisting of 14 electrons distributed over 10 orbitals, (14,10) (see table E.1), and 10 electrons distributed over 10 orbitals, (10,10) (see table E.2). Looking at the tables it is observed that excitation energies calculated with the aug-cc-pVDZ basis set are noticeably lower than those obtained with the other basis sets. The calculations with the bigger active space (see table E.2) involve a larger number of CSFs and this active space appeared to be too large for scattering calculations.

As the aug-cc-pVDZ basis set was found to be too diffuse for R-matrix calculations, it was replaced with the cc-pVTZ basis set. In table 8.17 are presented the CAS ground state energy, the vertical excitation energies and the ground state dipole moment of the two conformers of phosphoric acid calculated using the 6-31G, cc-pVDZ and cc-pVTZ basis sets, and the excitation energies obtained by Yekutiel et al. [301] using the EOM-CCSD method and the aug-cc-pV(T+d)Z basis set [305] for the C_3 symmetric conformer of phosphoric acid.

Several models were tested and it was observed that the number of calculated states affects the scattering results, and the orbitals obtained from ten-states calculations with the (14,10) active space and the cc-pVTZ basis set were employed in the close-coupling model.

The B3LYP/6-31+G* optimised uuu conformer possesses a lower ground state energy (-644.15495 Hartree) and dipole moment (0.19 D) than uud (-644.15388 Hartree, 3.38 D, respectively). Our five-states CAS calculations with the B3LYP/6-31+G* optimised structure, the (14,10) active space and the 6-31G and cc-pVDZ basis sets give the lower value of the ground state energy for uud (see table E.1). The same calculations with ten states show lower ground state energies for the uud conformer with all employed basis sets (see table 8.17). However, one-state calculations

using the cc-pVDZ and cc-pVTZ basis sets yield higher ground state energies for uud than for uuu. In our state-averaged CAS calculations the orbitals were optimised for an average of 10 states, and these calculations therefore do not yield accurate ground state energies. The B3LYP and one-state CAS calculations therefore likely give the correct energetic preference of the two phosphoric acid conformers. DFT generally gives lower energies than frozen-core ab initio calculations, because DFT correlates all electrons.

There are not many experimental or theoretical excitation energies to compare with, but the calculations with the cc-pVTZ basis set give the lowest excitation energies, and using this basis set uud has noticeably higher excitation energies than uuu.

There have been limited theoretical and experimental investigations of the electronic spectroscopy of H_3PO_4. Vapour-phase electronic absorption spectra of phosphoric acid were reported by Ali [306] and show a diffuse band at 5.1 eV. In 1965, Helmann and Platzer [307] recorded electronic absorption spectra of aqueous solution of phosphoric acid and the dominant features in their spectra were attributed to the dihydrogen phosphate ion $H_2PO_4^-$, with an absorption around 6.5-6.8 eV. These absorption bands are significantly lower in energy than our lowest calculated state using the cc-pVTZ basis set, but closer to the lowest excited state obtained with the aug-cc-pVDZ basis set (see tables E.1 and E.2). The excitation energies obtained by Yekutiel et al. [301] with the C_3 symmetric conformer are in quite good agreement with our results for the C_3 symmetric conformer using the cc-pVTZ basis set.

Table 8.17: The X^1A' ground state energy (in Hartree), the vertical excitation energies (in eV) and the ground state dipole moment (in D) of uuu and uud conformers of phosphoric acid calculated with ten states and the (14,10) active space.

State	**uuu**			**uud**			
	6-31G	**cc-pVDZ**	**cc-pVTZ**	**6-31G**	**cc-pVDZ**	**cc-pVTZ**	Ref. [301]
E^{RHF}	-641.7064	-642.0409	-642.0869	-641.7045	-642.0424	-642.0887	
			One state				
X^1A	-641.8113	-642.1473	-642.1945	-641.8134	-642.1460	-642.1930	
			Ten states				
X^1A	-641.7501	-642.0731	-642.2133	-641.7524	-642.0742	-642.2275	
2^1A	8.75	9.13	7.82	8.63	9.10	8.35	7.78
3^1A	8.81	9.17	7.87	8.69	9.15	8.42	8.74
4^1A	10.04	10.31	9.22	9.77	10.19	9.70	8.89
5^1A	10.24	10.50	9.53	10.29	10.66	10.20	9.04
1^3A	8.01	8.51	7.46	7.86	8.43	7.84	
2^3A	8.05	8.54	7.51	7.98	8.55	7.96	
3^3A	9.30	9.52	8.76	9.25	9.55	9.17	
4^3A	9.76	10.02	9.05	9.58	9.97	9.50	
5^3A	9.85	10.11	9.63	10.09	10.34	10.01	
μ^{RHF}	3.83	3.54	3.62	0.72	0.26	0.58	
μ^{CAS}	1.35	0.39	0.35	3.31	2.96	3.08	

8.6.3 R-matrix Calculations

Resonances

Figure 8.8 presents the eigenphase sums as a function of scattering model for the target calculation with the cc-pVTZ basis set. Inspection of the plots shows a resonance in the region above 7 eV. For the uuu conformer the CC calculations result in Feshbach resonances at 7.21, 7.27, 7.85 and 7.87 eV, and for the uud conformer at 7.74 and 7.88 eV. In appendix E.2 are shown the plots obtained from scattering calculations with the aug-cc-pVDZ basis set, but this basis set was found to be too diffuse for R-matrix calculations (see figures E.1, E.2, E.3, E.4). The SE and SEP calculations using the 6-31G, cc-pVDZ and cc-pVTZ basis sets, and all three models with the aug-cc-pVDZ basis set, were performed by Lilianna Bryjko, only the CC calculation using the cc-pVTZ basis set was done by Dr Amar Dora (see appendix F).

In table 8.18 are presented the resonances obtained by the SE, SEP, and CC models using the 6-31G, cc-pVDZ, cc-pVTZ and aug-cc-pVDZ basis sets. Table 8.18 shows that the predicted position of the resonances varies little between the two conformers. The position of uuu and uud conformer obtained with the cc-pVDZ and cc-pVTZ basis set is quite similar, but big differences in the scattering results are observed with the aug-cc-pVDZ basis set. The shape resonances obtained with the cc-pVTZ basis set are higher in energy than the resonances calculated with the 6-31G basis set. Also the appropriate shape resonances of uud are a little higher than those of conformer uuu.

Some of the SEP calculations show rather narrow, higher-energy resonances, which were not found in the SE calculations. Such resonances are better characterised by CC calculations, which in our case were performed with the cc-pVTZ basis set. Our scattering calculations result in very narrow Feshbach resonances. For the uuu conformer the lowest-two quasi-degenerate resonances at 7.21 and 7.27 eV are associated with the two quasi-degenerate triplet excited states at 7.46 an 7.51 eV, and the next two quasi-degenerate resonances at 7.85 and 7.87 eV are associated with the two quasi-degenerate singlet excited states at 7.82 and 7.87 eV. The two uud

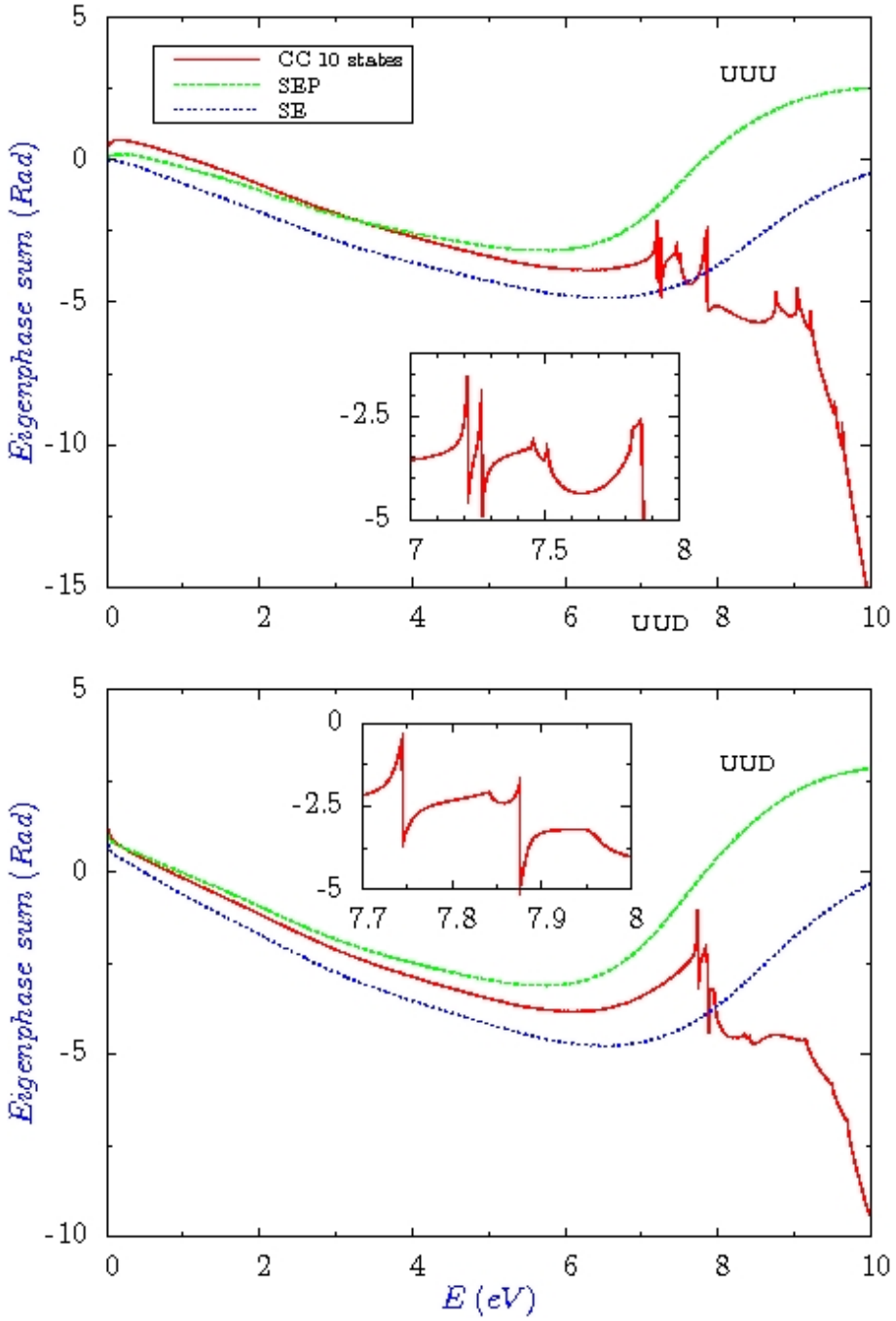

Figure 8.8: Eigenphase sums for electron scattering from phosphoric acid: upper panel uuu conformer, lower panel uud conformer. The SE and SEP calculations were performed by Lilianna Bryjko, and calculations with the CC model by Dr Amar Dora.

resonances at 7.74 an 7.88 eV can be associated with the two lowest triplet states at 7.84 and 7.96 eV. Resonances associated with singlet excited states were not found for the uud conformer. The reason for this could be that those resonances have become unbound or RESON did not find them. Previous studies identified broad resonances, as found for both our conformers, in the 6 to 9 eV region. Tonzani and Greene [22] found a resonance at 7.70 eV with a width of about 2.0 eV. Winstead and McKoy [20] identified broad resonances directly from peaks in the integral cross section and found the resonances at about 8.5 eV for the SE model and at about 7 eV for the SEP model, in good agreement with our results obtained with the cc-pVDZ and cc-pVTZ basis sets.

Table 8.18: Positions and widths (eV) of the resonances for phosphoric acid calculated with the SE and SEP and contracted CC model with the R-matrix box a=15a_0 using 15 virtual orbitals.

uuu			uud		
SE	SEP	CC	SE	SEP	CC
		6-31G			
6.90 (1.12)	5.71 (0.81)		7.07 (1.52)	5.75 (1.07)	
		cc-pVDZ			
8.59 (1.63)	7.31 (1.11)		8.71 (1.77)	7.39 (1.26)	
		cc-pVTZ			
8.55 (1.64)	7.54 (1.26)	7.21 (0.021)	8.64 (1.83)	7.51 (1.42)	7.74 (0.019)
		7.27 (0.017)			7.88 (0.014)
		7.85 (0.040)			
		7.87 (0.0007)			
		aug-cc-pVDZ			
no	no	2.35 (0.0009)	no	no	3.17 (0.0002)
		2.68 (0.0003)			3.75 (0.0013)
		6.92 (0.2150)			6.83 (0.0009)

Cross sections

The scattering matrix, related to the initial and final state of a scattering process is called S-matrix. The S-matrix for the collision gives the likelihood of each possibility. The scattering observables (such as the scattering cross sections and decay probabilities) can be extracted from K-matrix, which is related to S-matrix [29]:

$$S = \frac{(1 + iK)}{(1 - iK)} \tag{8.1}$$

The T-matrices are used to give a cross section, σ, for going from target state i to target state i' [29]:

$$\sigma(i \to i') = \frac{\pi}{k_i^2} \sum_S \frac{(2S+1)}{2(2S_i+1)} \sum_{\Gamma l l'} |T^{\Gamma S}_{i l i' i'}|^2 \tag{8.2}$$

where $\frac{k_i^2}{2}$ is energy of scattering electron relative to the initial state which has spin S_i. The first sum runs over the total spin states of the collision system, S, and the second sum runs over the spatial symmetries, Γ, and the degenerate channels associated with the initial and final states, denoted l and l' respectively. K-matrices are turned into T-matrices using the definition [29]:

$$T = \frac{2iK}{1 - iK} \tag{8.3}$$

Figure 8.9 presents elastic cross sections for the two conformers using different models employing the cc-pVTZ basis set. For both conformers the cross section increases rapidly at low energy, which is characteristic for electron collisions from targets with large permanent dipole moments. The Born correction significantly increases the cross section.

There are no reported measurements of the total elastic cross section for phosphoric acid, but our calculations give reasonable agreements with the previous studies (see also appendix F.1). Comparing our results to the previous calculations, our cross sections of the uuu conformer are about 10% larger than those of Tonzani and Greene [22] and show similar structure at lower energies. Below 5 eV, our cross section for both conformers is significantly larger than the cross sections obtained

by Winstead and McKoy [20], but it is unclear why their results do not show the low-energy peak characteristic of polar molecules.

Figure 8.10 shows electron impact electronic excitation cross sections of the two conformers for excitation to the two lowest singlet and triplet states. For the singlet states a Born correction computed by Dr Amar Dora has been added to the cross section based on the calculated transition dipole. The electronic excitation cross sections are very small in comparison to the elastic cross sections, which was also found for uracil [157].

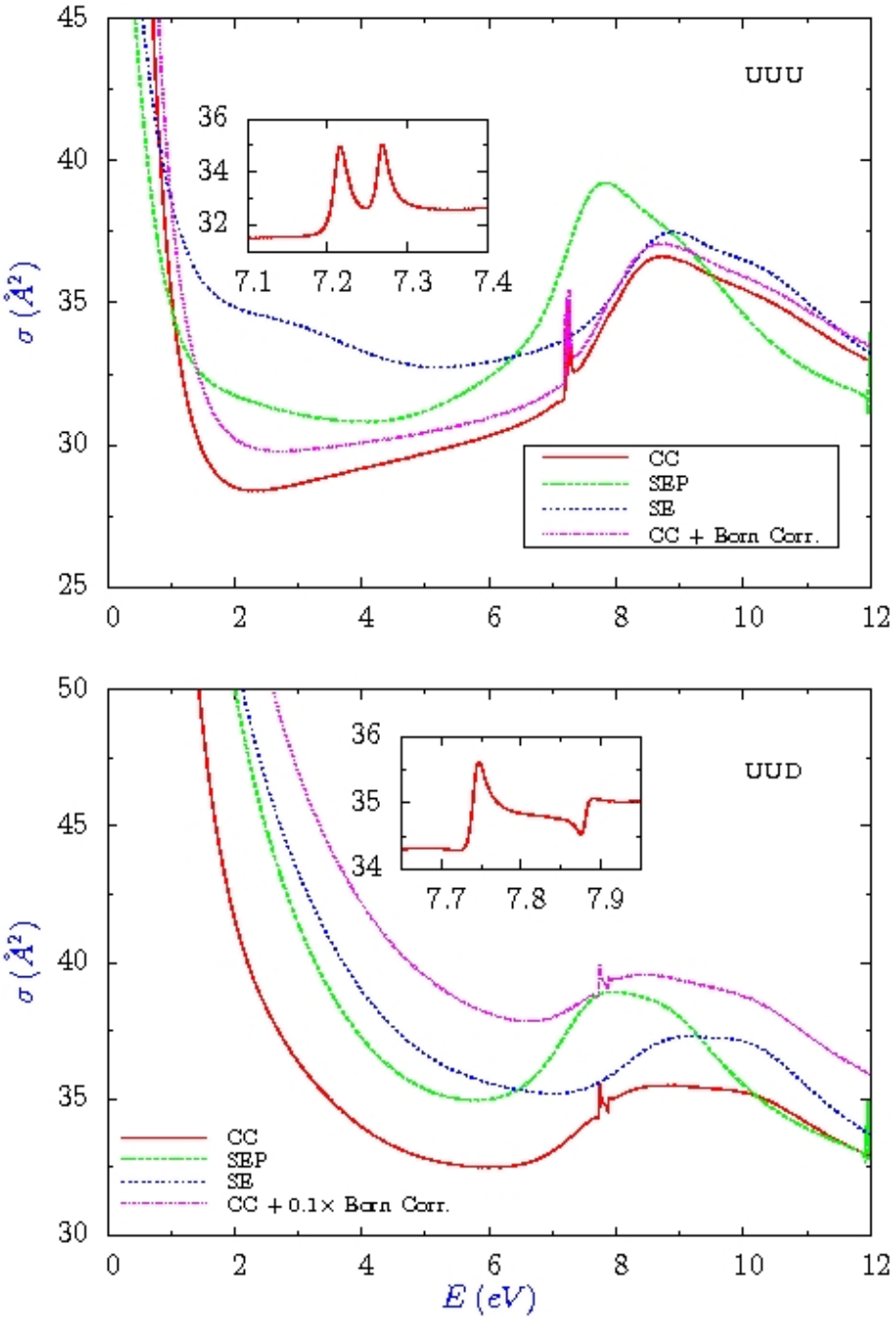

Figure 8.9: Elastic electron impact cross sections for phosphoric acid as a function of model: upper panel uuu conformer, lower panel uud conformer. The SE and SEP calculations were performed by Lilianna Bryjko, and calculations with the CC model by Dr Amar Dora. The Born correction that was added was also computed by Dr Amar Dora.

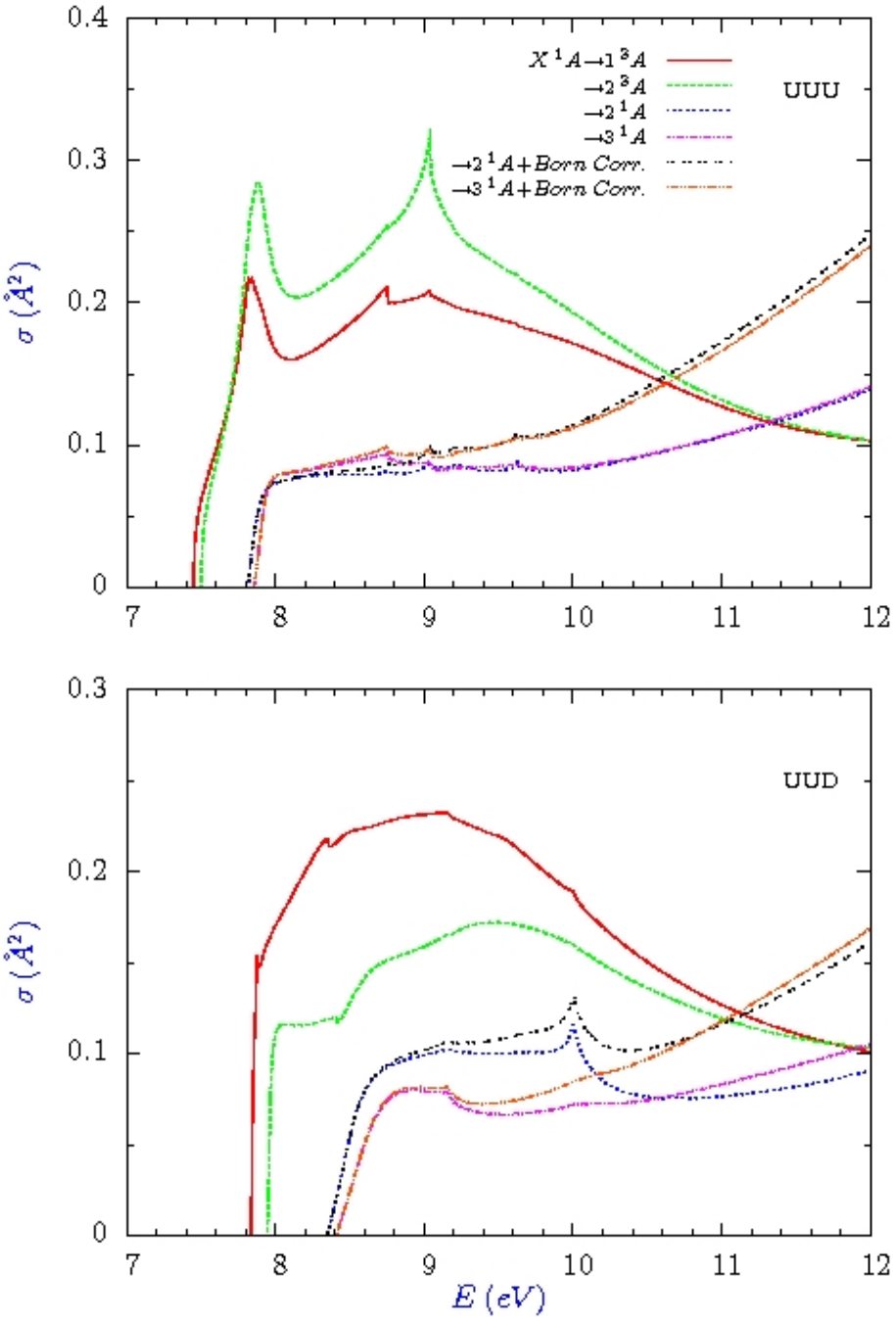

Figure 8.10: Electron impact excitation cross sections for excitation of the lowest two excited triplet and singlet states of phosphoric acid; calculations were performed by Dr Amar Dora using the close-coupling (CC) model; the upper curves have a Born correction calculated also by Dr Amar Dora: upper panel uuu conformer, lower panel uud conformer.

8.6.4 Conclusions

Electron collision calculations were performed on the two main conformers of phosphoric acid. The SE and SEP models employed the 6-31G, cc-pVDZ and cc-pVTZ basis sets. The CC calculations were performed at first with the aug-cc-pVDZ basis set, but this basis set was found to be too diffuse for R-matrix calculations and was exchanged for the cc-pVTZ basis set. The CC model used the target orbitals obtained from the ten-states CAS calculations using an active space consisting of 14 electrons distributed over 10 orbitals. The SE and SEP calculations were performed with HF orbitals. All scattering calculations were done with an R-matrix radius a=15a_0.

Both conformers display a broad feature at about 6-9 eV which may be associated with a shape resonance. This feature appears to be approximately the same for both conformers which can be understood from the fact that the two lowest unoccupied molecular orbitals (LUMOs) in the system are associated with P=O bonds, which are presumably not very sensitive to the conformerisation. For the uuu conformer the quasi-degenerate, very narrow Feshbach resonances were found, the first two at 7.21 and 7.27 eV and another two at 7.85 and 7.87 eV. However, for the uud conformer two Feshbach resonances at 7.74 an 7.88 eV were found.

A shape resonance had been found in previous SEP studies [20,22], but the Feshbach resonances obtained here using the close-coupling model have not been identified previously. Our calculations on the isolated H_3PO_4 molecule did not find any evidence for very low resonances or zero-energy states that could be the key to DNA strand breaks due to collisions with very-low-energy electrons.

Our calculations do not give a definitive, converged value for the resonance positions. They are very sensitive to the treatment of polarisation in the calculations. Better procedure for addressing this issue could be molecular R-matrix with pseudo states [308, 309], but it is not applied yet to a molecule as large as phosphoric acid. The behaviour of the two conformers is notably similar with resonance positions close to each other and cross sections that match quite closely, which suggests that calculations on either conformer would be appropriate input for modelling the phosphate group in studies of low-energy electron collisions in DNA. The uuu conformer

is chiral and this could be one area where the electron scattering between the two conformers may differ. Scattering of spin-polarised electrons from chiral systems can lead to enantiomer-dependent scattering [310], an effect known as electron circular dichroism.

8.7 2-Deoxyribose

Considering the action of deoxyribose, $C_5H_{10}O_4$, in DNA strand breaks, Simons' group [13–15] showed that electrons of ca. 1.0 eV can attach to the base to form a π^* anion, which then can break either a 3' or 5' O-C σ bond connecting the phosphate to either of the two sugar groups.

There have been few experimental or theoretical studies of low-energy electron scattering by deoxyribose. In order to describe the deoxyribose phosphate backbone in DNA, different model compounds were considered [22, 311–316].

Ptasińska et al. [3] have studied dissociative attachment and ionisation of gas-phase deoxyribose by low-energy electrons using a monochromatic electron bean in combination with a quadrupole mass spectrometer. They determined the ionisation energy of deoxyribose, $C_5H_{10}O_4$, at value 10.51 eV and, besides several peaks at very low energies, they see a peak in the $C_5H_5O_3^-$ fragment-ion spectrum at 6 eV, as well as a set of three peaks in the O^- yield at 7.3, 9.6, and 12.2 eV. Winstead and McKoy [317] have applied the Schwinger Multichannel Method (SMC) to study elastic scattering of low-energy electrons by 2-deoxyribose, 2-deoxyribose monophosphate and tetrahydrofuran (THF). For 2-deoxyribose and 2-deoxyribose monophosphate their SE integral cross section (ICS) shows a broad minimum near 6 eV and broad maxima at about 10 and 16 eV. By applying the polarisation shift they predicted the ICS exhibits broad maxima at about 8 eV and 13 eV for deoxyribose and a single, broader maximum at about 8 eV for 2-deoxyribose monophosphate.

The five-membered furanose ring is generally nonplanar. When one ring atom is out of the plane of the other four, the pucker type is envelope (E). More commonly, when two atoms deviate from the plane of the other three, with these two on either side of the plane, this is the twist conformation (T). If the major out-of -plane deviation of the atom in the ring is on the same side as the C4'-C5' bond it is an endo, if it is on the opposite side it is an exo conformer (see figures 8.11 and 8.12). In practice the pure envelope form is rarely observed, because of the differing substituents on the ring. The most commonly observed puckers in the crystal structures of isolated nucleosides and nucleotides are close to the C2'-endo or C3'-endo types. Purine

nucleosides prefer the C2'-endo pucker conformation type, whereas pyrimidine nucleosides favour C3'-endo. Deoxyribose nucleosides are primarily greater than 60% in the C2'-endo form [31]. The glycoside bond links a deoxyribose sugar and a base, being the C1'-N9 bond for purine nucleosides and the C1'-N1 bond for pyrimidine nucleosides.

In nucleotides, the pseudorotation phase angle P is calculated from the endocyclic sugar torsion angles according to [31]:

$$tanP = \frac{(\nu_4 + \nu_1) - (\nu_3 + \nu_0)}{2\nu_2(sin36^\circ + sin72^\circ)} \tag{8.4}$$

where the dihedral angles $\nu_0 = C_{4'}O_{4'}C_{1'}C_{2'}$, $\nu_1 = O_{4'}C_{1'}C_{2'}C_{3'}$, $\nu_2 = C_{1'}C_{2'}C_{3'}C_{4'}$, $\nu_3 = C_{2'}C_{3'}C_{4'}O_{4'}$, and $\nu_4 = C_{3'}C_{4'}O_{4'}C_{1'}$.

The pseudorotation phase angles are C3'-endo when $0^\circ \leq P \leq 36^\circ$ and C2'-endo when $144^\circ \leq P \leq 190^\circ$.

8.7.1 Methodology

The geometry of the two conformers of 2-deoxyribose was obtained from tight optimisation employing the B3LYP method and the 6-31+G* basis set [163] using the Gaussian03 with two frozen torsion angles, taken from the experimental data [312]. In both conformers, the ν_2 (36.9°) and ν_4 (20.8°) torsion angles for C3'-endo and the ν_2 (−35.7°) and ν_4 (0.2°) for C2'-endo were frozen. The C2'-endo conformer possesses slightly lower energy (-497.43632 Hartree, 1.82 D) than the C3'-endo conformer (-497.43307 Hartree, 2,69 D).

Seventy-two electrons of the nonplanar molecule occupy 36 orbitals, and the full active space includes 46 orbitals.

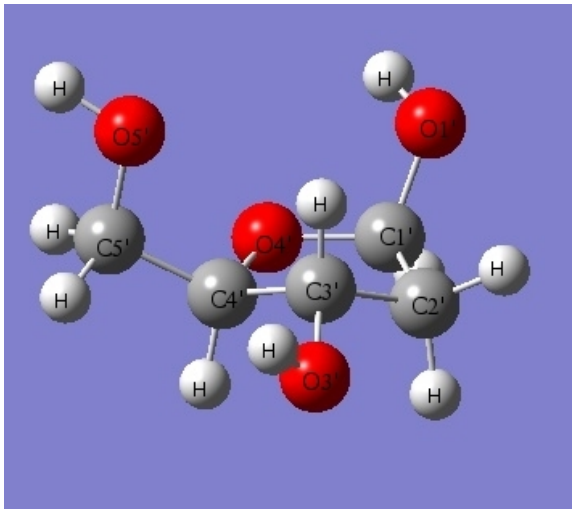

Figure 8.11: The structure of C3'-endo deoxyribose (Gaussview 4.1.2)

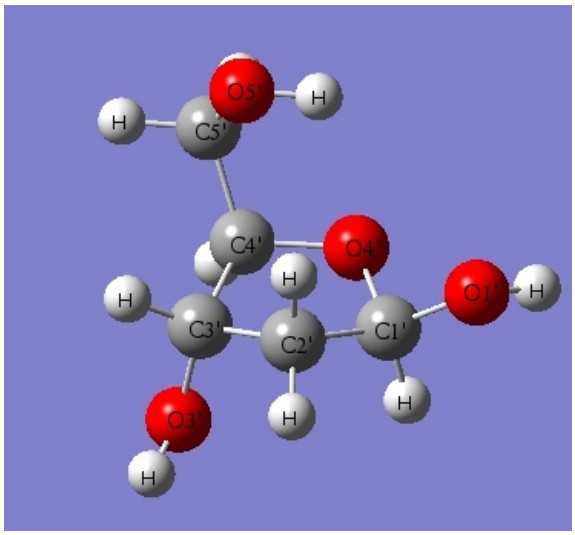

Figure 8.12: The structure of C2'-endo deoxyribose (Gaussview 4.1.2)

8.7.2 CAS calculations

Different active spaces were considered for the two conformers of deoxyribose. Table 8.19 compares the results obtained with the active space consisting of 10 electrons distributed over 10 orbitals, (10,10), and table 8.20 the results obtained with the active space consisting of 14 electrons distributed over 10 orbitals, (14,10), calculated with one and seven states using the 6-31G, cc-pVDZ and aug-cc-pVDZ basis sets. All calculations were performed with equal weights.

Looking at table 8.19 it is observed that noticeably the lowest values of the excitation energies were obtained with the aug-cc-pVDZ (a^d) basis set, and C3'-endo possesses higher excitation energies than the C2'-endo conformer. For the other basis sets the excitation energies for C2'-endo are higher than for C3'-endo. The RHF and one-state CAS ground state energies calculated with the B3LYP/6-31+G* optimised structure are lower for C2'-endo than for C3'-endo deoxyribose. The CAS ground state energy, obtained with calculations including seven states is lower for the C2'-endo conformer using the 6-31G basis set. However, considering the calculations with the other basis sets, C3'-endo possesses a lower CAS ground state energy than C2'-endo.

The active space consisting of 10 electrons distributed over 10 orbitals was too big for R-matrix calculations with phosphoric acid, which has a smaller number of electrons (50) than deoxyribose (72, see chapter 8.6). Therefore another active space, which generated less configurations was considered, the (14,10) active space (see table 8.20). Here also it is observed that the calculations using the aug-cc-pVDZ basis set give, in comparison to the other basis sets, noticeably lower values of the excitation energy. In this case for the C2'-endo conformer the RHF energy is lower than the CAS ground state energy calculated with seven states. Calculating a different number of states, or using different weights for the different states, may change this. Note that Molpro [24] by default uses equal weights for all states. The third singlet excitation energy of the C3'-endo conformer, obtained using the cc-pVDZ basis set, lies above the ionisation energy of deoxyribose, whereas for the calculations with the (10,10) active space all considered excitations lie below 10 eV.

Table 8.19: The X^1A' ground state energy (in Hartree), the vertical excitation energies (in eV) and the ground state dipole moment (in D) of deoxyribose calculated with one and seven states and the (10,10) active space. a^d means the aug-cc-pVDZ basis set.

State	**C2'-endo**			**C3'-endo**		
	6-31G	**cc-pVDZ**	**a**^{d}	**6-31G**	**cc-pVDZ**	**a**^{d}
E^{RHF}	-494.36592	-494.62761	-494.67138	-494.36238	-494.62379	-494.66909
			One state			
X^1A	-494.49700	-494.75572	-494.78344	-494.46563	-494.73960	-494.76930
			Seven states			
CSFs	19404					
X^1A	-494.40715	-494.66503	-494.68330	-494.39927	-494.66689	-494.74551
2^1A	8.90	8.57	5.81	8.74	8.31	6.50
3^1A	9.36	9.02	6.31	8.80	8.44	7.94
4^1A	9.65	9.38	6.35	9.58	9.03	8.32
CSFs	29700					
1^3A	8.13	7.91	5.74	7.94	7.75	6.28
2^3A	8.57	8.34	6.29	8.03	7.77	7.83
3^3A	8.94	8.70	6.33	8.91	8.32	8.28
μ^{RHF}	2.31	1.83	1.83	3.21	2.59	2.54
μ^{CAS}	2.38	1.90	2.94	3.70	3.07	2.17

Table 8.20: The X^1A' ground state energy (in Hartree), the vertical excitation energies (in eV) and the ground state dipole moment (in D) of deoxyribose calculated with one and seven states and the (14,10) active space. a^d means the aug-cc-pVDZ basis set.

State	**C2'-endo**			**C3'-endo**		
	6-31G	**cc-pVDZ**	**a**^{d}	**6-31G**	**cc-pVDZ**	**a**^{d}
E^{RHF}	-494.36592	-494.62761	-494.67138	-494.36238	-494.62379	-494.66909
			One state			
X^1A	-494.43480	-494.69312	-494.76722	-494.43050	-494.68915	-494.74094
			Seven states			
CSFs	4950					
X^1A	-494.38476	-494.63847	-494.58354	-494.38078	-494.63960	-494.67733
2^1A	8.69	8.41	4.28	8.54	8.26	6.37
3^1A	9.20	8.89	4.85	8.63	8.33	7.53
4^1A	9.27	9.04	4.88	9.21	10.78	8.40
CSFs	6930					
1^1A	8.12	7.87	4.22	7.95	7.71	6.11
2^1A	8.62	8.34	4.84	8.05	7.78	7.14
3^1A	8.63	8.44	4.86	8.62	10.13	8.05
μ^{RHF}	2.31	1.83	1.83	3.21	2.59	2.54
μ^{CAS}	2.25	1.77	3.46	3.22	2.28	2.28

8.7.3 Recommendations for R-matrix calculations

Because of evidence of temporary attachment of electrons to the base pair and the phosphate group (see section 8.6), we decided to first perform the scattering calculations with phosphoric acid, uracil and the DNA bases. However, consideration of electron collisions with deoxyribose could also be an interesting point for subsequent R-matrix calculations and investigation of DNA strand breaks.

We did not perform scattering calculations on deoxyribose, but also, in this case some difficulties may occur with the choice of the appropriate active space and basis set. Because the (10,10) active space was too large for the calculations with the close-coupling model on phosphoric acid, the smaller, (14,10) active space is recommended for scattering calculations on deoxyribose. The smallest values of the excitation energies of the sugar were obtained using the basis set with diffuse functions. However, the aug-cc-pVDZ basis set is too diffuse for scattering calculations on phosphoric acid. This suggests that scattering calculations on deoxyribose can not be performed with the aug-cc-pVDZ basis set. The calculations using the 6-31G and cc-pVDZ basis sets with the (14,10) active space are recommended for both conformers as starting point for the scattering calculations on deoxyribose.

It could be interesting to perform scattering calculations not only on the different conformers of deoxyribose with different basis sets and active spaces, but also on the different model compounds [22, 311–316] describing the deoxyribose phosphate backbone in DNA (see chapter 2), though complete nucleotides will be too large for R-matrix calculations.

Chapter 9

Conclusions and Future Work

CAS calculations were performed for the DNA/RNA bases uracil, cytosine, guanine, adenine, and thymine and for 2-deoxyribose and phosphoric acid. The main aim of the calculations was to provide CAS orbitals for use in R-matrix calculations using the CC model. A key problem with CAS calculations is scaling with system size: there is a factorial dependence on both the number of active electrons and particularly on the number of active orbitals generating many-electron configurations (full CI within the active space [37]). There is no clear-cut way to choose the active space. Usually, for small molecules, CAS calculations are done with a full valence active space. For conjugated systems all π orbitals should be included in the active space, if feasible [37]. Another way is to choose a one-to-one active space that has one anti bonding orbital for each bonding orbital.

An active space consisting of 14 electrons distributed over 10 MOs was chosen for uracil. The R-matrix calculations on cytosine will employ a similar active space. In the case of guanine, which is the largest DNA base, the active space which includes all π orbitals was too big for R-matrix calculations, and an active space consisting of 12 (4σ, 6π) electrons distributed over 9 orbitals was chosen. In the case of adenine, the same active space as for guanine will be considered, but with more states, because the ionisation potential of adenine is higher than that of guanine. For R-matrix calculations, the excitation energies should lie below the ionisation energy of the molecule. The scattering calculations were done for the planar bases, but also, for comparison, some CAS calculations for nonplanar molecules were per-

formed. For phosphoric acid the active space consisting of 14 electrons distributed over 10 orbitals was employed. A similar or smaller active space will be used for calculations on thymine and 2-deoxyribose, as the furanose sugar and the nonplanar base thymine are larger than phosphoric acid.

Most of the excited state calculations were performed with the 6-31G, 6-31G*, cc-pVDZ, aug-cc-pVDZ, and cc-pVTZ basis sets. Calculations with basis sets containing diffuse functions result usually in lower values of the excitation energies, which is noticeably observed in the case of 2-deoxyribose and phosphoric acid. Disagreements between our calculated excitation energies and the excitation energies obtained by experiment or other computational methods, could come from the fact that we could not use very large active spaces in the CAS calculations, as these would be too large for the R-matrix calculations. It must be noted that the considered molecules are rather large for scattering calculations.

The scattering calculations on phosphoric acid were done for the two most stable isomers [318]. With the SE and SEP model the 6-31G, cc-pVDZ, aug-cc-pVDZ and cc-pVTZ basis sets were employed. At first the CC calculations were performed with the aug-cc-pVDZ basis set, but this basis set was too diffuse for R-matrix calculations and was replaced with the cc-pVTZ basis set. All scattering calculations were done with radius a=15a_0. A broad shape resonance at about 7 eV was found for both isomers. Ten-state close-coupling calculations suggest the presence of narrow, Feshbach resonances in a very similar energy region. The resonances appear to be approximately the same for both isomers which can be understood from the fact that the two lowest unoccupied molecular orbitals (LUMO) in the system are associated with P=O bonds, which are presumably not very sensitive to the isomerisation.

The electron collision calculations on uracil were performed by the group from UCL [157] (see appendix F).

R-matrix calculations on cytosine, adenine, guanine and thymine using the CAS orbitals presented in this thesis will be done in the near future. We are currently performing the scattering calculations on guanine, but the results are not presented in this thesis. The calculations are very CPU time and memory demanding. The uncontracted close-coupling calculations (see section 6.2) on C_s-symmetric uracil

took more than one month, and the calculations on guanine are predicted to take a similar period of time. At the end it must be noted that the tables with the excitation energies presented in this thesis summarise the best feasible model for the R-matrix calculations.

Chapter 10

Presentations

10.1 Conferences attended

- 30th Royal Society of Chemistry Theoretical Chemistry Group Graduate Student meeting, April 2009, Nottingham, UK, PRESENTATION, **SA-CASSCF and low-energy electron collisions with uracil, guanine and phosphoric acid**

- Conference Collisions with Molecules and Clusters, April 2010, Milton Keynes, UK, POSTER, **SA-CASSCF and R-matrix calculations of low-energy electron collisions with uracil**

- 4th ScotCHEM Computational Chemistry Conference, April 2010, Glasgow, Scotland, UK, PRESENTATION, **SA-CASSCF and low-energy electron collisions with uracil, guanine and phosphoric acid**

- St Andrews Industry Chemistry Forum, September 2009, St Andrews, Scotland, UK, POSTER, **SA-CASSCF and R-matrix calculations of low-energy electron collisions with uracil**

- 7th Canadian Computational Chemistry Conference, July 2009, Halifax, Nova Scotia, Canada, POSTER, **SA-CASSCF and R-matrix calculations of low-energy electron collisions with uracil**

- 29th Royal Society of Chemistry Theoretical Chemistry Group Graduate Student meeting, April 2009, Cardiff, UK, POSTER, **SA-CASSCF and R-matrix calculations of low-energy electron collisions with uracil**
- 28th Royal Society of Chemistry Theoretical Chemistry Group Graduate Student meeting, April 2008, Manchester, UK, POSTER, **SA-CASSCF and R-matrix calculations of low-energy electron collisions with uracil**
- 3rd ScotCHEM Computational Chemistry Conference, May 2009, Edinburgh, Scotland, UK, POSTER, **SA-CASSCF and R-matrix calculations of low-energy electron collisions with uracil**
- 2nd ScotCHEM Computational Chemistry Conference, April 2008, Glasgow, Scotland, UK, POSTER, **Calculations of the excited states of biomolecules with CASSCF**
- RADAM Conference, June 2007, Dublin, Ireland
- 1st ScotCHEM Computational Chemistry Conference, April 2007, St Andrews, Scotland, UK

10.2 Publications

- A. Dora; J. Tennyson; L. Bryjko; T. van Mourik, **R-matrix calculation of low-energy electron collisions with uracil**, J. Chem. Phys. 130, 164307, 2009
- L. Bryjko, T. van Mourik, A. Dora, J. Tennyson, **R-matrix calculations of low-energy electron collisions with phosphoric acid**, J. Phys. B, At. Mol. Opt. Phys. 43, 235203, 2010

Appendices

Appendix A

Theory

A.1 Basis sets for calculations of excited states

Excited-state quantum chemical calculations require the use of large, diffuse, and flexible basis sets, which are able to describe at the same level valence, diffuse, Rydberg or anionic states.

The best general choice to get all types of excited states are Atomic Natural Orbitals (ANO) basis sets [319] supplemented with diffuse functions or augmented correlation-consistent basis sets (aug-cc-pVXZ, X=D,T,Q...) [320, 321].

ANO basis sets have a balanced construction and therefore get better results with a smaller number of functions than other sets. For a medium-sized molecule, an ANO contraction of the triple-zeta plus polarisation type has been shown to give accurate and reliable results for valence states [322]. Specific diffuse functions with small Gaussian exponents are required to compute Rydberg or anionic excited states.

Basis sets of type 6-31G* [323] are not as accurate but cheaper. They should be carefully calibrated for the studied problem, for example they may work where the Rydberg states are not competitive with the valence states in the studied energy region.

A.2 Types of correlation

The Electron Correlation Energy is the difference in energy between the HF and the lowest possible energy in a given basis set.
Two types of electron correlation can be identified [35]:

- **Radial Correlation**

  One electron is close to, and the other far from, the nucleus. To describe this, the basis set needs functions of the same type, but with different exponents.

- **Angular Correlation**

  Two electrons are on opposite sides of the nucleus. To describe this, the basis set needs functions with exponents of the same magnitude, but with different angular momenta.

The opposite-spin correlation is called **Coulomb correlation**, whereas the same-spin correlation is called **Fermi Correlation**. In the immediate vicinity of an electron the probability of finding another electron is reduced. For electrons of opposite spins this is called the **Coulomb hole**, whereas for electrons of the same spins this is called the **Fermi hole**.
There are three main ab initio methods for calculating electron correlation [35]:

1. Configuration Interaction (CI)
2. Many Body Perturbation Theory (MBPT)
3. Coupled Cluster (CC)

The correlation energy that arises from the overestimation of short-range electron repulsions in the Hartree-Fock wavefunction is referred to as **dynamical correlation**. The dynamical correlation is always reduced when a normal chemical bond (i.e. doubly occupied orbital) is broken. Where dynamical correlation effects are important, Hartree-Fock generally overestimates bond lengths and underestimates binding. An example is the rare-gas dimers, which are unbound at the Hartree-Fock

level, but in reality are held together by dispersion, which is a manifestation of dynamic correlation.

That part of the correlation energy arising from long-range correlation effects (like observed on molecular dissociation) is referred to as **non-dynamical or static correlation** [324–327].

It is difficult to define the division between dynamical and static correlation. For example, when thinking about electron correlation in a bond in a molecule, the radial and angular short-range concepts are blurred with the ideas of long-range dissociation. One visualisation is that the non-dynamical correlation is recovered with the minimum CI expansion describing properly all correlation effects. Convergence of the dynamical correlation energy with increasing size of CI expansion is very slow.

A.3 Molpro-Specific Orbital Subspace

The Molpro-specific orbital subspaces in accordance with the Molpro Manual [328] consist of:

- ***Occupied Orbitals***

  occ, n_1*,*n_2*,...,*n_8*;*

  n_i *specifies the number of occupied orbitals (including core and closed) in irreducible representation number i.*

- ***Frozen-Core Orbitals***

  Frozen, n_1*,*n_2*,...,;*

  n_i *specifies the number of frozen-core orbitals in irreducible representation number i.These orbitals are doubly occupied in all configurations and not optimised.*

- ***Closed Orbitals***

  Closed, n_1*,*n_2*,...,;*

  n_i *specifies the number of closed orbitals in irreducible representation number i. These orbitals do not form part of the active space, i.e., they are doubly occupied in all CSFs. In contrast to the frozen orbitals, these orbitals are fully optimised.*

- ***Frozen Orbitals***

  freeze, orb.sym;

  The specified orbital will not be optimised and will remain identical to the starting guess. orb.sym should be an active or closed-shell orbital. If orb.sym is a frozen core orbital, this card has no effect.

A.4 Modified Virtual Orbitals

The HF virtual orbitals could be too diffuse for the scattering calculations [19] and another way to receive virtual orbitals is the Modified Virtual Orbitals (MVO) scheme [162]. After convergence of the all-electron SCF or MCSCF calculation, all valence electrons are excluded and for the core electrons the Fock operator is constructed. This is transformed to a Fock matrix over molecular orbitals using the converged orbitals from the SCF or MCSCF calculations. The subspace corresponding to the virtual orbitals in the all-electron calculation is diagonalized. These new virtual orbitals are called Modified Virtual Orbitals (MVOs). This procedure does not mix occupied and virtual orbitals. Without the valence electrons, the lowest virtuals are drawn into the valence region and should be suitable for correlating the valence orbitals.

An alternative technique is to recompute the one-electron integrals with an increased nuclear charge for all the nuclei. Then an all-electron Fock operator can be constructed and the virtual subspace diagonalised. This process should be very similar to the elimination of valence electrons.

A.5 R-matrix

A.5.1 Configurations with an SCF target representation (SE and SEP model)

The R-matrix basis functions, ψ_k^{N+1}, in terms of orbital configurations are divided into two parts [18]:

1. The first part of each ψ_k^{N+1} corresponds to the configurations where one electron is in a continuum orbital and the rest of the electrons are in the target state.

2. The second part of each ψ_k^{N+1} consists of two types of configurations:

   - A one-particle term where the scattering electron drops down into the virtual orbitals.
   - A two-particle term in which there is one hole in the target and two particles in the virtual space.

Both of these types are L^2 configurations [29] because all the electrons are in short-range orbitals. The latter configurations are correlation configurations, sometimes called (short-range) polarisation configurations, which introduce correlation effects between target and projectile. A calculation in which the correlation configurations are omitted are at the static exchange level (SE), while the addition of correlation configurations is a static exchange plus polarisation approximation (SEP).

A.5.2 Configurations with a CI target representation (CC model)

In multistate scattering studies it is necessary to use a configuration interaction representation of the target states (see equation 4.1). The wavefunction is given by [18]:

$$\phi = \sum d_i \Delta_i \tag{A.1}$$

where the Δ_i are the set of CSFs, the choice of which defines different types of target state approximation, and the d_i are coefficients which are obtained by diagonalising the target state Hamiltonian in the basis Δ_i. The ψ_k^{N+1} can be analysed into parts as follows:

1. The first part of each R-matrix basis function consists of the Δ_i defining the target space with one electron in the continuum space.

2. The L^2 part of each ψ_k^{N+1} is divided into three parts:

    - Orthogonality CSFs, accounting for the fact that the continuum molecular orbitals are also orthogonal to the unoccupied virtual orbitals.
    - Correlation CSFs, where the scattering electron enters the charge cloud of the target state.
    - Two particle-one hole additional correlation CSFs. These CSFs are analogous to the two particle-one hole terms for the SCF target but are vastly increased in number with a CI target.

With a CI target it is not possible to describe the role of specific configurations as clearly as in the case of an SCF target.

Appendix B

Uracil

B.1 CAS calculations for uracil

B.1.1 The (12,9) active space

Table B.1: The X^1A' ground state energy (in Hartree) and the vertical excitation energies (in eV) for singlet and triplet uracil calculated with five states and the (12,9) active space. The orbital space consists of: closed 23,0; occupied 24,8.

State	**6-31G**	**6-31G***	**cc-pVDZ**	**aug-cc-pVDZ**	**cc-pVTZ**
X^1A'	-412.355293	-412.529336	-412.568635	-412.591036	-412.679678
$1^1A''$	4.45	4.65	4.65	4.60	4.62
$1^3A'$	3.75	3.83	3.83	3.80	3.81
$2^3A'$	5.41	5.56	5.56	5.54	5.56
$1^3A''$	4.27	4.47	4.47	4.43	4.44

Table B.2: The X^1A' ground state energy (in Hartree) and the vertical excitation energies (in eV) for singlet and triplet uracil calculated with 16 states and the (12,9) active space. The orbital space consists of: closed 23,0; occupied 24,8.

State	**6-31G**	**6-31G***	**cc-pVDZ**	**aug-cc-pVDZ**	**cc-pVTZ**
X^1A'	-412.347283	-412.519893	-412.559048	-412.556788	-412.668551
$2^1A'$	6.68	6.68	6.61	6.75	6.54
$3^1A'$	7.05	7.19	7.13	7.38	7.14
$4^1A'$	8.44	8.51	8.56	7.62	8.46
$1^1A''$	4.42	4.59	4.59	4.45	4.54
$2^1A''$	7.27	7.37	7.34	7.31	7.25
$3^1A''$	9.40	9.61	9.61	8.03	9.52
$4^1A''$	10.42	10.98	10.98	10.98	10.97
$1^3A'$	3.72	3.79	3.79	3.70	3.76
$2^3A'$	5.26	5.41	5.40	5.46	5.39
$3^3A'$	6.16	6.52	6.53	7.34	6.57
$4^3A'$	7.46	7.57	7.55	8.33	7.49
$1^3A''$	4.25	4.42	4.41	4.28	4.37
$2^3A''$	7.18	7.28	7.25	7.22	7.17
$3^3A''$	9.34	9.55	9.54	8.02	9.46
$4^3A''$	9.61	9.88	9.88	9.88	9.81

B.1.2 The (14,10) active space

Table B.3: The X^1A' ground state energy (in Hartree) and the vertical excitation energies (in eV) for singlet and triplet uracil calculated with five states and the (14,10) active space. The orbital space consists of: closed 22,0; occupied 24,8.

State	**6-31G**	**6-31G***	**cc-pVDZ**	**aug-cc-pVDZ**	**cc-pVTZ**
X^1A'	-412.355694	-412.529896	-412.569203	-412.591698	-412.680323
$1^1A''$	4.39	4.59	4.59	4.55	4.56
$1^3A''$	3.76	3.84	3.84	3.80	3.82
$2^3A''$	5.42	5.57	5.58	5.56	5.58
$1^3A''$	4.20	4.40	4.40	4.36	4.38

Table B.4: The X^1A' ground state energy (in Hartree) and vertical excitation energies (in eV) for singlet and triplet uracil calculated with 16 states and the (14,10) active space. The orbital space consists of: closed 22,0; occupied 24,8.

State	**6-31G**	**6-31G***	**cc-pVDZ**	**aug-cc-pVDZ**	**cc-pVTZ**
X^1A'	-412.350985	-412.524426	-412.563490	-412.585088	-412.673907
$2^1A'$	6.61	6.66	6.59	6.46	6.54
$3^1A'$	6.96	7.06	7.00	6.94	6.98
$4^1A'$	8.63	8.74	8.77	8.62	8.72
$1^1A''$	4.69	4.93	4.92	4.92	4.93
$2^1A''$	6.17	6.49	6.49	6.47	6.50
$3^1A''$	7.73	7.92	7.89	7.87	7.89
$4^1A''$	7.88	8.03	7.96	7.90	7.93
$1^3A'$	3.79	3.87	3.87	3.84	3.85
$2^3A'$	5.31	5.50	5.49	5.48	5.50
$3^3A'$	6.04	6.34	6.36	6.34	6.38
$4^3A'$	7.58	7.73	7.70	7.62	7.69
$1^3A''$	4.52	4.76	4.75	4.76	4.76
$2^3A''$	5.97	6.29	6.29	6.28	6.31
$3^3A''$	7.62	7.82	7.78	7.76	7.78
$4^3A''$	7.86	8.00	7.93	7.87	7.91

B.1.3 The (14,11) active space

Table B.5: The X^1A' ground state energy (in Hartree) and the vertical excitation energies (in eV) for singlet and triplet uracil calculated with five states and the (14,11) active space. The orbital space consists of: closed 22,0; occupied 24,9.

State	**6-31G**	**6-31G***	**cc-pVDZ**	**aug-cc-pVDZ**	**cc-pVTZ**
X^1A'	-412.366466	-412.540814	-412.580116	-412.600904	-412.691920
$1^1A''$	4.39	4.60	4.59	4.47	4.61
$1^3A'$	3.76	3.84	3.84	3.86	3.80
$1^3A'$	5.40	5.54	5.55	5.61	5.55
$1^3A''$	4.20	4.40	4.40	4.28	4.44

Table B.6: The X^1A' ground state energy (in Hartree) and the vertical excitation energies (in eV) for singlet and triplet uracil calculated with 16 states and the (14,11) active space. The orbital space consists of: closed 22,0; occupied 24,9.

State	**6-31G**	**6-31G***	**cc-pVDZ**	**aug-cc-pVDZ**	**cc-pVTZ**
X^1A'	-412.361860	-412.535080	-412.574134	-412.588112	-412.685028
$2^1A'$	6.61	6.62	6.55	6.65	6.46
$3^1A'$	6.95	7.05	6.99	7.12	6.96
$4^1A'$	8.62	8.73	8.76	7.24	8.70
$1^1A''$	4.69	4.92	4.91	4.81	4.92
$2^1A''$	6.18	6.52	6.52	6.71	6.54
$3^1A''$	7.73	7.93	7.89	7.72	7.89
$4^1A''$	7.89	8.02	7.96	8.14	7.93
$1^3A'$	3.79	3.86	3.86	3.82	3.84
$2^3A'$	5.29	5.50	5.48	5.53	5.49
$3^3A'$	6.05	6.34	6.37	6.56	6.39
$4^3A'$	7.56	7.70	7.67	7.17	7.64
$1^3A''$	4.52	4.75	4.74	4.64	4.75
$2^3A''$	5.97	6.31	6.32	6.52	6.34
$3^3A''$	7.63	7.82	7.78	7.62	7.78
$4^3A''$	7.87	7.99	7.93	8.13	7.90

Table B.7: The X^1A' ground state energy (in Hartree) and the vertical excitation energies (in eV), the number of configurations, and time of the calculations with five states for singlet and triplet uracil depending on the number of active orbitals for 14 electrons in the active space. Here (a,b) means: a-orbitals of first symmetry, b-orbitals of second symmetry.

	6-31G			**cc-pVDZ**	
	10 (2,8)	**14 (4,10)**	**16 (5,11)**	**10 (2,8)**	**14 (4,10)**
CSFs	2598	1382535	13911370	2598	1382535
X^1A'	-412.35569	-412.44393	-412.45922	-412.56920	-412.65691
CSFs	2352	1378080	13899270	2352	1378080
$1^1A''$	4.39	5.05	4.91	4.59	5.27
CSFs	3458	2504645	26544650	3458	2504645
$1^3A'$	3.76	3.85	3.87	3.84	3.91
$2^3A'$	5.42	5.61	5.59	5.58	5.79
CSFs	3472	2505360	26548390	3472	2505360
$1^3A''$	4.20	4.83	4.70	4.40	5.06
time	84[sec]	46[hour]	40[day]	129[sec]	44[hour]

B.2 MRCI calculations for uracil

Table B.8: The MRCI X^1A' ground state energy (in Hartree) and vertical excitation energies (in eV) for singlet and triplet uracil. The orbital space consists of core 22,0; occ 24,8. The reference wavefunction is obtained from CAS calculations with 16 states and the (14,10) active space, see table B.4.

State	**6-31G**	**6-31G***	**cc-pVDZ**	**aug-cc-pVDZ**	**cc-pVTZ**
X^1A'	-412.478472	-412.722747	-412.766562	-412.806134	-412.915363
$2^1A'$	6.17	6.26	6.18	5.96	6.09
$3^1A'$	6.72	6.93	6.84	6.72	6.82
$4^1A'$	7.76	7.97	8.01	7.69	7.90
$1^1A''$	4.97	5.26	5.24	5.25	5.24
$2^1A''$	6.44	6.79	6.76	6.73	6.75
$3^1A''$	7.69	7.98	7.92	7.85	7.91
$4^1A''$	7.74	7.92	7.83	7.72	7.78
$1^3A'$	3.86	3.97	3.96	3.92	3.95
$2^3A'$	5.33	5.60	5.56	5.54	5.59
$3^3A'$	6.10	6.43	6.44	6.38	6.45
$4^3A'$	7.06	7.28	7.24	7.09	7.22
$1^3A''$	4.77	5.07	5.04	5.07	5.06
$2^3A''$	6.21	6.57	6.54	6.53	6.56
$3^3A''$	7.62	7.88	7.83	7.76	7.83
$4^3A''$	7.72	7.92	7.80	7.69	7.76

Table B.9: The MRCI with Davidson correction X^1A' ground state energy (in Hartree) and vertical excitation energies (in eV) for singlet and triplet uracil. The orbital space consists of core 22,0; occ 24,8. The reference wavefunction is obtained from CAS calculations with 16 states and the (14,10) active space, see table B.4.

State	**6-31G**	**6-31G***	**cc-pVDZ**	**aug-cc-pVDZ**	**cc-pVTZ**
X^1A'	-412.487386	-412.738785	-412.783026	-412.826961	-412.936797
$2^1A'$	6.06	6.14	6.05	5.74	5.92
$3^1A'$	6.63	6.84	6.75	6.56	6.70
$4^1A'$	7.52	7.73	7.76	7.24	7.59
$1^1A''$	5.01	5.32	5.28	5.29	5.30
$2^1A''$	6.48	6.83	6.79	6.73	6.78
$3^1A''$	7.66	7.97	7.89	7.75	7.85
$4^1A''$	7.70	7.86	7.76	7.59	7.68
$1^3A'$	3.87	3.98	3.97	3.93	3.96
$2^3A'$	5.32	5.60	5.55	5.51	5.57
$3^3A'$	6.09	6.43	6.43	6.33	6.43
$4^3A'$	6.93	7.15	7.10	6.87	7.03
$1^3A''$	4.81	5.12	5.09	5.11	5.11
$2^3A''$	6.24	6.61	6.57	6.54	6.58
$3^3A''$	7.59	7.85	7.81	7.68	7.78
$4^3A''$	7.67	7.88	7.73	7.56	7.66

Appendix C

Guanine

Table C.1: The X^1A' ground state total energy (in Hartree), the vertical excitation energies (in eV) and the ground state dipole moment, μ (in D) for planar keto-N7H guanine calculated with 16 states and the (16,12) active space. The orbital space consists of: closed 31,0; occupied 32,11.

State	**6-31G**	**6-31G***	**cc-pVDZ**	**aug-cc-pVDZ**	**cc-pVTZ**
E^{RHF}	-539.13204	-539.38339	-539.43763	-539.47311	-539.58097
CSFs	41745				
X^1A'	-539.22923	-539.46813	-539.52139	-539.52805	-539.66162
$2^1A'$	5.75	5.82	5.80	5.90	5.76
$3^1A'$	6.15	6.18	6.20	6.47	6.15
$4^1A'$	7.39	7.39	7.43	6.61	7.37
CSFs	29040				
$1^1A''$	6.24	6.55	6.52	6.46	6.44
$2^1A''$	7.44	7.81	7.82	7.76	7.76
$3^1A''$	9.17	9.48	9.49	8.44	9.43
$4^1A''$	10.71	11.17	11.18	9.92	11.08

Continued on Next Page...

Table C.1 – Continued

State	**6-31G**	**6-31G***	**cc-pVDZ**	**aug-cc-pVDZ**	**cc-pVTZ**
CSFs	63888				
$1^3A'$	3.75	3.81	3.81	3.87	3.77
$2^3A'$	4.76	4.93	4.97	5.13	4.95
$3^3A'$	5.32	5.41	5.41	5.48	5.37
$4^3A'$	6.17	6.38	6.39	6.55	6.41
CSFs	49368				
$1^3A''$	5.89	6.25	6.23	6.22	6.16
$2^3A''$	6.98	7.34	7.34	7.26	7.28
$3^3A''$	9.14	9.43	9.45	8.39	9.37
$4^3A''$	9.87	10.32	10.33	9.82	10.24
μ^{RHF}	2.14	2.09	2.10	1.95	2.03
μ^{CAS}	2.75	2.45	2.58	1.91	2.45

Table C.2: The X^1A' ground state total energy (in Hartree), the vertical excitation energies (in eV) and the ground state dipole moment, μ (in D) for nonplanar keto-N7H guanine calculated with 16 states and the (16,12) active space.

State	**6-31G**	**6-31G***	**cc-pVDZ**	**aug-cc-pVDZ**	**cc-pVTZ**
E^{RHF}	-539.12796	-539.38484	-539.43943	-539.47428	-539.58204
CSFs	70785				
X^1A	-539.22269	-539.46874	-539.52237	-539.53639	-539.66290
2^1A	5.01	5.40	5.41	5.32	5.45
3^1A	5.91	5.97	5.95	6.08	5.91
4^1A	6.24	6.31	6.32	6.69	6.29
5^1A	6.52	6.89	6.86	6.84	6.83
6^1A	6.59	7.03	7.06	7.01	7.04
7^1A	7.24	7.61	7.65	7.27	7.63
8^1A	7.57	7.66	7.70	7.44	7.72
CSFs	113256				
1^3A	3.64	3.72	3.73	3.90	3.71
2^3A	4.72	4.90	4.93	5.14	4.92
3^3A	4.85	5.24	5.26	5.31	5.30
4^3A	5.35	5.50	5.50	5.73	5.49
5^3A	6.09	6.34	6.36	6.56	6.36
6^3A	6.19	6.48	6.46	6.66	6.45
7^3A	6.25	6.69	6.73	7.21	6.71
8^3A	7.17	7.31	7.30	7.24	7.27
μ^{RHF}	1.93	1.74	1.70	1.58	1.62
μ^{CAS}	2.34	2.00	1.94	1.64	1.84

Appendix D

Adenine

Table D.1: The X^1A' ground state total energy (in Hartree), the vertical excitation energies (in eV) and the ground state dipole moment, μ (in D) for planar adenine-N9H calculated with 16 states and the (16,12) active space. The orbital space consists of: closed 27,0; occupied 29,10.

State	**6-31G**	**6-31G***	**cc-pVDZ**	**aug-cc-pVDZ**	**cc-pVTZ**
E^{RHF}	-464.292106	-464.513393	-464.558845	-464.586147	-464.676974
CSFs	36465				
X^1A'	-464.395633	-464.607596	-464.651958	-464.676881	-464.768173
$2^1A'$	5.18	5.25	5.26	5.20	5.23
$3^1A'$	6.91	6.80	6.78	6.68	6.73
$4^1A'$	7.36	7.38	7.36	7.31	7.33
CSFs	34320				
$1^1A''$	5.67	5.98	5.98	5.94	5.96
$2^1A''$	6.09	6.40	6.40	6.38	6.38
$3^1A''$	7.08	7.46	7.45	7.40	7.42
$4^1A''$	7.76	8.11	8.11	8.07	8.07

Continued on Next Page...

Table D.1 – Continued

State	**6-31G**	**6-31G***	**cc-pVDZ**	**aug-cc-pVDZ**	**cc-pVTZ**
CSFs	56760				
$1^3A'$	3.86	3.95	3.95	3.90	3.93
$2^3A'$	5.19	5.22	5.23	5.17	5.20
$3^3A'$	5.35	5.36	5.37	5.33	5.35
$4^3A'$	5.63	5.70	5.69	5.67	5.68
CSFs	56496				
$1^3A''$	5.37	5.70	5.71	5.66	5.69
$2^3A''$	5.65	5.98	5.98	5.97	5.96
$3^3A''$	6.88	7.24	7.24	7.18	7.20
$4^3A''$	7.59	7.93	7.93	7.89	7.89
μ^{RHF}	2.62	2.47	2.41	2.46	2.44
μ^{CAS}	2.68	2.61	2.55	2.58	2.57

Table D.2: The X^1A' ground state total energy (in Hartree), the vertical excitation energies (in eV) and the ground state dipole moment, μ (in D) for nonplanar adenine-N9H calculated with 16 states and the (16,12) active space. The CI calculations with the cc-pVDZ basis set were not converged.

State	**6-31G**	**6-31G***	**aug-cc-pVDZ**	**cc-pVTZ**
E^{RHF}	-464.291272	-464.513490	-464.586227	-464.677060
CSFs	70785			
X^1A	-464.389380	-464.606650	-464.620723	-464.763683
2^1A	5.21	5.29	5.20	5.26
3^1A	5.60	5.89	5.48	5.90
4^1A	6.05	6.44	6.17	6.39
5^1A	6.61	7.00	6.28	6.84
6^1A	7.03	7.02	6.73	6.91
7^1A	7.16	7.38	7.09	7.22
8^1A	7.27	7.64	7.84	7.62
CSFs	113256			
1^3A	3.82	3.94	4.49	3.87
2^3A	5.14	5.28	5.15	5.22
3^3A	5.30	5.33	5.45	5.29
4^3A	5.35	5.62	5.98	5.64
5^3A	5.61	5.77	6.25	5.70
6^3A	5.64	6.01	6.29	5.98
7^3A	6.12	6.57	6.67	6.47
8^3A	6.89	6.77	6.72	6.90
μ^{RHF}	2.70	2.53	2.51	2.49
μ^{CAS}	2.56	2.59	3.10	2.42

Appendix E

Phosphoric acid

E.1 CAS calculations

Table E.1: The X^1A' ground state energy (in Hartree), the vertical excitation energies (in eV) and the ground state dipole moment (in D) of phosphoric acid calculated with five states and the (14,10) active space. a^d means the aug-cc-pVDZ basis set.

State		**uud**			**uuu**	
	6-31G	**cc-pVDZ**	**a**^{d}	**6-31G**	**cc-pVDZ**	**a**^{d}
CSFs	4950					
X^1A	-641.76745	-642.08706	-642.11891	-641.74853	-642.08346	-642.12091
2^1A	8.66	8.70	6.62	8.22	8.53	6.59
3^1A	8.72	8.98	7.03	8.29	8.89	6.98
CSFs	6930					
1^3A	7.80	8.13	6.42	7.52	8.10	6.41
2^3A	7.96	8.45	6.84	7.61	8.41	6.78
μ^{RHF}	3.83	3.54	3.62	0.72	0.26	0.58
μ^{CAS}	3.77	3.99	4.25	0.63	0.66	0.93

Table E.2: The X^1A' ground state energy (in Hartree), the vertical excitation energies (in eV) and the ground state dipole moment (in D) of phosphoric acid calculated with five states and the (10,10) active space. a^d means the aug-cc-pVDZ basis set

State	**uud**			**uuu**		
	6-31G	**cc-pVDZ**	**a**^{d}	**6-31G**	**cc-pVDZ**	a^d
E^{RHF}	-641.70644	-642.04087	-642.08692	-641.70454	-642.04245	-642.08866
CSFs	19404					
X^1A	-641.81922	-642.14730	-642.18480	-641.81713	-642.14928	-642.20894
2^1A	8.58	8.84	6.98	8.70	8.97	7.62
3^1A	8.91	9.25	7.43	9.04	9.32	7.71
CSFs	29700					
1^3A	7.87	8.40	6.81	8.03	8.57	7.42
2^3A	8.31	8.89	7.29	8.42	8.95	7.51
μ^{RHF}	3.83	3.54	3.62	0.72	0.26	0.58
μ^{CAS}	4.15	4.02	4.13	0.47	0.62	1.33

E.2 R-matrix calculations

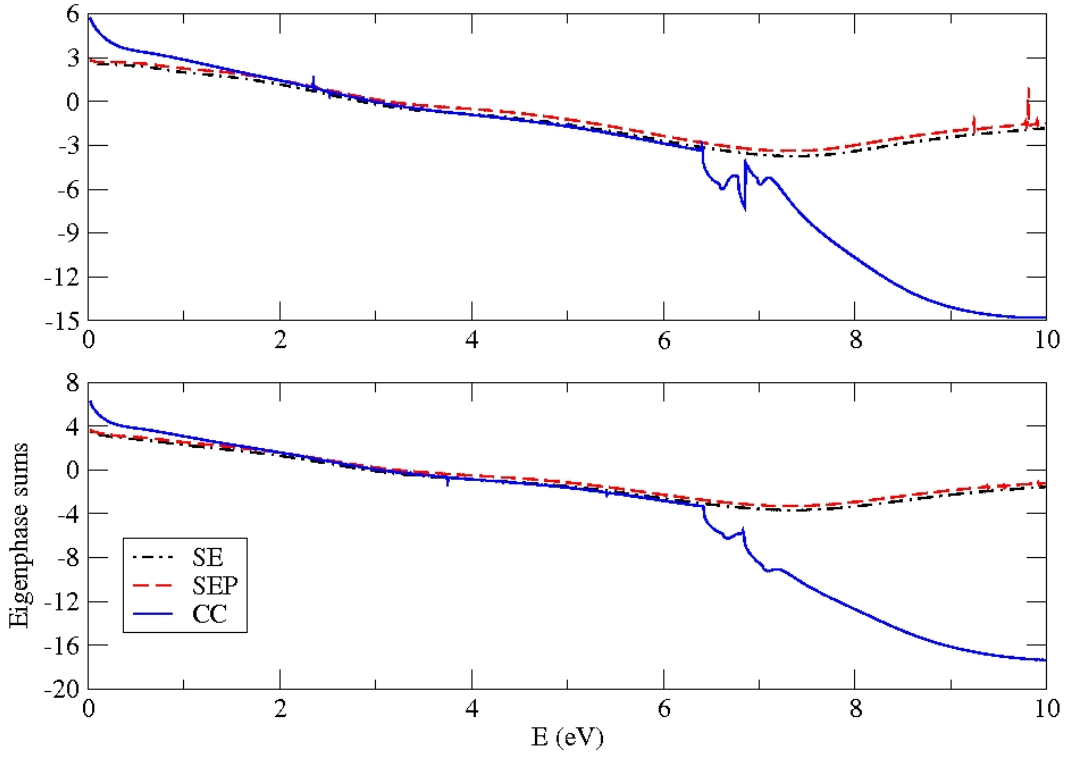

Figure E.1: Eigenphase sums for electron scattering from phosphoric acid: upper panel uuu isomer, lower panel uud isomer. The scattering calculations were performed with the aug-cc-pVDZ basis set. The CC calculations were done using the orbitals from five-state CAS calculations with the (14,10) active space (see table E.1).

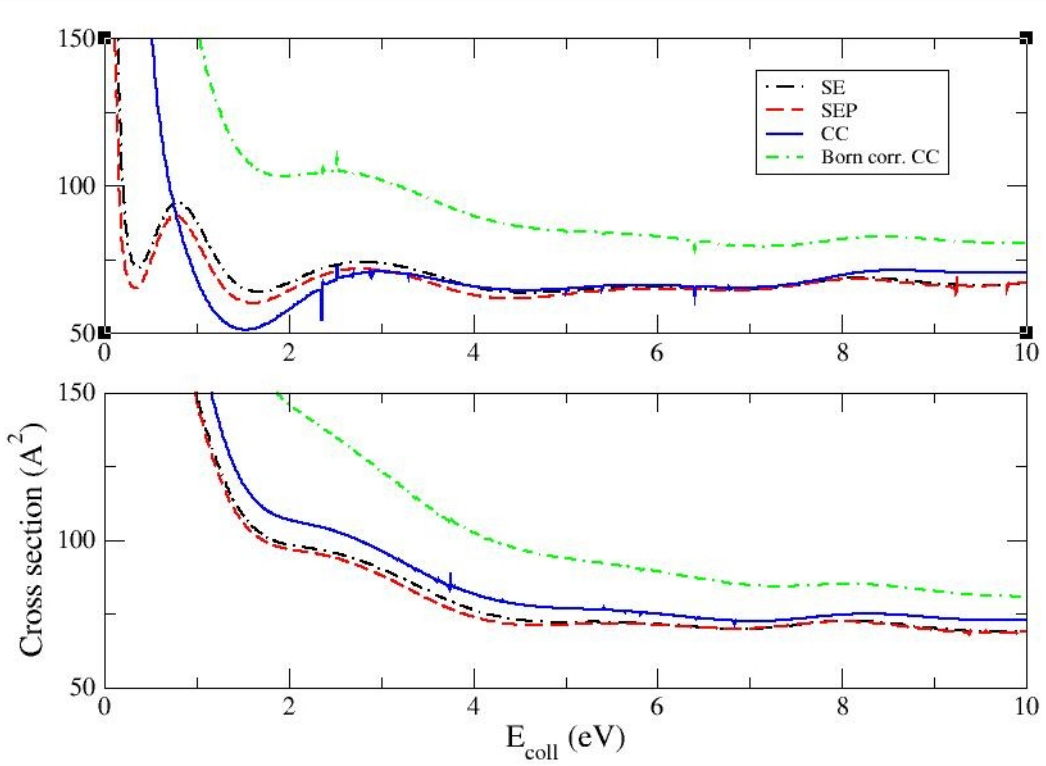

Figure E.2: Elastic electron impact cross sections for phosphoric acid as a function of model: upper panel uuu isomer, lower panel uud isomer. The Born correction that was added was computed by Dr Amar Dora. The scattering calculations were performed with the aug-cc-pVDZ basis set. The CC calculations were done using the orbitals from five-state CAS calculations with the (14,10) active space (see table E.1).

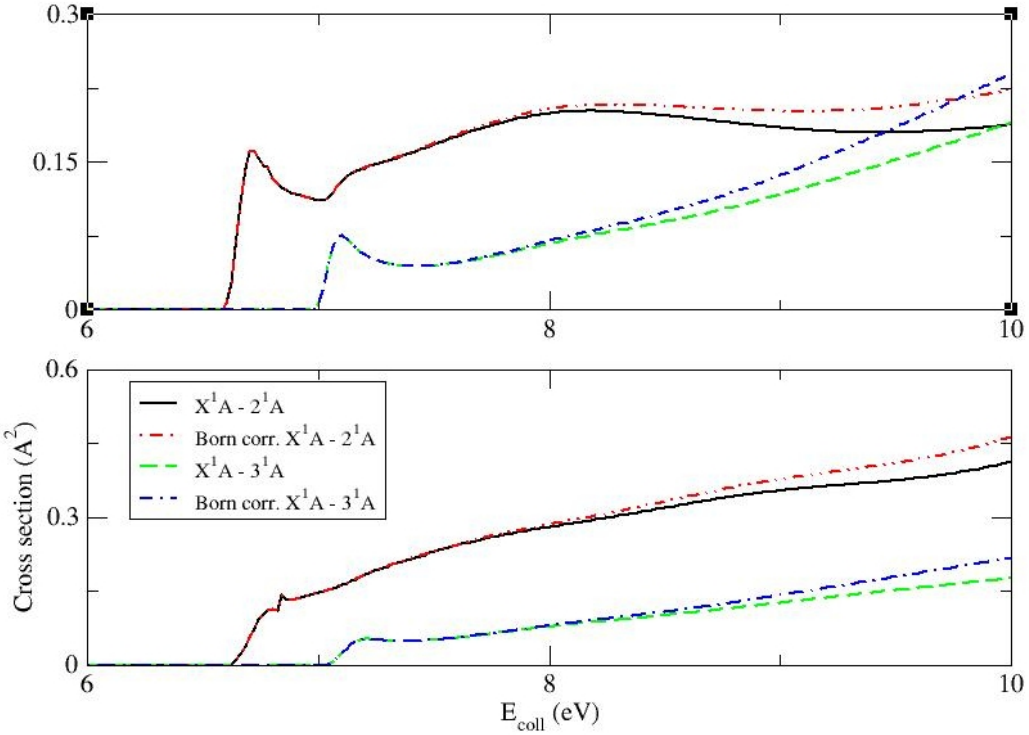

Figure E.3: Electron impact excitation cross sections for excitation of the lowest two excited singlet states of phosphoric acid; calculations were performed using the CC model; the upper curves include a Born correction calculated by Dr Amar Dora: upper panel uuu isomer, lower panel uud isomer. The scattering calculations were performed with the aug-cc-pVDZ basis set. The CC calculations were done using the orbitals from five-state CAS calculations with the (14,10) active space (see table E.1).

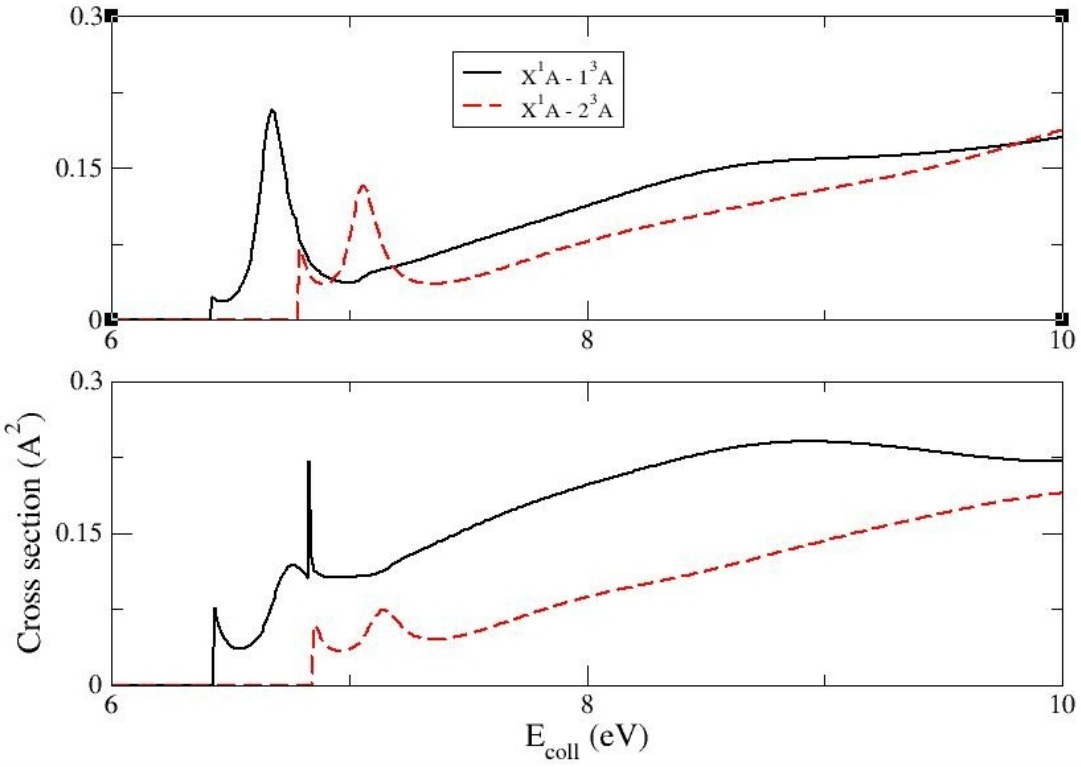

Figure E.4: Electron impact excitation cross sections for excitation of the lowest two excited triplet states of phosphoric acid; calculations were performed using the CC model; upper panel uuu isomer, lower panel uud isomer. The scattering calculations were performed with the aug-cc-pVDZ basis set. The CC calculations were done using the orbitals from five-state CAS calculations with the (14,10) active space (see table E.1).

Appendix F

Publications

F.1 R-matrix calculation of low-energy electron collisions with uracil

F.2 R-matrix calculation of low-energy electron collisions with phosphoric acid

Bibliography

[1] B. Boudaiffa; P. Clutier; A. Hunting; M. A. Huels; L. Sanche, *Science*, **2000**, *287*, 1658.

[2] K. Aflatooni; G. A. Gallup; P. D. Burrow, *J. Phys. Chem. A*, **1998**, *102*, 6205.

[3] S. Ptasińska; S. Denifl; P. Scheier; T. D. Märk, *J. Chem. Phys.*, **2004**, *120*, 8505.

[4] T. D. Mark S. Ptasińska; S. Denifl; S. Gohlke; P. Scheier; E. Illenberger, *Angev. Chem.,Int. Ed.*, **2006**, *45*, 1893.

[5] Y. Zheng; P. Cloutier; D. J. Hunting; J. R. Wagner; L. Sanche, *J. Chem. Phys.*, **2006**, *124*, 064710.

[6] A. Scheer; K. Aflatooni; G. A. Gallup; P. D. Burrow, *Phys. Rev. Lett.*, **2004**, *92*, 068102.

[7] X. Bao; J. Wang; J. Gu; J. Leszczyński, *Proc. Natl. Aca. Sci. USA*, **2006**, *103*, 5658.

[8] J. Gu; J. Wang; J. Rak; J. Leszczyński, *Ang. Chem.*, **2007**, *119*, 3549.

[9] A. Kumar; M. D. Sevilla, *J. Phys. Chem. B*, **2007**, *111*, 5464.

[10] S. Ptasińska; L. Sanche, *Phys. Rev. E*, **2007**, *75*, 31915.

[11] R. Panajotovic; M. Michaud; L. Sanche, *Phys. Chem. Chem. Phys.*, **2007**, *9*, 138.

[12] S. Ptasińska; L. Sanche, *Phys. Chem. Chem. Phys.*, **2007**, *9*, 1730.

[13] R. Barrios; P. Skurski; J. Simons, *J. Phys. Chem. B*, **2002**, *10*, 7991.

[14] J. Berdys; I. Anuszkiewicz; P. Skurski; J. Simons, *J. Am. Chem. Soc.*, **2004**, *126*, 6441.

[15] J. Berdys; I. Anuszkiewicz; P. Skurski; J. Simons, *J. Phys. Chem. A*, **2004**, *108*, 2999.

[16] V. Cobut; Y. Fongillo; J. P. Patau; T. Goulet; M. J. Fraser; J. P. Jay-Gerin, *Radiat. Phys. Chem.*, **1998**, *51*, 229243.

[17] J. M. Berg; J. L. Tymoczko; L. Stryer, *Biochemistry;* W. H. Freeman, 2002.

[18] W. M. Huo; F. A. Gianturco, Eds., *Computational Methods for Electron-Molecule Collisions;* Plenum Press, New York, 1995.

[19] C. Winstead; V. McKoy, *J. Phys. Chem*, **2006**, *125*, 174304.

[20] C. Winstead; V. McKoy, *Int. J. Mass Spect.*, **2008**, *277*, 279.

[21] C. Winstead; V. McKoy, *Rad. Phys. Chem.*, **2008**, *77*, 1258.

[22] S. Tonzani; Ch. Greene, *J. Chem. Phys.*, **2006**, *125*, 094504.

[23] S. Tonzani; Ch. Greene, *J. Chem. Phys.*, **2006**, *124*, 054312.

[24] P. Celani; T. Korona; A. Mitrushenkov; G. Rauhut; T. B. Adler; R. D. Amos; A. Bernhardsson; A. Berning; D. L. Cooper; M. J. O. Deegan; A. J. Dobbyn; F. Eckert; E. Goll; C. Hampel; G. Hetzer; T. Hrenar; G. Knizia; C. Köppl; Y. Liu; A. W. Lloyd; R. A. Mata; A. J. May; S. J. McNicholas; W. Meyer; M. E. Mura; A. Nicklass; P. Palmeri; K. Pflüger; R. Pitzer; M. Reicher; U. Schumann; H. Stoll; A. J. Stone; R. Tarroni; T. Thorsteinsson; M. Wang; A. Wolf H.J. Werner; P. J. Knowles; R. Lindh; F. R. Manby; M. Schütz, *MOLPRO, version 2006.1, http://www.molpro.net.*

[25] M. J. Frisch; G. W. Trucks; H. B. Schlegel; G. E. Scuseria; M. A. Robb; J. R. Cheeseman; J. A. Montgomery; Jr.; T. Vreven; K. N. Kudin; J. C. Burant; J. M. Millam; S. S. Iyengar; J. Tomasi; V. Barone; B. Mennucci; M. Cossi;

G. Scalmani; N. Rega; G. A. Petersson; H. Nakatsuji; M. Hada; M. Ehara; K. Toyota; R. Fukuda; J. Hasegawa; M. Ishida; T. Nakajima; Y. Honda; O. Kitao; H. Nakai; M. Klene; X. Li; J. E. Knox; H. P. Hratchian; J. B. Cross; V. Bakken; C. Adamo; J. Jaramillo; R. Gomperts; R. E. Stratmann; O. Yazyev; A. J. Austin; R. Cammi; C. Pomelli; J. W. Ochterski; P. Y. Ayala; K. Morokuma; G. A. Voth; P. Salvador; J. J. Dannenberg; V. G. Zakrzewski; S. Dapprich; A. D. Daniels; M. C. Strain; O. Farkas; D. K. Malick; A. D. Rabuck; K. Raghavachari; J. B. Foresman; J. V. Ortiz; Q. Cui; A. G. Baboul; S. Clifford; J. Cioslowski; B. B. Stefanov; G. Liu; A. Liashenko; P. Piskorz; I. Komaromi; R. L. Martin; D. J. Fox; T. Keith; M. A. Al-Laham; C. Y. Peng; A. Nanayakkara; M. Challacombe; P. M. W. Gill; B. Johnson; W. Chen; M. W. Wong; C. Gonzalez; and J. A. Pople, *Gaussian 03, Revision E.01, Wallingfort, CT*, **2004**.

[26] M. W. Schmidt; K. K. Baldridge; J. A. Boatz; S. T. Elbert; M. S. Gordon; J. H. Jensen; S. Koseki; N. Matsunga; K. A. Nguyen; S. J. Su; T. L. Windus; M. Dupuis; J .A. Montgomery, *J. Comput. Chem.*, **1993**, *14*, 1347.

[27] O. Christiansen; R. Cimiraglia; S. Coriani; P. Dahle; E. K. Dalskov; T. Enevoldsen; B. Fernandez; Ch. Haetting; K. Hald; A. Halkier; H. Heiberg; T. Helgaker; H. Hettema; H. J. Aa. Jensen; D. Jonsson; P. Joergensen; S. Kirpekar; w. Klopper; R. Kobayashi; H. Koch; A. Ligabue; O. B. Lutnaes; K. V. Mikkelsen; P. Norman; J. Olsen; M. J. Packer; T. B. Pedersen; z. Rinkevicius; E. Rudberg C. Angeli; K. L. Bak; V. Bakken, *Dalton, Release 2.0; rev.0; http;//www.kjemi.uio.no/software/dalton/dalton.html*.

[28] G. Schaftenaar; J. H. Noordik, *J. Comput.-Aided Mol. Design*, **2000**, *14*, 123.

[29] J. Tennyson, *Phys. Rep.*, **2010**, *491*, 29.

[30] B. Rosenberg, *Biochimie*, **1978**, *60*, 859.

[31] W. Saenger, *Principles of Nucleic Acid Structure;* Springer-Verlag, New York, Inc., 1983.

[32] N. Mills, *J. Am. Chem. Soc*, **2006**, *41*, 13649.

[33] A. D. McLean; B. Liu, *J. Chem. Phys.*, **1973**, *58*, 1066.

[34] W. G. Richards; D. L. Cooper, *Ab Initio Molecular orbital Calculations for Chemists;* Clarendon Press, 1983.

[35] F. Jensen, *Introduction to Computational Chemistry;* John Wiley and Sons Ltd., 1999.

[36] P. R. Taylor, *Advan. Chem. Phys.*, **1990**, *77*, 103.

[37] M. W. Schmidt; M. S. Gordon, *Annu. Rev. Phys. Chem.*, **1998**, *49*, 233.

[38] P. Knowles; M. Schütz; H. J. Werner, *Modern Methods and Algorithms of Quantum Chemistry;* Vol. 3; John von Neumann Institute for Computing, Jülich, NIC Series, 2000.

[39] T. L. Gilbert, *J. Chem. Phys.*, **1965**, *43*, 248.

[40] G Das; A. C. Wahl, *J. Chem. Phys.*, **1966**, *44*, 87.

[41] L. G. Yaffe; W. A. Goddard, *Phys. Rev. A*, **1976**, *13*, 1682.

[42] B. Levy; G. Berthier, *Int. J. Quantum Chem*, **1968**, *2*, 307.

[43] J. Hinze, *Int. J. Quantum Chem*, **1981**, *S15*, 69.

[44] K. Ruedenberg; L. M. Cheung; S. T. Elbert, *Int. J. Quantum Chem*, **1979**, *16*, 1069.

[45] B. O. Roos, *Int. J. Quantum Chem*, **1980**, *S16*, 175.

[46] L. M. Cheung; K. R. Sundberg; K. Ruedenberg, *Int. J. Quantum Chem*, **1979**, *16*, 1103.

[47] K. Ruedenberg; K. R. Sundberg, *In Quantum Science;* Plenum, 1976.

[48] E. Dalgaard; P. Jørgensen, *J. Chem. Phys.*, **1978**, *69*, 3833.

[49] D. L. Yeager; P. Jørgensen, *J. Chem. Phys.*, **1979**, *71*, 755.

[50] B. H. Lengsfield, *J. Chem. Phys.*, **1980**, *73*, 382.

[51] D. R. Yarkony, *Chem. Phys. Lett.*, **1981**, *77*, 634.

[52] R. Shepart; J. Simons, *Int. J. Quantum Chem.*, **1980**, *S14*, 211.

[53] H. J. A. Jensen; P. Jørgensen, *J. Chem. Phys.*, **1984**, *80*, 1204.

[54] W. T. Zemke; P. G. Lykos; A. C. Wahl, *J. Chem. Phys.*, **1969**, *51*, 5635.

[55] A. Karo; M. Krauss; A. C. Wahl, *J. Chem. Phys.*, **1973**, *S7*, 143.

[56] F. Grein; A. Banerjee, *Int. J. Quantum Chem.*, **1975**, *S9*, 147.

[57] D. L. Yeager; P. Jørgensen, *Mol. Phys.*, **1980**, *39*, 587.

[58] K. K. Docken; J. Hinze, *J. Chem. Phys.*, **1972**, *57*, 4928.

[59] H. J. Werner; M. Meyer, *J. Chem. Phys.*, **1981**, *74*, 5794.

[60] M. Meyer; V. Staemmler, *Theor. Chim. Acta*, **1989**, *76*, 95.

[61] H. Chaban; M. W. Schmidt; M. S. Gordon, *Theor. Chim. Acta*, **1997**, *97*, 88.

[62] B.O. Roos, *Adv. Chem. Phys.*, **1987**, *69*, 399.

[63] A. Dreuw, *ChemPhysChem*, **2006**, *7*, 2259.

[64] M. J. Bearpark; F. Ogliaro; T. Vreven; M. Boggio-Pasqua; M. J. Frisch; S. M. Larkin; M. Morrison; M. A. Robb, *J. Photochem. Photobiol. A; Chem.*, **2007**, doi;10.1016/j.jphotochem.2007.05.008.

[65] R. Puncz, *The Symmetric Group in Quantum Chemistry;* CRC, Boca Raton, 1995.

[66] A. Kutateladze, *Computational Methods in Photochemistry;* CRCPress Boca Raton, 2005.

[67] R. N. Diffenderfer; D. R. Yarkony, *J. Chem. Phys.*, **1982**, *86*, 5098.

[68] M. K. Shukla; J. Leszczyński, Eds., *Radiation Induced Molecular Phenomena in Nucleic Acids;* Springer, Jackson, 2007.

[69] P. J. Knowles; H. J. Werner, *Chem. Phys. Lett.*, **1985**, *115*, 259.

[70] H. J. Werner; P. J. Knowles, *Chem. Phys. Lett.*, **1988**, *145*, 514.

[71] H. J. Werner; P. J. Knowles, *Theor. Chim. Acta*, **1992**, *84*, 95.

[72] P. E. M. Siegbahn, *J. Chem. Phys.*, **1979**, *70*, 5391.

[73] J. Lorentzon; M. P. Fülscher; B. O. Roos, *J. Am. Chem. Soc.*, **1995**, *117*, 9265.

[74] R. J. Buenker; S. D. Peyerimhoff, *Theor. Chim. Acta*, **1974**, *35*, 33.

[75] R. J. Buenker; S. D. Peyerimhoff, *Mol. Phys.*, **1978**, *35*, 771.

[76] B. R. Brooks; H. F. Schaefer III, *J. Chem. Phys.*, **1979**, *70*, 5092.

[77] B. R. Brooks; D. Ladig; P. Saxe; N. C. Bandy; H. F. Schaefer III, *Phys. Scr.*, **1980**, *21*, 312.

[78] W. Duch; J. Karwowski, *Theor. Chim. Acta*, **1979**, *51*, 175.

[79] W. Duch, *Theor. Chim. Acta*, **1980**, *57*, 299.

[80] P. Tavan; K. Schulten, *J. Chem. Phys.*, **1980**, *72*, 3547.

[81] P. R. Taylor, *J. Chem. Phys.*, **1981**, *74*, 1256.

[82] B. Liu; M. Yoshimine, *J. Chem. Phys.*, **1981**, *74*, 612.

[83] H. Lischka; R. Shepard; F. B. Brown; I. Shavitt, *J. Chem. Phys.*, **1981**, *S15*, 91.

[84] H. J. Werner; P. J. Knowles, *J. Chem. Phys.*, **1988**, *89*, 5803.

[85] P. E. M. Siegbahn, *Chem. Phys.*, **1977**, *25*, 197.

[86] P. E. M. Siegbahn, *J. Quantum Chem.*, **1983**, *23*, 1869.

[87] W. Mayer, *In Modern Theoretical Chemistry;* Plenum, 1977.

[88] P. E. M. Siegbahn, *J. Quantum Chem.*, **1980**, *18*, 1229.

[89] H. J. Werner; E. A. Reinsch, *J. Chem. Phys.*, **1982**, *76*, 3144.

[90] A. F. Fuciarelli; J. D. Zimbrick, Eds., *Radiation Damage in DNA; Structure/Function Relationship at Early Times;* Battelle, Columbus, OH, 1995.

[91] S. G. Lias; R. D. Levin; S. A. Kafafi, *In NIST Chemistry WebBook, NIST Standard Reference Database Number 69;* National Institute of Standards and Technology, Gaithersburg, MD.

[92] R. Barrios; P. Skurski; J. Simons, *J. Phys. Chem. B.*, **2002**, *106*, 7991.

[93] X. Pan; L. Sanche, *Chem. Phys. Lett.*, **2006**, *421*, 404.

[94] X. Pan; L. Sanche, *Phys. Rev. Letts.*, **2005**, *94*, 198104.

[95] X. Pan; P. Cloutier; D. Hunting; L. Sanche, *Phys. Rev. Letts.*, **2003**, *90*, 208102.

[96] S. M. Pimblott; J. A. LaVerne, *Radiat. Phys. Chem.*, **2007**, *76*, 1244.

[97] J. Tennyson; J. D. Gorfinkiel; I. Rozum; C. S. Trevisan; N. Vinci, *Rad. Phys. Chem.*, **2003**, *68*, 65.

[98] P. G. Burke; A. Hibbert; W. D. Robb, *J. Phys. B*, **1971**, *4*, 1153.

[99] P. G. Burke; M. J. Seaton, *Methods. Comput. Phys.*, **1971**, *10*, 1.

[100] P. G. Burke, *Comput. Phys. Comm.*, **1973**, *6*, 288.

[101] P. G. Burke; W. D. Robb, *J. Phys. B*, **1972**, *5*, 44.

[102] P. G. Burke; W. D. Robb, *Adv. At. Mol. Phys.*, **1975**, *11*, 143.

[103] P. G. Burke; K. A. Berrington, *R-matrix Theory of Atomic and Molecular Processes;* IOP Publishing, Bristol, 1993.

[104] B. I. Schneider, *Chem. Phys. Lett.*, **1975**, *2*, 237.

[105] B. I. Schneider, *Phys. Rev.*, **1975**, *A11*, 1957.

[106] B. I. Schneider; P. J. Hay, *Phys. Rev.*, **1976**, *A13*, 2049.

[107] B. I. Schneider; M. A. Morrison, *Phys. Rev.*, **1977**, *A16*, 1003.

[108] P. G. Burke; I. Mackey; I. Shimamura, *J. Phys. B*, **1977**, *10*, 2497.

[109] B. D. Buckley; P. G. Burke; Vo Ky Lan, *Comput. Phys. Commun.*, **1979**, *17*, 175.

[110] C. J. Noble; P. G. Burke; S. Salvini, *J. Phys. B*, **1979**, *15*, 3779.

[111] B. I. Schneider; T. N. Rescigno, *Phys. Rev. A*, **1988**, *37*, 3749.

[112] K. Takatsuka; V. McKoy, *Phys. Rev. A*, **1981**, *24*, 2473.

[113] K. Takatsuka; V. McKoy, *Phys. Rev. A*, **1984**, *30*, 1734.

[114] C. Winstead; Q. Y. Sun; P. G. Hipes; M. A. P. Lima; V. McKoy, *Australian J. Phys.*, **1992**, *45*, 325.

[115] P. G. Burke; K. A. Berrington, *Atomic and Molecular Processes - An R-matrix Approach;* Bristol; IOPP, 1993.

[116] L. A. Morgan; J. Tennyson; C. J. Gillan, *Comput. Phys. Commun*, **1998**, *114*, 120.

[117] C. J. Gillan; O. Nagy; P. G. Burke; L. A. Morgan; C. J. Noble, *J. Phys. B; At. Mol. Phys.*, **1987**, *20*, 4585.

[118] P. G. Burke; I. Mackey; I. Shimamura, *J. Phys. B; At. Mol. Opt. Phys.*, **1977**, *10*, 2497.

[119] B. M. Nestman; R. K. Nesbett; S. D. Peyerimhoff, *J. Phys. B; At. Mol. Opt. Phys.*, **1991**, *24*, 5133.

[120] L. A. Morgan; C. J. Gillan; J. Tennyson; X. Chen, *J. Phys. B; At. Mol. Opt. Phys.*, **1997**, *30*, 4087.

[121] W. M. Huo; D. Brown, *Phys. Rev. A*, **1999**, *60*, 295.

[122] P. Kolerec; M. Cizek; J. Horacek; G. Mil'nikov; H. Nakamura, *Physica Scripta*, **2002**, *65*, 328.

[123] M. Telmini; C. Jungen, *Phys. Rev. A*, **2003**, *68*, 062704.

[124] M. Hiyama; N. Kosugi, *J. Theor. Comput. Chem.*, **2005**, *4*, 35.

[125] S. Tonzani, *Computer Phys. Comm.*, **2007**, *176*, 146.

[126] J. Almlöf; P. R. Taylor; C. E. Dykstra (Ed.), *Advanced Theories and Computational Approaches to the Electronic Structure of Molecules;* Reidel, 1984.

[127] J. Almlöf; P. R. Taylor; E. Clementi (Ed.), *Modern Techniques in Computational Chemistry; MOTECC-91;* Escom, Leiden, 1991.

[128] C. P. Ballace; K. A. Berrington; B. M. McLaughlin, *J. Phys. B; At. Mol. Opt. Phys.*, **2001**, *34*, 3775.

[129] S. Kaur; K. L. Baluja, *J. Phys. B; At. Mol. Opt. Phys.*, **2005**, *38*, 3917.

[130] M. Tashiro, *J. Chem. Phys*, **2008**, *129*, 164308.

[131] K. Baluja; A. Msezane, *J. Phys. B; At. Mol. Opt. Phys.*, **2002**, *35*, 437.

[132] K. Baluja; J. A. Tossell, *J. Phys. B; At. Mol. Opt. Phys.*, **2004**, *37*, 609.

[133] M. Tashiro; K. Morokuma, *Phys. Rev. A*, **2007**, *75*, 012720.

[134] M. Gupta; K. L. Baluja, *Euro. Phys. J. D*, **2007**, *41*, 475.

[135] B. Yan; S. F. Pan; J. H. Yu, *Chin. Phys.*, **2007**, *16*, 1956.

[136] R. Curik; C. H. Greene, *Mol. Phys.*, **2007**, *105*, 1565.

[137] D. J. Haxton; C. H. Greene, *Phys. Rev. A*, **2008**, *78*, 052704.

[138] C. S. Trevisan; A. E. Orel; T. N. Rescigno, *J. Phys. B; At. Mol. Opt. Phys.*, **2006**, *39*, L255.

[139] J. Tennyson; C. J. Noble, *J. Phys. B; At. Mol. Opt. Phys.*, **1986**, *19*, 4025.

[140] D. Bouchiha; J. D. Gorfinkiel; L. G. Caron; L. Sanche, *J. Phys. B; At. Mol. Opt. Phys.*, **2007**, *40*, 1259.

[141] J. Tennyson; D. B. Brown; J. J. Munro; I. Rozum; H. N. Varambhia; N. Vinci, *J. Phys. Conf. Series*, **2007**, *86*, 012001.

[142] L. A. Morgan; J. Tennyson, *Phil. Trans. R. Soc. A*, **1999**, *357*, 1161.

[143] P. G. Burke; J. Tennyson, *Mol. Phys.*, **2005**, *103*, 2537.

[144] I. Rozum; N. J. Mason; J. Tennyson, *J. Phys. B; At. Mol. Opt. Phys.*, **2003**, *36*, 2419.

[145] J. Tennyson, *J. Phys. B; At. Mol. Opt. Phys.*, **1996**, *29*, 6185.

[146] K. Higgins; C. J. Noble; P. G. Burke, *J. Phys. B; At. Mol. Opt. Phys.*, **1994**, *27*, 3203.

[147] A. Faure; J. D. Gorfinkiel; J. Tennyson, *J. Phys. B; At. Mol. Opt. Phys.*, **2004**, *37*, 801.

[148] J. Tennyson; J. D. Gorfinkiel; I. Rozum; C. S. Trevisan; N. Vinci, *Rad. Phys. Chem.*, **2003**, *68*, 65.

[149] H. N. Varambhia; J. Tennyson, *J. Phys. B; At. Mol. Opt. Phys.*, **2007**, *40*, 1211.

[150] J. D. Gorfinkiel; A. Faure; S. Taioli; C. Piccarreta; G. Halmová; J. Tennyson, *Eur. Phys. J. D*, **2005**, *35*, 231.

[151] W. M. Huo; F. A. Gianturco, *Computational Methods for Electron Molecule Collisions;* Plenum Press, New York, 1995.

[152] W. Domcke, *Phys. Rep.*, **1991**, *208*, 97.

[153] M. Larsson; A. E. Orel, *Dissociative Recombination of Molecular Ions;* Cambridge University Press, 2008.

[154] J. Tennyson; C. J. Noble, *Comp. Phys. Comm.*, **1984**, *33*, 421.

[155] G. Breit; E. Wigner, *Phys. Rev.*, **1936**, *49*, 519.

[156] A. U. Hazi, *Phys. Rev. A*, **1979**, *19*, 920.

[157] A. Dora; J. Tennyson; L. Bryjko; T. van Mourik, *J. Chem. Phys.*, **2009**, *130*, 164307.

[158] J. Tennyson, *J. Phys. B; At. Mol. Opt. Phys.*, **1996**, *29*, 1817.

[159] J. Tennyson, *J. Phys. B; At. Mol. Opt. Phys.*, **2004**, *37*, 1061.

[160] A. Faure; J. D. Gorfinkiel; J. Tennyson, *J. Phys. B; At. Mol. Opt. Phys.*, **2004**, *37*, 801.

[161] K. K Rohatgi-Mukherjee, *Fundamentals of Photochemistry;* Wiley Eastern Limited, 1978.

[162] Jr. Ch. W. Bauschlicher, *J. Chem. Phys.*, **1980**, *72*, 880.

[163] W. J. Hehre; R. Ditchfield; J. A. Pople, *J. Chem. Phys.*, **1972**, *56*, 2257.

[164] T. H. Dunning Jr., *J. Chem. Phys.*, **1989**, *90*, 1007.

[165] R. A. Kendall; T. H. Dunning Jr.; R. J. Harrison, *J. Chem. Phys.*, **1992**, *96*, 6796.

[166] J. D. Petke; G. M. Maggiora; R. E. Chistoffersen, *J. Phys. Chem.*, **1992**, *96*, 6992.

[167] J. Leszczynski, *In Advances in Molecular Structure Research;* JAI Press; London, 2000.

[168] J. Leszczynski, *J. Phys. Chem.*, **1992**, *96*, 1649.

[169] J. Sponer; P. Hobza; J. Leszczynski, *In Computational Molecular Biology, Theoretical and Computational Book Series;* Vol. 8; Elsevier; Amsterdam, 1999.

[170] E. S. Kryachko; M .T. Nguyen; T. Zeegers-Huyskens, *J. Phys. Chem. A*, **2001**, *105*, 1288.

[171] J. Leszczynski, *Int. J. Quantum. Chem.; Quantum. Biol. Symp.*, **1991**, *18*, 9.

[172] D. A. Estrin; L. Paglieri; G. Korongiu, *J. Phys. Chem.*, **1994**, *98*, 5653.

[173] J. Leszczynski, *Int. J. Quantum. Chem.; Quantum. Biol. Symp.*, **1991**, *18*, 9.

[174] K. Szczepaniak; W. B. Person; J. Leszczynski; J. S. Kwiatkowski, *Pol. J. Chem.*, **1998**, *72*, 402.

[175] A. C. Drohat; T. J. Stivers, *J. Am. Chem. Soc.*, **2000**, *122*, 1840.

[176] R. F. Stewart, *Acta Crystallogr.*, **1967**, *23*, 1102.

[177] A. F. Bell; L. Hecht; L. D. Barron, *J. Chem. Soc. Faraday Trans.*, **1997**, *93*, 553.

[178] R. D. Brown; P. D. Godfrey; D. McNaughton; A. P. Pierlot, *J. Am. Chem. Soc.*, **1998**, *107*, 2329.

[179] I. Kulakowski; M. Geller; B. Lesyng; K. L. Wierzchowski, *Biochim. Biophys. Acta*, **1974**, *361*, 119.

[180] J. Schiedt; R. Weinkauf; D. M. Neumark; E. Schlag, *Chem. Phys.*, **1998**, *239*, 511.

[181] M. Piacenza; S. Grimme, *J. Comp. Chem.*, **2003**, *25*, 83.

[182] V.Vaquero; M. E. Sanz; J. C. López; J. L. Alonso, *Phys. Chem. Letts A*, **2007**, *111*, 3443.

[183] J. W. Boughton; P. Pulay, *Inter. J. Quantum Chem.*, **1993**, *47*, 49.

[184] H. H. Jaffé; M. Orchin, *Symmetry in Chemistry;* John Wiley and Sons Inc, 1967.

[185] S. R. Langhoff; E. R. Davidson, *Int. J. Quantum Chem.*, **1974**, *8*, 61.

[186] I. Rozum; N. J. Mason; J. Tennyson., *New J. Phys*, **2003**, *5*, 155.

[187] N. Russo; M. Toscano; A. Grand, *J. Comp. Chem.*, **2000**, *21*, 1243.

[188] B. I. Verkin; L. F. Sukodub;I. K. Yanson, *Dokl Akad Nauk SSSR*, **1976**, *228*, 1452.

[189] R. B. Brown; P. D. Godfrey; D. McNaughton; A. P. Pierlot, *J. Am. Chem. Soc*, **1988**, *110*, 2329.

[190] A. Broo; Holmén, *J. Phys. Chem. A*, **1997**, *101*, 3589.

[191] M. K. Shukla; J. Leszczyński, *J. Phys. Chem. A*, **2002**, *106*, 8642.

[192] M. K. Shukla; P. C. Mishra, *Chem. Phys*, **1999**, *240*, 319.

[193] Y. Marcier; F. Santoro; M. Reguero; R. Importa, *J. Phys. Chem. Lett. B*, **2008**, *112*, 10769.

[194] T. Climent; R. González-Luque; M. Merchán; L. Serrano-Andrès, *Chem. Phys. Lett.*, **2007**, *441*, 327.

[195] S. Grimme; M. Waletzke, *J. Chem. Phys.*, **1999**, *111*, 5645.

[196] M. R. Silva-Junior; M. Schreiber; S. P. A. Sauer; W. Thiel, *J. Chem. Phys.*, **2008**, *129*, 104103.

[197] C. M. Marian; F. Schneider; M. Kleinschmidt; J. Tatchen, *Eur. Phys. J. D*, **2002**, *20*, 357.

[198] Ch. Neiss; P. Saalfrank; M. Parac; S. Grimme, *J. Phys. Chem A*, **2002**, *107*, 140.

[199] D. W. Miles; R. K. Robins; H. Eyring, *Proc. Natl. AcSci. U.S.A.*, **1967**, *57*, 1139.

[200] C. A. Sprecher; W. C. Johnson;, *Biopolymers*, **1977**, *16*, 2243.

[201] J. S. Novros; L. B. Clark, *J. Phys. Chem.*, **1986**, *90*, 5666.

[202] L. B. Clark; G. G. Paschel; O. Tinoco, *J. Phys. Chem.*, **1965**, *69*, 3615.

[203] B. B. Brady; L. A. Pateanu; D. H. Levy, *Chem. Phys. Lett.*, **1988**, *147*, 538.

[204] C. Zazza; A. Amadei; N. Sanna; A. Grandi; G. Chillemi; A. Di Nola; M. D'Abramo; M. Aschi, *Phys. Chem. Chem. Phys.*, **2006**, *8*, 1385.

[205] N. Sanna; F. Gianturco, *Comput. Phys. Commun.*, **1998**, *114*, 142.

[206] W. Voelter; R. Records; E. Bunnenburg; C. Djerasi, *J. Am. Chem. Soc*, **1968**, *90*, 6113.

[207] W. C. Brunner; M. F. Maestre, *Bioplymers*, **1975**, *14*, 555.

[208] J. S. Novros; L. B. Clark, *J. Phys. Chem.*, **1986**, *90*, 5666.

[209] Y. Matsuoks; B. Norden, *J. Phys. Chem.*, **1982**, *86*, 1378.

[210] A. Holmen; A. Broo; B. Albinsson, *J. Phys. Chem.*, **1994**, *98*, 4998.

[211] D. Voet; W. B. Gratzer; R. A. Cox; P. Doty, *Biopolymers*, **1963**, *1*, 193.

[212] M. T. Fujii; T. Tamura; N. Mikami; M. Ito, *Chem. Phys. Lett.*, **1986**, *126*, 583.

[213] P. Vigny; J. P. Ballini; B. Pullman; N. Goldblum; Reidel; Dordrecht, Eds., *Excited states in Organic Chemistry and Biochemistry;* 1997.

[214] L. B. Clark; I. Tinocco, *J. Am Chem. Soc.*, **1965**, *87*, 11.

[215] A. Kaito; M. Hatano; T. Ueda; S. Shibuya, *Bull. Chem. Soc. Jpn.*, **1980**, *53*, 3073.

[216] R. Kobayashi, *J. Phys. Chem. A*, **1998**, *102*, 10813.

[217] R. Kobayashi, *Angew. Chem. Int. Ed.*, **2009**, *48*, 9030.

[218] J. Šponer; P. Hobza, *J. Phys. Chem.*, **1994**, *98*, 3161.

[219] A. Aamouche; M. Ghomi; L. Gracjar; M. H .Baron; F. Romain; V. Baumruk; J. Stepanek; C. Coulombeau; H. Jobic; G. Berthier, *J. Phys. Chem.A*, **1997**, *101*, 10063.

[220] A. D. Becke, *J. Chem. Phys.*, **1993**, *98*, 5648.

[221] C. Lee; W. Yang; R. G. Parr, *Phys. Rev. B*, **1988**, *37*, 785.

[222] S. H. Vosko; L. Wilk; M. Nusair, *Can. J. Phys.*, **1980**, *58*, 1200.

[223] P. J. Stephens; F. J. Devlin; C. F. Chabalowski; M. J. Frisch, *J. Phys. Chem.*, **1994**, *98*, 11623.

[224] P. R. Callis, *Ann. Rev. Phys. Chem.*, **1983**, *34*, 329.

[225] C. A. Sprecher; W. C. Jr. Johnson, *Biopolymers*, **1977**, *16*, 2243.

[226] D. Voet; W. B. Gratzer; R. A. Cox; P. Doty, *Biopolymers*, **1963**, *1*, 193.

[227] L. B. Clark; I. Tinoco, *J. Am. Chem. Soc.*, **1965**, *87*, 11.

[228] T. Yamada; H. Fukutome, *Biopolymers*, **1968**, *6*, 43.

[229] F. Zaloudek; J. S. Novros; L. B. Clark, *J. Am. Chem. Soc.*, **1985**, *107*, 7344.

[230] W. C. Jr Johnson; P. M. Vipond; J. C. Girod, *Biopolymers*, **1971**, *10*, 923.

[231] A. Kaito; M. Hatano; T. Ueda; S. Shibuya, *Bull. Chem. Soc. Jpn.*, **1980**, *53*, 3073.

[232] K. Raksany; I. Foldvary, *Biopolymers*, **1978**, *17*, 887.

[233] M. K. Shukla; J. Leszczyński, *J. Biomol. Struct. Dyn*, **2007**, *25*, 93.

[234] K. Kowalski; P. Piecuch; I. S. O. Pimienta; M. NcGuire, *Int. Rev. Phys. Chem.*, **2002**, *21*, 527.

[235] K. Kowalski; P. Piecuch, *J. Chem. Phys.*, **2004**, *120*, 1715.

[236] K. Kowalski; M. Valiev, *J. Phys. Chem. A*, **2008**, *112*, 5538.

[237] K. A. Kistler; S. Matsika, *J. Phys. Chem. A*, **2009**, *113*, 12396.

[238] M. W. Schmidt; K. K. Baldridge; J. A Boatz; S. T. Elbert; M. S. Gordon; J. H. Jensen; S. Koseki; N. Matsunaga; K. A. Nguyen; S. Su; T. L. Windus; M. Dupuis; J. A. Montgomery, *J. Comput. Chem.*, **1993**, *14*, 1347.

[239] K. A. Kistler; S. Matsika, *J. Phys. Chem.A*, **2007**, *111*, 2650.

[240] M. K. Shukla; J. Leszczyński, *J. Comput. Chem.*, **2004**, *25*, 768.

[241] K. Tomić; T. Jörg; C. M. Marian, *J. Phys. Chem.A*, **2005**, *109*, 8410.

[242] M. Schreiber; M. R. Silva-Junior; S. P. A. Sauer; W. Thiel, *J. Chem. Phys.*, **2008**, *128*, 134110.

[243] A. L. Sobolewski; W. Domcke, *Phys. Chem. Chem. Phys.*, **2004**, *6*, 2763.

[244] N. Ismail; L. Blancafort; M. Olivucci; B. Kohler; M. A. Robb, *J. Am. Chem. Soc.*, **2002**, *124*, 6818.

[245] L. Blancafort; M. A. Robb, *J. Phys. Chem. A*, **2004**, *108*, 10609.

[246] M. Z. Zgierski; S. Patchkovskii; E. C. Lim, *J. Chem. Phys.*, **2005**, *123*, 1081101.

[247] M. Z. Zgierski; S. Patchkovskii; T. Fujiwara; E. C. Lim, *J. Phys. Chem. A*, **2005**, *109*, 8410.

[248] M. Merchán; L. Serrano-Andrés, *J. Am. Chem. Soc.*, **2003**, *125*, 8108.

[249] M. Merchán; L. Serrano-Andrés; L. Robb; M. Blancafort, *J. Am. Chem. Soc.*, **2005**, *127*, 1820.

[250] K. M. Guckian; B. A. Schweitzer; R. X. Ren; C. J. Sheils, *J. Am. Chem. Soc.*, **2000**, *122*, 2213.

[251] W. Caminati, *Angew. Chem. Int. Ed.*, **2009**, *48*, 9030.

[252] M. Schreiber; M. R. Silva-Junior; S. P. A. Sauer; W. Thiel, *J. Chem. Phys.*, **2008**, *128*, 134110.

[253] K. Aflatooni; G. A. Gallup; P. D. Burrow, *J. Phys. Chem. A*, **1998**, *102*, 6205.

[254] D. W. Miles; R. K. Robins; H. Eyring, *Proc. Natl. Acad. Sci. U.S.A*, **1967**, *57*, 1139.

[255] W. Woelter; R. Records; E. Bunnenberg; C. Djerassi, *J. Am. Chem. Soc.*, **1968**, *90*, 6163.

[256] D. W. Miles; M. J. Robins; R. K. Robins; M. W. Winkley; H. Eyring, *J. Am. Chem. Soc.*, **1969**, *91*, 825.

[257] W. C. Brunner; M. F. Maestre, *Biopolymers*, **1975**, *14*, 555.

[258] B. G. Anex; A. F. Fucaloro; A. Durra-Ahmed, *J. Phys. Chem.*, **1975**, *79*, 2636.

[259] D. B. Jones; F. Wang; D. A. Winkler; M. J. Brunger, *Biophys. Chem.*, **2006**, *121*, 105.

[260] M. K. Shukla; J. Leszczyński, *J. Phys. Lett*, **2006**, *429*, 261.

[261] Ch. M. Marian, *J. Phys. Chem. A*, **2007**, *111*, 1545.

[262] L. Gorb; A. Kaczmarek; A. Gorb; A. J. Sadlej; J. Leszczyński, *J. Phys. Chem.B*, **2005**, *109*, 13770.

[263] M. Sabio; S. Topiol; W. C. Lumma, *J Phys. Chem*, **1990**, *94*, 1366.

[264] J. D. Petke; G. M. Maggiora; R. E. Christoffersen, *J Am. Chem. Soc*, **1990**, *112*, 5452.

[265] L. Gorb; J. Leszczyński, *J Am. Chem. Soc*, **1998**, *120*, 50249.

[266] M. K. Shukla; J. Leszczyński, *Chem. Phys. Lett.*, **2006**, *429*, 261.

[267] A. Broo; A. Holmén, *J. Phys. Chem. A*, **1997**, *101*, 3589.

[268] I. Pugliesi; K. Müller-Dethlefs, *J. Phys. Chem. A*, **2006**, *110*, 13045.

[269] P. S. Kushwaha; A. Kumar; P. C. Mishra, *Spectrochem. Acta A*, **2004**, *60*, 719.

[270] H. Chen; S. Li, *J. Phys. Chem. A*, **2006**, *110*, 12360.

[271] M .K. Shukla; S. K. Mishra; A. Kumar; P. C. Mishra, *J. Comp. Chem.*, **2000**, *21*, 826.

[272] M. K. Shukla; J. Leszczyński, *J. Phys. Chem. A*, **2005**, *109*, 7775.

[273] H. Langer; N. L. Doltsinis, *J. Chem. Phys.*, **2003**, *118*, 5400.

[274] J. Cerny; V. Spirko; M. Mons; P. Hobza; D. Nachtigallová, *Phys. Chem. Chem. Phys.*, **2006**, *8*, 1985.

[275] K. Kowalski; M. Valiev, *Res. Lett. Phys. Chem.*, **2007**, *2007*, Article ID 85978.

[276] P. Markus; M.P. Fülscher; L. Serrano-Andrés; B.O. Roos, *J. Am. Chem. Soc*, **1997**, *119*, 6168.

[277] C. Winstead; V. McKoy, *J. Chem. Phys.*, **2006**, *125*, 224302.

[278] L. Sanche; G. Schulz, *Phys. Rev. A*, **1972**, *5*, 1672.

[279] V. M. Orlov; A. M. Smirnov; Y. M. Varshavsky, *Tetrahedron Lett.*, **1976**, *48*, 4377.

[280] L. B. Clark, *J. Am. Chem. Soc.*, **1994**, *116*, 5265.

[281] M. Mons; F. Piuzzi; I. Dimicoli; L. Gorb; J. Leszczyński, *J. Phys. Chem. A*, **2002**, *110*, 10921.

[282] E. Nir; Ch. Janzen; P. Imhof; K. Kleinermanns; M. S. de Vires, *J. Chem. Phys.*, **2001**, *115*, 4604.

[283] M. Mons; I. Dimicoli; F. Piuzzi; B. Tardivel; M. Elhanine, *J. Phys. Chem. A*, **2002**, *106*, 5088.

[284] A. Holmén; A. Broo, *Int. J. Quantum Chem.*, *56*, 113.

[285] O. Isayev; A. Furmanchuk; O. V. Shishkin; L. Gorb; J. Leszczynski, *J. Phys. Chem. B*, **2007**, *111*, 3476.

[286] P. Hobza; J. Šponer, *Chem. Rev.*, **1999**, *99*, 3247.

[287] M. P. Fülscher; S. Serrano-Andrés; B. O. Roos, *J. Am. Chem. Soc*, **1997**, *119*, 6168.

[288] C. T. Hwang; C. L. Stumpt; Y. Q. Lu; H. I. Keuttämaa, *Int J Mass Spectrom*, **1999**, *182/183*, 253.

[289] N. J. Kim; G. Jeong; Y. S. Kim; J. Sung; S. K. Kim; Y. D. Park, *J. Chem. Phys.*, **2000**, *113*, 10051.

[290] D. C. Luhrs; J. Viallon; I. Fisher, *Phys. Chem. Chem. Phys.*, **2001**, *3*, 1827.

[291] E. Nir; K. Kleinermanns; L. Grace; M. S. de Vries, *J. Phys. Chem. A*, **2001**, *105*, 5106.

[292] L. B. Clark, *J. Phys. Chem.*, **1995**, *99*, 4466.

[293] L. B. Clark;, *J. Phys. Chem.*, **1990**, *94*, 2873.

[294] A. Holmén; A. Broo; B. Albinsson; B. Norden, *J. Am. Chem. Soc.*, **1997**, *119*, 12240.

[295] N. A. Richardson; J. Gu; S. Wang; Y. Xie; H. F. Schaefer, *J. Am. Chem. Soc.*, **2004**, *126*, 4404.

[296] X. Li; M. D. Sevilla; L. Sanche, *J. Am. Chem. Soc*, **2003**, *125*, 3668.

[297] C. König; J. Kopyra; I. Bald; E. Illenberg, *Phys. Rev. Lett.*, **2006**, *97*, 018105.

[298] C. König; J. Kopyra; I. Bald; E. Illnberger, *Phys. Rev. Letts.*, **2006**, *97*, 018105.

[299] K. Aflatooni; A. M Scheer; P. D. Burrow, *J. Chem. Phys.*, **2006**, *125*, 054301.

[300] P. D. Burrow; G. A. Gallup; A. Modelli, *J. Phys. Chem. A*, **2008**, *112*, 4106.

[301] M. Yekutiel; J. R. Lane; P. Gupta; H. G. Kjaergaard, *J. Phys. Chem. A*, **2010**, page 7544.

[302] A. Faure; J. D. Gorfinkiel; L. A. Morgan; J. Tennyson, *Computer Phys. Comms.*, **2002**, *144*, 224.

[303] R. Zhang; A. Faure; J. Tennyson, *Physica Scripta*, **2009**.

[304] J. Tennyson; C. J. Noble, *Computer Phys. Comms.*, **1984**, *33*, 421.

[305] T.H. Dunning Jr.; K.A. Peterson; A.K. Wilson, *J. Chem. Phys.*, **114**, page 9244.

[306] S. N. Ali, *Indian J. Phys.*, **1939**, *13*, 309.

[307] M. Helmann; I. Platzer, *J. Chem. Soc.*, **1965**, page 1440.

[308] J. D. Gorfinkiel; J. Tennyson, *J. Phys. B; At. Mol. Opt. Phys*, **2005**, *38*, 1607.

[309] J. D. Gorfinkiel; J. Tennyson, *J. Phys. B; At. Mol. Opt. Phys*, **2004**, *37*, L343.

[310] K. Blum; D. Thompson, *J. Phys. B; At. Mol. Opt. Phys.*, **1998**, *38*, 39.

[311] N. Foloppe; A. D. MacKerell, *J. Phys. Chem. B*, **1998**, *102*, 6669.

[312] K. Miaskiewicz; R. Osman, *J. Am. Chem. Soc.*, **1994**, *116*, 323.

[313] K. A. Bramed; W. A. Goddard, *J. Am. Chem. Soc.*, **1999**, *121*, 985.

[314] D. Antic; L. Parenteau; L. Sanche, *J. Phys. Chem. B*, **2000**, *104*, 4711.

[315] D. Antic; L. Parenteau; L. Sanche, *J. Phys. Chem. B*, **2000**, *104*, 4711.

[316] D. Antic; L. Parenteau; M. Lepage; L.Sanche, *J. Phys. Chem.*, **1999**, *103*, 6611.

[317] C. Winstead; V. McKoy, *J. Chem. Phys.*, **2006**, *125*, 074302.

[318] L. Bryjko; T. van Mourik; A. Dora; J. Tennyson, *J. Phys. B; At. Mol. Opt. Phys., submitted.*

[319] J. Almöf; T. Helgaker; P. R. Taylor, *J. Phys. Chem.*, **1988**, *92*, 3029.

[320] T. H. Dunning Jr., *J. Chem. Phys.*, **1989**, *90*, 1007.

[321] R. A. Kendall; T. H. Dunning Jr.; R. J. Harrison, *J. Chem. Phys.*, **1992**, *96*, 6796.

[322] M. Merchán; L. Serrano-Andrés; M.P. Fülscher; B.O. Roos, *Recent Advances in Multireference Methods;* World Scientific Publishing, 1999.

[323] R. Krisham; J. S. Binkley; R. Seeger; J. A. Pople, *J. Chem. Phys.*, **1980**, *72*, 650.

[324] H. J. Silverstone; O. Sinanoglu, *J. Chem. Phys.*, **1966**, *44*, 1999.

[325] O. Sinanoglu; D. F. Tuan, *J. Chem. Phys.*, **1963**, *38*, 1740.

[326] D. F. Tuan; O. Sinanoglu, *J. Chem. Phys.*, **1964**, *41*, 2677.

[327] V. McKoy; O. Sinanoglu, *J. Chem. Phys.*, **1964**, *41*, 2689.

[328] H.J. Werner; P. J. Knowles, *MOLPRO User's Manual Version 2006.1.*